DEPARTMENT OF MECHANICAL ENGINEERING
COLLEGE OF ENGINEERING & TECHNOLOGY
OLD DOMINION UNIVERSITY
NORFOLK, VIRGINIA 23529

NON-LINEAR BOUNDARY-LAYER RECEPTIVITY DUE TO DISTRIBUTED SURFACE ROUGHNESS

By

Tahani R. Amer, Graduate Research Assistant

Principal Investigator: Gregory V. Selby

Summary of Research (Final Report)
For the period ended November 30, 1994

Prepared for
National Aeronautics and Space Administration
Langley Research Center
Hampton, VA 23681-0001

Under
Research Grant NAG-1-1603
Robert Yang, Technical Monitor
Technology Applications Group

August 1995

DEPARTMENT OF MECHANICAL ENGINEERING
COLLEGE OF ENGINEERING & TECHNOLOGY
OLD DOMINION UNIVERSITY
NORFOLK, VIRGINIA 23529

NON-LINEAR BOUNDARY-LAYER RECEPTIVITY DUE TO DISTRIBUTED SURFACE ROUGHNESS

By

Tahani R. Amer, Graduate Research Assistant

Principal Investigator: Gregory V. Selby

Summary of Research (Final Report)
For the period ended November 30, 1994

Prepared for
National Aeronautics and Space Administration
Langley Research Center
Hampton, VA 23681-0001

Under
Research Grant NAG-1-1603
Robert Yang, Technical Monitor
Technology Applications Group

Submitted by the
Old Dominion University Research Foundation
P.O. Box 6369
Norfolk, VA 23508

August 1995

ABSTRACT

NON-LINEAR BOUNDARY-LAYER RECEPTIVITY DUE TO DISTRIBUTED SURFACE ROUGHNESS

Tahani Reffet Amer

Old Dominion University

Advisor: Dr. Gregory V. Selby

The process by which a laminar boundary layer internalizes the external disturbances in the form of instability waves is known as boundary-layer receptivity. The objective of the present research was to determine the effect of acoustic excitation on boundary-layer receptivity for a flat plate with distributed variable-amplitude surface roughness through measurements with a hot-wire probe. Tollmien-Schlichting mode shapes due to surface-roughness receptivity have also been determined, analyzed, and shown to be in agreement with theory and other experimental work. It has been shown that there is a linear relationship between the surface roughness and receptivity for certain roughness configurations with constant roughness wavelength. In addition, strong non-linear receptivity effects exist for certain surface roughness configurations over a band where the surface roughness and T-S wavelength are matched. The results from the present experiment follow the trends predicted by theory and other experimental work for linear receptivity. In addition, the results show the existence of non-linear receptivity effects for certain combinations of surface roughness elements.

ACKNOWLEDGEMENTS

This is a thesis being submitted in lieu of a final report for the research project entitled "Supersonic Suction Laminar Flow Control Experiments with Applications to the High Speed Civil Transport" for the period December 1, 1993 through November 30, 1994. This work was supported by the NASA Langley Research Center through NAG-1603, Robert Yang, Technical Monitor, Technology Applications Group, NASA Langley Research Center, Mail Stop 211.

TABLE OF CONTENTS

LIST OF TABLES

LIST OF FIGURES

NOMENCLATURE

Symbol	Definition
A_{sc}	Complex amplitude of Stokes-layer profile.
a_i	Hot-wire calibration polynomial coefficients.
d	Diameter of hot-wire.
e	Output voltage from hot-wire anemometer.
e_c	Temperature-compensated output voltage from hot-wire.
f	Acoustic forcing frequency.
F	Dimensionless frequency of T-S wave, $F = \frac{\omega}{R \times 10^6} = \frac{2\pi f \nu}{U_\infty^2 \times 10^{-6}}$
H	Boundary-layer shape factor. $H = \frac{\delta^*}{\theta}$
h	Two-dimensional roughness height.
k	Wave number, $K = \frac{2\pi}{\lambda}$

OHR — Over-heat ratio,

$$OHR = \frac{r_{hw}}{r_{cold}}$$

p_{atm} — Atmospheric pressure.

p_{static} — Static pressure.

r_{hw} — Operating resistance of hot-wire.

r_{cold} — Resistance of hot-wire at ambient temperature.

Re — Boundary-layer Reynolds number,

$$Re = \frac{U_\infty x}{\nu}$$

Re_v — Virtual boundary-layer Reynolds number,

$$Re_v = \frac{U_\infty x_v}{\nu}$$

Re_h — Reynolds number based on roughness height,

$$Re_h = \frac{U_\infty h}{\nu}$$

Re_{tr} — Transition Reynolds number.

T — Ambient temperature.

T_0 — Average temperature during hot-wire calibration.

u — Mean streamwise velocity.

U_∞	Freestream velocity.
u'	Fluctuating velocity amplitude.
u'_{ac}	Fluctuating velocity amplitude due to acoustic forcing.
$u'_{ac,\infty}$	Fluctuating velocity amplitude due to freestream acoustic forcing.
u'_t	Fluctuating velocity amplitude due to forcing frequency.
u'_{ts}	Fluctuating velocity amplitude due to T-S component.
x	Streamwise distance from the actual leading edge.
x_v	Streamwise distance from the virtual leading edge.
y	Normal distance from upper surface of model.
α	Resistance - temperature coefficient for RTD.
α_a	Angle-of-attack of boundary-layer plate.
δ	Boundary-layer thickness.
δ^*	Boundary-layer displacement thickness.
η	Boundary-layer similarity variable, $\equiv y/\delta_r$
θ	Boundary-layer momentum thickness.
λ_{ac}	Wavelength of acoustic wave $\equiv f/c$
λ_{ts}	Wavelength of T-S disturbance.
λ_w	Wavelength of surface waviness.
μ	Dynamic viscosity.
ν	Kinematic viscosity.

ρ	Fluid density.
ϕ	Relative phase.
ϕ_{sc}	Relative phase of Stokes-layer to acoustic source.
ϕ_{ts}	Relative phase of T-S wave to acoustic source.

CHAPTER 1

INTRODUCTION

In order to increase aircraft performance and lower operating cost, scientists and aerodynamicists have been searching for ways to reduce aircraft drag. Drag on an aircraft consists of profile drag, drag-due-to-lift , and compressibility drag. Low-drag aircraft have been designed by taking advantage of the inherently low friction drag in laminar boundary layers. Therefore, increasing the extent of the laminar boundary layer by delaying transition provides a great opportunity to improve aircraft performance. However, the actual physics of transition from laminar to turbulent flow is a complex boundary-layer process, and must be understood in order to conceive techniques for predicting and delaying transition.

1.1 The Transition Process

The process of laminar to turbulent transition usually begins with the excitation of instabilities in the laminar boundary layer. Most engineering flows are considered to be unstable, if they are excited. The excitation phase is very important because it effects the overall transition process. The transition process goes through several stages as the flow moves downstream on a smooth flat plate. These stages are as follows (White, 1991):

1. Stable laminar flow
2. Formation of unstable two-dimensional Tollmien-Schlichting waves
3. Formation of three-dimensional waves and vortex formation
4. Vortex breakdown
5. Formation of turbulent spots
6. Fully-developed turbulent flow

Figure 1 shows the six stages of the transition process for flow over a flat plate. In step two, Tollmien-Schlichting (T-S) waves are formed and amplified due to instabilities in the flow. T-S waves are important phenomenon in the transition process; therefore, the present research has focused on understanding the effect of surface roughness on T-S waves. In addition, acoustic excitation has been used as an external disturbance which can couple with unstable T-S waves in the boundary layer.

Tollmien-Schlicting (T-S) instabilities are created in the stable region of the flow close to the leading edge and pass through the neutral stability point into the unstable region. These waves are two-dimensional planar traveling waves. T-S wave stability is frequency dependent (Ball, 1987) and waves are in the stable mode when the wave fronts are normal to the flow (Squire, 1933). The possible sources of T-S waves are free-stream vorticity, entropy disturbances, surface vibrations, and external sound waves. What is known as boundary-layer receptivity is the process by which the boundary layer

internalizes the environmental disturbances in the form of instability waves. Moreover, receptivity is the mechanism by which an external disturbance couples with the boundary layer to create an unstable T-S wave (Morkovin, 1969).

Until recently, transition research has focused on the linear and non-linear development of already existing instabilities within the boundary layer. In the last few years, there has been a rapid growth in the understanding of the receptivity of a laminar boundary layer to acoustic disturbances. Most of the research has been directed towards locating the regions of the boundary layer where sound waves excite T-S waves. The laminar boundary layer can be categorized into three regions, according to Goldstein and Hultgren (1989). They defined the domains in which various models can be used to perform perturbation analyses. The three regions are as follows:

Region 1. Navier-Stokes equations are used to model the flow, where non-linear relationships exist between perturbed velocities and flow velocities.

Region 2. Linearized equations can be used to model the flow, where perturbations are small relative to flow quantities.

Region 3. Parallel flow models can be used to model the flow, where the flow is parallel to the model, and flow quantities are changing slowly. Stable T-S waves are formed and started (Goldstein, 1983).

In transition research, it is very important to identify a method which can be used to predict transition location. Two approaches that are used to predict transition from laminar to turbulent flow are the exponential growth (e^N) and amplitude methods.

The most widely used transition prediction technique is the e^N method, which was developed by Smith and Gamberoni (1956) and developed further by Mack (1975) and Malik (1993). The e^N method states that boundary-layer transition occurs when the amplitude of the most unstable disturbance has grown by a factor of e^N relative to the amplitude at the lower branch of the neutral stability curve. Disturbance growth can be calculated, from linear stability theory, after the value of "N" is determined empirically from the experimentally determined transition location. A range of "N" between 9 and 11 corresponds to the general class of flows. The e^N method is still open to question, in spite of its success in predicting transition location. The e^N method incorporates calculations from the linear amplification stage, and does not take into account receptivity and non-linear instabilities. So, this method absorbs receptivity considerations and non-linear flow development into the constant "N" (Heinrich, Choudhari, and Kerschen (1988)). Neglect of the receptivity process is reflected in the different values of "N" for flows with greatly different disturbance environments. Knowledge of the receptivity process would provide the realistic estimates for primary instability amplitudes which are required for calculating the value for the constant "N".

Neglect of the non-linear stage in the e^N method is justified by the fact that the non-linear process leading to transition is a very rapid process; therefore, it occupies a negligible portion of the transition region compared to the linear stage. However, experimental (Saric, et al.,1990) research has shown that the non-linear stage may occur at different Reynolds numbers, depending on the initial amplitude and frequency spectrum of the disturbances inside the boundary layer.

In summary, an effective transition prediction method should consider both receptivity and the non-linear growth region. Such an approach would provide a link between the disturbance environment and unsteady motion in the boundary layer. Moreover, a method that combines receptivity and linear stability would include the influence of the unsteady motion in the boundary layer, and eliminate the uncertainty in the "N" factor associated with environmental disturbances. Thus, including receptivity effects in theoretical and experimental prediction methods is important in the process of transition prediction.

1.2 The Receptivity Phenomena

Receptivity, as defined by Kerschen (1989,1987), is the process by which external disturbances generate instability waves in the boundary-layer. The understanding of the physics behind the receptivity process is the accomplishment of Goldstein and his co-workers (1987). The receptivity phenomenon targets the generation and initiation of

instability waves in the boundary layer; however, classical linear stability theory targets the propagation and amplification of instabilities in boundary layer. To understand the overall picture of the transition process, the aerodynamicist must understand the receptivity problem, as well as the stability problem, which means that the generation and propagation of boundary layer instability waves have to be addressed. Classical stability theory has been studied for many years, and methods have been identified to control the propagation of instabilities, such as wall suction, heating or cooling, and favorable pressure gradients.

In recent years, there has been a great effort to understand the receptivity concept and its features. Fortunately, great progress has been made in predicting receptivity and understanding stability. A complete overview of the transition process, with an emphasis on receptivity, has been given by Goldstein (1987), Nishioka and Morkovin (1986), Kerschen (1989,1987), Heinrich (1988), Goldstein and Hultgren (1987), Choudhari and Streett (1990), Wiegel and Wlezien (1993), and Wlezien (1989,1990,1994).

Acoustic receptivity refers to the excitation of boundary-layer T-S instability waves by acoustic disturbances. Usually, the wavelengths of the acoustic disturbances are much longer than those of T-S waves (Choudhari, 1990); therefore, a wavelength conversion process is required to tune the signature of the external acoustic disturbance to the T-S wavelength in the boundary layer. Energy transfer from the acoustic

disturbance to the T-S instability waves occurs when the two wavelengths match. Goldstein showed that the spatial tuning required for the wavelength conversion process occurs when the acoustic disturbance is scattered by short-scale irregularities in the flow. Goldstein defines three cases of short-scale irregularities:

a) Sharp leading edge (Goldstien,1989; Wlezien, et al.,1990)

b) Adverse pressure gradients (Smith, 1956; Nishioka and Morkovin,1986)

c) Short-scale variations in surface, such as surface roughness (Aizin,1979; Saric, et al., 1990; Wiegel and Wlezien,1993)

Occurrence of receptivity requires an unsteady scattered field to have the wavelength of the T-S instability wave. Moreover, Goldstein 's work suggests that in subsonic regions, overall receptivity in the boundary layer is dominated by surface irregularities in the region near the lower branch of the neutral stability curve. Consistent with this finding, the present research focuses on the effect of acoustic disturbances and surface roughness on T-S waves.

Previous experiments have helped to provide further understanding of the receptivity mechanism. In the early work of Schubauer and Skramstad (1947), sound was identified as one of the factors that affected transition location. Their experiment was considered to be the first leading-edge receptivity experiment. They attached a sound

source to the top of the tunnel at the leading edge of the plate. It was demonstrated that a T-S disturbance could be induced by choosing the appropriate frequency for a given flow speed. In a subsequent experiment, Spangler and Wells (1968) directed pure sound into the inlet of the wind tunnel. They noticed that the degree to which the transition location was shifted was determined by the frequency of the sound. The first published results from an investigation of the effect of a surface inhomogeneity coupled with acoustic excitation was performed by Aizin and Polyakov (1979). Strong effects on receptivity were observed. In 1984, Ruban showed analytically, by using an asymptotic method, that a small surface roughness on a plate could excite T-S waves. The sound waves interacted with local surface roughness to excite the T-S waves.

In recent works by Wlezien (1989) and Wlezien and Parekh (1990), acoustic receptivity phenomena associated with two different geometries (the leading edge and a suction slot) were investigated. It was difficult to distinguish between different receptivity mechanisms; thus, it is important to remove any receptivity mechanism which is extraneous to an experiment. Leehey and Shapiro (1980) showed that T-S waves can be generated at a low-aspect ratio leading edge of 6:1. This result was consistent with the analytical result obtained by Goldstein and Hultgren (1987) in which leading-edge receptivity was addressed. Recent experiments performed by Saric, et al. (1980) and Wiegel and Wlezien (1993), and recent theory developed by Crouch (1990) and Choudhari (1990) have addressed the effect of wall roughness on the receptivity process

and considered either localized irregularities or non-localized surface irregularities. These irregularities usually create steady short-wavelength disturbances that interact with the external unsteady acoustic disturbance to produce a traveling wave field. The traveling wave has the frequency of the acoustic wave and the wave number of the surface irregularities. Receptivity occurs when the frequency and wave number of the generated traveling wave match the T-S wave. Localized receptivity generated by a wall roughness has been analyzed using asymptotic analysis by Crouch and Bertolotti (1992). Non-localized receptivity generated by surface irregularities over an extended streamwise distance has been analyzed by non-linear mode-interaction theory, which is based on the Orr-Sommerfeld equation (Crouch,1991). Crouch's results have shown that in general, non-localized receptivity is an order-of-magnitude stronger than localized receptivity because non-localized receptivity occurs over an extended streamwise range, which results in T-S wave streamwise growth rate. In the present experiment, non-localized receptivity was studied and analyzed in terms of the mode shape of the T-S waves.

Choudhari (1994) and Crouch (1992) analyzed non-localized receptivity due to acoustic forcing. Both predicted that receptivity would be produced only at a narrow band of wall wavelengths near the instability wavelength of the acoustic forcing frequency. An experiment by Wiegel and Wlezien (1993) showed that strong receptivity occurred over a narrow band where the waviness of the surface irregularities and the T-S wavelength were matched.

Crouch (1991) developed an analytical model for acoustic receptivity of a boundary layer for a collection of modes resulting from surface irregularities. He studied the complex process in which freestream disturbances with long wavelengths initiate short-wave disturbances in a boundary layer. Crouch attempted to determine if non-linear receptivity existed with multiple forced modes. By using an analytical model, he predicted that nonlocalized receptivity over rough surfaces with multiple forced modes would act to energize the T-S mode. He determined that the calculation of the T-S mode amplitude and phase must account for the contributions from all relevant forced modes, which would allow the calculation of the total disturbance of the T-S mode as the sum of the forced modes. Crouch showed that the total amplitude of the T-S waves has a larger-than-linear growth over a region extending well downstream of branch I of the stability curve.

1.3 Present Research

In the present experiment, receptivity as a function of wall roughness has been investigated under the influence of external forced acoustic disturbances. The present research is related to the work of Saric (1990) and Wiegel and Wlezien (1993). The primary purpose of the present research was to determine if non-linear receptivity due to wall roughness exists and to make measurements to be used to validate theoretical and

numerical results. Moreover, secondary objectives were to investigate the effect of a range of wall roughness heights and locations on T-S wave amplitude.

There were several tasks that had to be accomplished. One task was to obtain a zero-pressure-gradient boundary layer ($\nabla p = 0$). A second task was to develop a technique for obtaining a plane traveling acoustic wave. A third task was to develop a periodic wall-roughness surface condition. A fourth task was to identify a method for separating the signal due to T-S waves from the total fluctuating hot-wire signal. Finally, a fifth task was to evaluate the effect of roughness height on the stability of the laminar boundary layer.

CHAPTER 2

EXPERIMENTAL SET-UP

2.1 Experimental Equipment

2.1.1 Wind Tunnel

The experiment was conducted in the 2 ft x 3 ft (0.6m x 0.9m) Low-Speed Wind Tunnel in the Flow Modeling and Control Branch of NASA Langley Research Center. Figures 2 and 3 are schematics of the plan and side views of the closed-loop wind tunnel. The tunnel fan is powered by a 150 (maximum) horsepower motor, delivering a maximum velocity of 43 m/s tunnel test section. The tunnel has four sets of turning vanes and several sets of honeycomb and screens to straighten the airflow in the test section. The tunnel has been modified to improve the quality of the airflow in the test section by the installation of a newly designed fan fairing to the fan housing, by the removal of several of the 1/2-in copper tubes originally used as heat exchangers, and by design and installation of a new adjustable test-section ceiling.

2.1.2 Test Model

The test model consisted of a flat plate made of aluminum jig plate, a leading edge, and a variable-angle flap. The flap was attached to the aft end of the model in order to adjust the stagnation line by varying the flap angle. The test model was 2.74m

long, 0.91m wide, and 0.0127m thick. The elliptical leading edge had an aspect ratio of 24:1. This aspect ratio was chosen for the leading edge because it was found by Wlezien (1990) that leading-edge receptivity is minimized with a leading-edge aspect ratio of 24:1. The test model had to be very smooth to minimize surface roughness effects on receptivity. To accomplish this, the test model was buffed with a fine-grade material and polished with jewelry polish. The test model was supported by four screw jacks. Two of the screw jacks were located downstream of the leading edge and the other two were upstream of the flap hinge connection (see Figure 4). For the present tests, the angle-of-attack of the test model was set at 0.0107° using the screw jacks.

2.1.3 Traverse System

In the wind tunnel test section, a newly designed traverse system (Smith, 1995) was installed in the test section to position the probe. The traverse system was mounted in the top of the test section by aluminum brackets. The system was placed at the center of the test-section ceiling through a slot (0.02m wide and 2.44m long). This slot was covered with fine black brushes, manufactured by Power Brushes,Iinc., to minimize the air flowing from the test-section (see Figure 5). The traverse system was two-dimensional. The streamwise (x) range of the traverse system was from 0.0 to 2.1m and the vertical (y) range was from 0.0 to 0.1524m. The accuracy of the traverse system was $\pm$ 160 μm/m in the streamwise range and $\pm$ 33 μm/m in the vertical range. The traverse

system was controlled by a SUN SPARC workstation computer using a Unidex 12 traverse control unit.

2.1.4 Acoustic System

Acoustic disturbances were used to excite the T-S waves in the boundary layer. These disturbances were created by four acoustic sources installed in the wind tunnel. Four speakers were placed upstream of the fourth set of turning vanes and honeycomb section in a square arrangement to provide a plane sound wave in the test section. The fifth speaker was located after the first set of turning vans and honeycomb section downstream of the test section. Each 8-ohm speaker consisted of 203 mm diameter polypropylene woofers, which provided a frequency response of 40-3000 hz. The speakers were driven by a Hewlett Packard Universal Source that generated sine waves at varying frequency. This signal was fed to an amplifier and then to the speakers. Each speaker was placed inside an airtight wooden box to normalize the pressure between the inside and outside of the wind tunnel. Moreover, a 6.35 mm hole was drilled through the tunnel wall into the wooden box to equalize the pressure across the diaphragm of the speakers.

2.2 Instrumentation and Data Acquisition

2.2.1 Pitot-Static Probes

Two standard pitot-static probes were used to measure the differential pressure (total - static). The differential pressure was measured in mm Hg with an electronic manometer whose ports were connected through tubing to the probe orifices. The velocity in the test section was calculated from this pressure differential measurement. One probe used to determine freestream velocity was placed near the front of the test model. The other pressure probe used to calibrate the hot-wire probe was located above the test model next to the resistance temperature detector (see Figure 6). The inherent error associated with a pitot-static probe is usually about 0.01 % of the pressure reading (Rae & Pope, 1984). To minimize system errors, each manometer was zeroed before taking any measurements.

2.2.2 Resistance Temperature Detector

The freestream temperature was measured using a resistance temperature detector (RTD). The RTD consisted of a sensing element, a sheath, lead wire, and connection. The sensing element is made of 99.99% pure platinum wound about a ceramic core and sealed in a ceramic capsule. Platinum wire is chosen because it is mechanically and electrically stable and the sensing elements conform to a standard curve with $\alpha = 0.000385$ ohms/ohm/°C. The RTD sheath is a closed end tube that provides protection to the

sensing element. The RTD operates on the principle of change in electrical resistance in the wire as a function of temperature. The resistance of the circuit was dependent on the temperature in the freestream. The RTD has a temperature range from -50 to 600°C. The error inherent in such an instrument, according to the manufacture (Omega), is about 0.02% of the total temperature.

2.2.3 Hot-Wire Anemometer

A constant-temperature hot-wire anemometer was used to measure the streamwise component of the instantaneous velocity in the test section. The hot-wire probe consisted of a fine tungsten wire with a diameter of 5μm and a length of 1.25mm.

The electrical circuit for the constant-temperature anemometer kept the wire temperature constant through adjustment of the current. When the flow passed through the probe, the hot-wire cooled down by convection cooling and the resistance of hot-wire changed causing an unbalance of the electric circuit. The current was adjusted to keep the temperature constant. A TSI, Incorporated, Intelligent Flow Analyzer 100 was used in operating the hot-wire anemometer system with an overheat ratio of 1.8.

2.2.4 Data Acquisition System

The 2'x 3' Low Speed Wind Tunnel was equipped with a Hewlett Packard Data Acquisition and Control System. This system was used to process data from the

experimental instruments. The system had 8 slots which served 6 multiplexers plus other devices. A multiplexer is an electronic device that switches each channel for a short finite period of time from analog to digital (Rae & Pole, 1984). Each multiplexer had 20 channels and each channel had an electrical input from an experimental instrument such as a pitot-static probe, RTD and etc. The control system was connected to the Sun workstation by a GPIB(General Purpose Interface Bus)- IEEE interface.

2.2.5 Spectrum Analyzer

A Spectrum Analyzer manufactured by Hewlett Packard was used to acquire data from the hot-wire anemometer. The analyzer displayed the amplitude and the relative phase of the hot-wire signal. The analyzer consisted of two channels. One was connected to a signal generator which provided a sinusoidal wave with maximum amplitude of 0.5v and a variable frequency. The other channel was connected to the hot-wire anemometer. The signal from the hot-wire probe was passed through a filter that eliminated undesired frequencies in the signal.

2.2.6 Computer System

A SPARC SUN workstation was used to gather data from the experimental devices via GPIB-IEEE cable. The software for experimental data acquisition was developed by J. Smith. She used the LabView graphics-based programming language.

CHAPTER 3

EXPERIMENTAL TECHNIQUES

3.1 Hot-Wire Calibration

During the experiment, calibration of the hot-wire probe was required several times. Freestream temperature and voltage as a function of freestream velocity were required for each calibration of the hot-wire probe. Because the wind tunnel is a closed-loop type, the temperature normally drifts until it reaches equilibrium inside the tunnel. Therefore, the wind tunnel was warmed-up prior to taking any measurements in order to minimize temperature drift. The warm-up time for the tunnel was found to be about five minutes. The output voltage was corrected for ambient temperature drift in the tunnel. The correction was accomplished using the following equation (Wiegel,1992):

$$e_c = e\left[1 - \frac{\alpha}{OHR-1}\,(T - T_0)\right]^{-0.5}$$

where:

e_c	=	corrected voltage
e	=	output voltage
OHR	=	overheat ratio
T	=	air temperature (°C)
T_0	=	average temperature (°C)
α	=	temperature coefficient of resistance (1/°C)

Calibration was accomplished by positioning the hot-wire at the same streamwise and vertical coordinates as the aft pitot-static probe. The flow velocity measured by the aft pitot-static probe at these coordinates was considered the reference calibration velocity. A fourth-order polynomial was fit to the acquired calibration data to obtain the applicable coefficients. The form of the polynomial relationship between velocity and voltage is:

$$U = a_0 + a_1 e + a_2 e^2 + a_3 e^3 + a_4 e^4$$

Where: $U \equiv$ freestream velocity

$e \equiv$ voltage

$a_0, a_1, a_2, a_3, a_4 \equiv$ polynomial coefficients

Several methods were utilized to minimize the error in calibrating the hot-wire probe: 1) using a wide range of velocities (0.0-20.0 m/s), 2) providing adequate time averaging (3 seconds) when taking measurements, 3) applying a fourth-order polynomial to calibration data, 4) repeating the calibration process if the standard deviation from the measured calibration curve was more than 2.5%, and 5) allowing the tunnel to warm up before taking measurements (to reduce temperature drift).

3.2 Chordwise Pressure Gradient

Pressure gradients influence the initial linear instability and the breakdown of the laminar boundary layer. The neutral stability curve is strongly influenced by pressure gradient, as described by White (1979) (see Figure 7). Therefore, it was important to

have zero freestream pressure gradient in the tunnel test section in order to minimize the effect of pressure gradient on receptivity and to be able to compare results to the Blasius boundary-layer solution.

Three steps were taken to obtain zero pressure gradient in the freestream direction in the test section. The first step was to adjust the stagnation point on the test model, which was done by deflecting the variable-angle flap (see Figure 6). The flap was deflected in incremental angles and an oil/fluorescent dye mixture was used to visualize the flow by applying it on and around the leading edge on both the top and bottom surfaces. By focusing a black light on the leading edge, separation bubbles and stagnation lines were noted at each flap angle. Results showed that a flap deflection angle of 1.80 degrees ensured that the stagnation line was on the upper surface and there was no separation bubble on the lower surface. The second step was to define the streamwise static pressure and then adjust the plate to attain $dp/dx = 0$. Measurement of the pressure gradient was accomplished by using a pitot-static probe mounted on the traverse mechanism. The angle-of-attack of the plate was adjusted by using four screw jacks located under the plate, until approximately zero streamwise pressure gradient was achieved. Typical results are presented in terms of pressure coefficient as a function of position in Figure 8.

The next step was to obtain boundary-layer velocity profiles every 200 mm in the x-direction from 400mm to 1800mm from the leading edge of the plate. For each case,

values of the displacement thickness, momentum thickness, and shape factor were calculated. After several velocity profiles were measured, the pressure gradient was evaluated by plotting shape factor as a function of position in the streamwise direction. The final velocity profiles were compared to the Blasius profile to confirm the existence of a zero-pressure-gradient laminar boundary layer.

3.3 Transition Reynolds Number

Transition Reynolds number (Re_{tr}) is defined as the Reynolds number at which transition from laminar to turbulent flow occurs. Transition Reynolds Number is considered to be a measure of the flow quality in a wind tunnel. If the wind tunnel has a transition Reynolds Number on the order of 1.5 million or greater, there is an extensive region of laminar flow present (Rae & Pope,1984).

In the present experiment, transition Reynolds Number was measured using a hot-wire probe. Measurements with the hot-wire probe were made at two different streamwise locations (1800mm and 1950mm from the leading edge) for each run, and at the vertical location where $u/U_\infty = 0.2$ at a freestream velocity of 12.5 m/s. Next, freestream velocity was incrementally increased and three parameters were measured u/U_∞, U_∞, and temperature. In the laminar regime, u/U_∞ increases slowly with increasing freestream velocity (maximum U_∞ =43m/s). However when transition occurs in the flow, a noticeable increase occurs in the value of u/U_∞. A value for transition Reynolds

number was determined to be 4.6 million for the present experiment, which established the wind tunnel as having excellent flow quality.

3.4 Acoustic Field Characterization

It was important to characterize the test-section acoustic environment and identify what kind of waves existed in the test section. Reference data for the acoustic wave components were obtained in the freestream outside the boundary layer. Freestream acoustic measurements were alternately obtained using the upstream speakers and the downstream speaker. A sinusoidal voltage with an amplitude of 0.5 volts was supplied to the speakers via an amplifier at a frequency of 80 Hz. Acoustic waves were emitted by the upstream speakers at forcing frequencies of 72, 80, 86, and 90 hz. Downstream measurements were made with a hot-wire probe at each frequency. Data were obtained at 64 streamwise locations in increments of 34 mm so as to cover a distance of 2.1 meters (equal to half a wavelength at a forcing frequency of 80 hertz). These streamwise measurements were used to determine the type of waves present in the test section. In addition, acoustic measurements were made in the vertical direction at three streamwise positions. For acoustic measurements, the signal from the hot-wire anemometer was passed at a gain of 100 through a filter with a bandwidth of 10 to 100 Hz. At each frequency, the amplitude of the signal and the relative phase between the measured signal and supply signal were recorded.

Because this experiment was conducted in a closed-loop wind tunnel with acoustically reflective surfaces, the acoustic wave was always a combination of traveling waves and a standing-wave (see Figure 9). It was important to have a plane traveling wave in lieu of standing waves or a combination of two different waves. For a traveling wave, the amplitude is constant while the phase varies linearly. For a standing wave, the amplitude has a sinusoidal shape and the phase oscillates between +90° and -90°(Wiegel and Wlezien,1992). In this experiment, the method developed by Wiegel (1992) was used to decompose the acoustic wave and its reflection. Figures 20 and 21 show the results of applying this decomposition method.

3.5 Mode-Shape Measurements

The primary purpose of this experiment was to acquire data for the unstable T-S mode shape under different conditions. Velocity profiles were defined by taking hot-wire measurements at sixty-four data points in the y-direction. For each velocity profile, the displacement thickness, momentum thickness, and the shape factor were calculated. In addition, acoustic phase and amplitude were obtained outside the boundary layer by taking four data points in the y-direction in increments of 15 mm starting at 120 mm above the test plate. These data were required to decompose the fluctuating component of the total signal into T-S and acoustic wave components.

To determine the T-S mode-shapes, it was required that of the Stokes wave be removed from the total fluctuating velocity (u'_t). The theoretical Stokes-layer profile is

an exact solution for a plate oscillating in its own plane. This is similar to the case of a fixed plate in an oscillating fluid. Characterization of the Stokes-layer profile is presented by Panton (1984), and also discussed by Wiegel (1992) in the following form:

$$A_{ac} = u'_{ac,\infty}\{ (1 - e^{-ys} \cos ys) + i(e^{-ys} \sin ys)\} = u'_{ac} e^{i\phi_{ac}}$$

where:

A_{ac} ≡ Complex value of amplitude and phase of acoustic wave

$u'_{ac,\infty}$ ≡ Fluctuating freestream acoustic velocity

u'_{ac} ≡ Fluctuating acoustic velocity

ν ≡ Kinetic viscosity

f ≡ Acoustic frequency

y ≡ Normal distance above the plate

$$s = \sqrt{\frac{\pi f}{\nu}}$$

and

$$\phi_{ac} = \tan^{-1}\left[\frac{e^{-ys} \sin ys}{1 - e^{-ys}\cos ys}\right] = acoustic\ wave\ phase$$

The theoretical Stokes-layer profile equations presented above were evaluated numerically and the results are shown in Figures 10a and 10b. The T-S, acoustic, and total measured signal components are related vectorially (Wlezien,1990). Figure 11

shows a schematic representation of the decomposition of the total signal. Since u'_{ac}, u'_t, ϕ_{ac}, and ϕ_t are known from acquired data, the T-S amplitude and phase can be obtained by:

$$Amplitude: u'_{ts} = \{u'^2_t + u'^2_{ac} - 2u'_t\, u'_{ac}\, cos(\phi_t - \phi_{ac})\}^{1/2}$$

$$Phase: \phi_{ts} = \phi_t - cos^{-1}\left[\frac{u'^2_{ts} + u'^2_t - u'^2_{ac}}{2u'_{ts}\, u'_t}\right]$$

where additional variables include:

$u'_{ts} \equiv$ T-S fluctuating velocity amplitude

$u'_t \equiv$ Total fluctuating velocity amplitude

$\phi_{ts} \equiv$ T-S wave phase angle

$\phi_t \equiv$ Total phase angle

Typical experimental and theoretical mode shapes are shown in Figure 12a (Wiegel, 1993). Figure 12b shows the resulting of mode shapes measured with a hot-wire at x=1350 mm and Re=1830 for thirteen strips of wall roughness for the present experiment (configuration #2).

CHAPTER 4

CHARACTERIZATION OF TEST-SECTION FLOW

Characterization of the flow over the test plate was accomplished by measuring the boundary-layer velocity profiles, flow quality, acoustic field, and Tollmien-Schlichting wave parameters.

4.1 Boundary-Layer Velocity Profiles

In this experiment, it was required to precisely locate the effective leading-edge of the boundary layer. The physical leading edge of the test model was not the effective leading edge of the experimental model due to non-zero pressure gradients and test-section physical geometry. In order to precisely locate the effective leading edge of the model, which is called the virtual leading edge, several boundary-layer velocity profiles were measured using a hot-wire anemometer. The experimental data and the following equation from White (1991) were used to obtain the virtual leading edge for the present experimental conditions.

$$\delta^* = 1.7208 \frac{\sqrt{(x_v)\nu}}{\sqrt{U_\infty}}$$

where:

δ^* ≡ displacement thickness

U_∞ ≡ freestream velocity

x_v ≡ virtual leading edge

ν ≡ kinematic viscosity= $1.49 \times 10^{-5} \pm 0.21 \times 10^{-5}$ (T/20-1) in (m^2/s)

T = ambient temperature in °C

Measurements of boundary-layer velocity profiles were taken every 200 mm along the plate between 400 mm to 2000 mm at U_∞ = 12.5 m/s. For all profiles, δ^*, Θ, and shape factors were computed (see Table 1 and Figures 13-15).

TABLE 1

Mean Flow Measurements to Determine the Virtual Leading Edge

x(mm)	δ^*	U_∞(m/s)	x_v(mm)	x-x_v(mm)
400	1.16	12.50	371	30
600	1.41	12.55	551	49
800	1.60	12.58	711	89
1000	1.81	12.52	905	95
1200	1.98	12.49	1081	119
1400	2.21	12.52	1350	50
1600	2.36	12.53	1540	59
1800	2.44	12.55	1649	150

The x-xv data were curve-fit using the least-squares technique to obtain a new reference location which was 80.0 mm downstream of the physical leading edge. Figures 16 and 17 show the relationship of the Blasius boundary layer to the experimental results.

4.2 Flow Quality

An important parameter in this experiment is Re_{tr}, the transition Reynolds number. The flow quality of the wind tunnel is related to Re_{tr}. The value of Re_{tr} is about 1.5×10^6 for a tunnel with good flow quality (Rae & Pope,1984). In this experiment, Re_{tr} is 4.6×10^6; therefore, the tunnel exhibited exceptionally good flow quality and was considered acoustically quiet (see Figure 18).

Moreover, flow contamination interference due to the tunnel sidewalls was measured using flow visualization. The model was sprayed with naphthalene from the leading edge to the trailing edge, then the tunnel was run to 12.5 m/s and the region of sidewall contamination was easily distinguished. Flow interference was confined to a 11.4 wedge at both sidewalls (see Figure 19).

4.3 Acoustic-Field

It was noted that in a closed-loop wind tunnel, the acoustic field inside the test section is a combination of downstream and upstream traveling wave components. The process of characterizing the acoustic field included activating the upstream speakers at

various frequencies from 72 to 90 Hz and then independently activating the downstream speaker.

For all experimental measurements, the reconstruction data, that was obtained by combining superposing the decomposed upstream traveling wave, which should have reproduced the same acoustic amplitude and phase, did not match the original data well, except at higher frequencies (see Figure 20). It was noted that with an at 80-hz signal from the upstream speakers, the amplitude was fairly constant and the phase was linear in the streamwise direction. Therefore, it was concluded that a plane traveling wave existed at 80 hz, along with a weak standing wave. Figure 21 shows both amplitude and phase for the 80 hz. signal. The frequency of 80 hz was found to be the most suitable for the experiment (using the upstream speakers only).

Measurements of wave amplitude and phase variations normal to the test plate were acquired for three different streamwise (x) locations. All three profiles showed fairly constant amplitude and phase variations in the y-direction, which indicated that an acoustic field of plane waves existed in the tunnel test section above the plate.

It is very important to address the issue of ambient background noise when conducting receptivity experiments, because the response to acoustic excitation is of small amplitude. In this experiment, freestream hot-wire measurements were made at x =

1345 mm with and without an 80 hz. acoustic signal. For the case without acoustic input, the measurements are of the ambient acoustic signal due to a combination of the turbulent boundary layer in the tunnel, freestream turbulence, and the tunnel fan. For the case with acoustic input, the measurements included the effect on the laminar boundary layer through the receptivity mechanism (see Figure 22). Preliminary boundary-layer measurements indicated a response of T-S waves to acoustic excitation.

It is desirable in the region of interest to have the T-S wave scales vary linearly with the level of acoustic excitation. To verify linearity, T-S mode shapes were acquired at three different level of acoustic excitation. The ratio between two runs of maximum amplitude of the T-S wave ($u'_{ts,max}$) is 1.73, and the ratio between two runs of ($u'_{ac,e}$) is 1.70 for Runs 1 and 2. See Table 2 for a summary of the results for Runs 1 and 3. These results verify the linearity.

Table 2. T-S and Acoustic Amplitudes for Linearity Verification Test

Run	T-S Wave $u'_{ts,max}$ (m/s)	Acoustic Force $u'_{ac,\infty}$ (m/s)	Sound Pressure (dB)
I	0.0457	0.0018	-46
II	0.0791	0.0030	-50
III	0.1315	0.0045	-48
Ratio I of 2 Runs	1.73	1.70	4.0
Ratio III of 2 Runs	1.63	1.58	2.0

The mode shape of the T-S waves due to the effect of surface-roughness receptivity was extracted by removing the Stokes-layer receptivity effects. For example, measurements for varying surface-roughness configurations were taken at x = 1345 mm and at U_∞ = 12.5 m/s. Figures 33a and 33b show the results for one configuration. The normalized mode shape is presented to enable comparison to an appropriate theoretical stability analysis. The phase variation of the T-S waves is plotted as a function of normalized y-position in Figure 33b.

4.4 Tollmien-Schlichting Wave Characteristics

In this experiment, it was important to determine the growth of T-S waves in the streamwise direction. This task has been accomplished by making several mode-shape measurements in the streamwise direction from x = 1105 mm to x = 1345 mm in

increments of 30 mm. Moreover, measurements were made at x = 1545, 1745, and 1945 mm to determine further changes in the T-S wave amplitude. For this test, the surface roughness was configured as follows: eleven tape strips of 1" wide x 2.3 mil thickness and between them were four strips of 1/8 " wide x 5 mil thickness all located at the lower branch. The freestream velocity for all cases was 12.5 m/s. Figure 42 shows the normalized streamwise T-S wave growth, with external forcing for all cases.

CHAPTER 5

EXPERIMENTAL RESULTS

5.1 Surface Waviness Configurations

In the present experiment, geometric simulation of a sinusoidal wavy wall was necessary to provide wall wavelengths on the order of the wavelength of the T-S waves, in order for the receptivity phenomenon to occur. However, this ideal geometry is not possible to construct, so a more realistic approach had to be devised. Acoustic waves which matched the T-S waves in frequency and wavelength could provide a mechanism for energy transfer to the boundary layer; however, the mismatch in wavelengths would prevent this transfer from occurring. Since the acoustic wavelength is much longer than the T-S wavelength, a reduction in length scale was required to facilitate the aforesaid energy transfer. This was accomplished through using various surface roughness configurations (rectangular tape strips) to serve as scattering sites for the acoustic waves. The scattered acoustic field contained acoustic waves at wavelengths and frequencies on the order of the T-S waves, thus providing a mechanism for energy transfer from the acoustic field to the T-S waves. As a consequence of linear receptivity, the amplitude of the resulting T-S wave was expected to be linearly related to the height of the distributed surface roughness and the acoustic wave amplitude.

Mathematically, the addition of two sine waves (linear interaction) with wave numbers K_2 and K_4 separated by an amount of $2K_1$ with $K_1 << K_2 < K_4$ will result in the same aggregate wave as the product of two sine waves (non-linear interaction) with wave numbers K_1 and $K_3=(K_2+K_4)/2$ (see Figures 24,25). Consequently, the sine wave with wave number K_1 (long wavelength on the order of the T-S waves) can be considered the results of the non-linear interaction of the wave modes at K_2 and K_4; therefore, accommodating a transfer of energy at the wave number K_1 (to the T-S waves) through the non-linear receptivity phenomenon. The wave number spectrum associated with the present wall-roughness configurations is similar to that for a purely sinusoidal wall (e.g. at wave number K_1) for wall-roughness configurations 1, 2, and 3 (spectrum also includes higher harmonics due to sharp edges). Then, these configurations are expected to have an effect on T-S waves through the phenomenon of linear receptivity. In addition, the wave number spectrum associated with wall-roughness configurations 5, 6, and 7 resembles the spectrum previously described as composed of dual modes K_2 and K_4. Then, these latter configurations are expected to affect the T-S waves through the non-linear receptivity phenomenon. Schematics of the seven surface roughness configurations tested in the present experiment are presented in Figure 23.

Tape height and thickness variations effect boundary-layer receptivity and were concerns when choosing the thickness of each configuration. Saric, Hoos, and

Radeztsky (1991) have stated that departure from linear behavior occurs when the reattachment length exceeds the roughness height. This could result in the formation of a free shear layer that has its own instability, which may effect the receptivity process. In addition, they observed that the critical roughness-height Reynolds number is approximately $Re_h \approx 150$. Thus, Re_h defines a hydraulically smooth surface. In the present research, Re_h was varied, but remained below the critical value for all seven cases (see Table 3).

Table 3. Reynolds Number Based on Roughness Height for All Roughness Configurations

Configuration	Description	Tape Size	Re_h
1	11 type-1 tape strips	1" W x 1.5×10^{-3} thk.	31
2	11 type-2 tape strips	1" wide x 2.5×10^{-3}" thk.	52
3	11 type-3 tape strips	1" wide x 4.6×10^{-3}" thk.	95
4	40 type-4 tape strips	⅛" wide x 5.0×10^{-3}" thk.	103
5	11 type-5 tape strips & 40 type-4 tape strips	1" wide x 2.3×10^{-3}" thk. ⅛" wide x 5.0×10^{-3}" thk.	103
6	11 type-6 tape strips & 40 type-4 tape strips	1" wide x 3.8×10^{-3}" thk. ⅛" wide x 5.0×10^{-3}" thk.	103
7	11 type-7 tape strips & 40 type-4 tape strips	1" wide x 4.6×10^{-3}" thk. ⅛" wide x 5.0×10^{-3}" thk.	103

5.2 Surface Wave-Number Spectra

It was desirable to study the wave number spectra of all seven roughness configurations with respect to the thickness of the tape strips and consequently, the effect on linear and non-linear receptivity. For configurations 1, 2, and 3, a power spectrum

analysis using discrete Fourier spectra was accomplished and the results are shown in Figures 26, 27, and 28. The case in Figure 26 simulates the addition of sine waves that produces one large peak at low wave number and several small peaks at multiples of the first wave number, due to harmonics in the signal resulting from the fact that the wall was not a pure sine wave wall (rectangular tape strips). As tape thickness increased (see configurations 2 and 3), the peak amplitude increased at the same wave number that provided input to the linear receptivity phenomena.

The power spectra for configurations 5, 6, and 7 are shown in Figures 30, 31, and 32. Figure 30 illustrates the case that is considered to correspond to purely weak non-linear receptivity effects, because the height of the wider tape (longer wavelength) was almost half of the thinner tape (shorter wavelength). Therefore, the linear receptivity effect for this configuration was attenuated and non-linear receptivity effects dominated. With increases to the thickness of the longer wavelength tape, the linear receptivity effect increased linearly. The results of these cases are shown in Figures 30 and 31. Notice that in these configurations, the non-linear portion of the power spectra was distorted due to the increase of harmonics in the signal (caused by the rectangular tape corners).

For configuration 4 which included only short wavelength tapes, the power spectrum analysis showed that both linear and non-linear receptivity effects existed and

there were phase shifts in the non-linear portion. At this time, the power spectrum results for this case are difficult to reconcile with the other results (see Figure 32).

5.3 Tollmien-Schlichting Mode Shapes

Mode-shape profiles were acquired at a constant streamwise position of x = 1345 mm from the leading edge for nine different freestream velocities ranging from 10.5 m/s to 14.5 m/s. Measurements for different configurations were taken at the same y-position. Phase and amplitude of the acoustic field was calculated outside the boundary layer because these data were needed to decompose the total fluctuating signal into a T-S wave component and an acoustic-field wave component.

Figures 33 to 39 show the mode shape of the T-S waves due to wavy-wall receptivity for the different configurations of wall roughness strips. From these figures, it can be concluded that the ratio between the T-S wave amplitude and the acoustic wave amplitude increases with an increase in roughness height. Mode shapes shown in Figures 33a to 39a match well for values below the zero crossing. All phase variations of decomposed T-S waves show the expected 180° phase shift at a value of $y/\delta^* \approx 2.0$, which is the exact position of the zero crossing of the mode shape.

5.4 Detuning of Tollmien-Schlichting Waves

There are two parameters that can affect the wavelength of T-S waves; one is freestream velocity and the other is acoustic frequency. In the experiments by Wlezien (1989) and Parekh, el al.(1990), the freestream acoustic frequency was varied and the effect on T-S wavelength was determined. In this experiment, the freestream velocity was the parameter which was varied because with an acoustic forcing frequency of 80 hz, a minimal standing wave component existed in the test section. Therefore, it was important to conduct the experiments at a single acoustic frequency, which left the freestream velocity as the parameter to vary. The resulting change in T-S wavelength was used to investigate the effect of mismatching the excited T-S wavelength and the wavelength associated with surface roughness configurations, which is called the detuning effect.

Crouch (1992) and Choudhari (1990) made theoretical predictions covering a detuning range of $\sigma = \pm 10\%$. Therefore, freestream velocity was varied from U_∞ = 10.5 m/s to 14.5 m/s to investigate the detuning effect upon changing the freestream velocity. The position of the lower branch of the stability curve changes about two surface-roughness wavelengths downstream and upstream of the first surface roughness tape strip over the detuning range (Crouch,1992). There is only a narrow region around the lower branch that is sensitive to surface roughness, as shown from previous research (Wiegel,1992). Therefore, in the present experiment, two wavelengths of surface

roughness were simulated by extending roughness strips far upstream and downstream of the lower branch.

Detuning effects are displayed in Figures 40 and 41 for all seven configurations. These figures display the ratio between the maximum amplitude of the T-S wave and the freestream acoustic wave amplitude, as a function of freestream velocity. The T-S detuning results for these configurations indicate that $u'_{ts,max}/u'_{ac}$ decreases symmetrically with increasing and decreasing freestream velocity about a freestream velocity of 12.5 m/s. A strong detuning effect with little scatter of the data is observed, which is consistent with Wiegel's (1992) measurements. Figure 40 also shows the same strong detuning effects for the other surface roughness configurations. For each configuration, maximum tuning occurs around a freestream velocity of 12.5 m/s and resulting values of $u'_{ts,max}/u'_{ac}$ are shown in Table 4.

Table 4. $u'_{ts,max}/u'_{ac}$ for All Roughness Configurations

Configuration No.	Figure #	$u'_{ts,max}/u'_{ac}$
1	34	29.4
2	35	49.0
3	36	69.0
4	37	76
5	38	16.73
6	39	29.0
7	40	38.0

Figure 40 shows the T-S detuning effects for configurations 1, 2, and 3, which are based on the one-inch wide wall roughness element with varying tape thicknesses. Results show that an increase in the roughness thickness (wavy-wall height) results in a linear increase in the T-S wave amplitude.

Figure 41 shows the detuning effects for configurations 4, 5, 6, and 7, which are composed of combinations of tape widths of 1" and ⅛" with varying thicknesses. The results show that an increase in the roughness height increases the amplitude of the T-S waves linearly, but the magnitude of the T-S amplitude in these configurations is lower than for configurations 1, 2, 3, and 4.

5.5 Streamwise Tollmien-Schlichting Wave Growth

Mode shape measurements were obtained at different streamwise positions to determine the T-S wave growth in the streamwise direction. These measurements were obtained with hot-wire probe positions from x = 1105 mm to x = 1345 mm with a spacing of 30 mm in the x-direction. The freestream velocity was U_∞ = 12.5 m/s. Figure 42 shows the normalized streamwise T-S growth with external acoustic forcing as a function of the boundary-layer Reynolds number. These results match the findings of Wiegel and Wlezien (1992), which matched theoretical results obtained from Choudhari (1990). The matching of these results confirms the presence of a zero-pressure gradient

in the streamwise direction, since the growth of the T-S wave amplitude is affected by the streamwise pressure gradient.

5.6 Linear and Non-Linear Receptivity

Finally, for each configuration, results from the mode-shape analysis provided the T-S wave amplitude and the results from the power-spectrum analysis provided the wall roughness wave number. Figure 43 shows the fluctuating velocity component of the T-S wave as a function of the wave number for configurations 1 and 3. Figure 44 includes these results for configurations 4, 5, 6, and 7. For configurations 1 and 3, it is seen that there is a linear receptivity phenomenon present, which means that the amplitude of the T-S waves produced by the 2-D roughness elements increases linearly with roughness height. This agrees with the results that Wiegel (1992) and Saric (1991) obtained experimentally,and Crouch (1992) and Choudhari (1990) obtained theoretically. Results from configuration #2 were disregarded because the surface roughness element peeled from the edge of the test plate due to the poor adhesive property of the tape. Therefore, results from this case were misleading and not representative of the effect of surface roughness on receptivity.

Figure 45 shows the measurements of the fluctuating velocity component of the T-S waves at a fixed location near branch II of the stability curve for two conditions. One condition was the single configurations tapes with longer wavelengths, which shows the

existence of linear receptivity for these tests. If the line representing linear receptivity effects is extended, it will cross the origin; however, this case of zero linear receptivity can't be achieved in actuality. It is observed that an increase in tape thickness causes a linear increase in the T-S wave amplitudes. The second condition covers all the combined configurations (long wavelength and short wavelength), and indicates that there is a non-linear receptivity phenomenon present for configurations 5, 6 and 7. If the line for this condition is extended, it will not cross the origin, and this intersection with the ordinate is considered to be the case of purely non-linear receptivity (does not actually exist). The difference between these two lines is due to the non-linear receptivity effect and the slopes of the two lines are the same (linear receptivity effect).

Therefore, the present research has shown that both linear and non-linear receptivity effects exist for the present test conditions. This experiment is unique because it is the first to demonstrate the non-linear receptivity phenomena. More receptivity experiments are required to clarify and verify the results from this experiment.

CHAPTER 6

SUMMARY, CONCLUSIONS AND RECOMMENDATIONS

Summary and Conclusions

The principal experiments in this investigation have facilitated a study of the unsteady T-S mode shape under different conditions. A leading edge with a 24:1 ratio was used to reduce the leading-edge effect on receptivity. A scheme was used to subtract the acoustic signal from the total hot-wire fluctuating signal. This decomposition scheme has been documented in the literature and is limited to the case where there is a fairly large ratio between acoustic amplitude and T-S amplitude. Furthermore, great care was taken to eliminate any extraneous influences that would effect the validity of the experiment. Thus, the normalized amplitudes of the mode shape and detuning results are reliable.

In conducting acoustic receptivity experiments, one must consider the effect of all parameters when controlling variables and the mean flow must be thoroughly characterized. For these reasons, it was important to have the following:

a. A plane traveling wave which was obtained by placing four speakers upstream of the test plate which produced acoustic waves at a fixed frequency of 80 hz.

b. Zero pressure gradient, which was achieved by varying the ceiling shape and adjusting the flap angle. (Measurement of velocity profiles and determination of the boundary-layer shape factor showed that zero pressure gradient was achieved.)

c. Good flow quality, which was shown by attaining a high limit of the transition Reynolds number.

After taking the aforesaid issues under consideration, excitation of the T-S wave by freestream acoustic frequency was accomplished. The total fluctuating velocity component was decomposed into the T-S amplitude and the freestream acoustic amplitude. Documentation of the amplitude and phase of T-S waves for different configurations of surface roughness elements have resulted in observation of the non-linear receptivity phenomenon. Non-linear receptivity exists when we have different combinations of wall-roughness elements that have long and short wavelength, which produce non-linear phenomena in the fluctuating velocity component of the T-S waves. This experiment has shown that linear and non-linear receptivity effects exist under the present experimental conditions.

Increasing the wall roughness height resulted in a linear relationship between the amplitude of the T-S wave and the roughness height. The effect of detuning on the T-S wave was that all different configurations which have been tested "tune" at the same

velocity with different amplitude ratios, which was expected. This experiment indicated that there is a strong detuning effect. Theoretical predictions by Crouch (1990) and Choudhari (1992) show similar results. The strong effect of acoustic receptivity on the T-S wave amplitude shows the importance of receptivity on an accurate prediction of transition.

Recommendation

The present experiment provides a basis for studying the non-linear receptivity phenomenon. Further experiments addressing non-linear receptivity would help in understanding acoustic receptivity. In addition, it is important to investigate the effect on the T-S mode shape of different orientations of wall roughness. Studying three-dimensional wall roughnesses might provide interesting results that clarify additional physics beyond the acoustic receptivity phenomenon. These are some areas which can provide further research opportunities in acoustic receptivity and which might result in an increased ability to predict transition.

REFERENCES

Aizin, L. B. and Polyakov, M. F., "Acoustic Generation of T-S Waves Over Unevenness of Surfaces Immersed in Streams," Theor. Appl. Mech., 1979.

Ball, N.G., "Acoustic Excitation of Tollmien-Schlichting Waves in a Laminar Boundary-Layer," UTIAS Report No. 321, 1987.

Choudhari, M. and Streett, C., "Boundary-Layer Receptivity Phenomena in Three-Dimensional and High-Speed Boundary-Layers," Second International Aerospace Planes Conference, Orlando, FL, October 29-31, 1990.

Choudhari, M. and Streett, C., "Theoretical Prediction of Boundary-Layer Receptivity," 25th AIAA Fluid Dynamics Conference, Colorado Springs, CO, June 20-30, 1994.

Choudhari, M. and Kerschen, E.J., "Instability Wave Patterns Generated by Interaction of Sound Waves with Three-Dimensional Wall Suction or Roughness," Vol. 90-0119, 1990.

Crouch, J.D., "A Nonlinear Mode-Interaction Model for Boundary-Layer Receptivity," Bull. Am. Phys. Soc., Vol. 35, 1990, pp. 2262.

Crouch, J.D. and Bertolotti, F. P., "Non-Localized Receptivity of Boundary-Layers to Three-Dimensional Disturbances," 30th Aerospace Sciences Meeting & Exhibit, Reno, NV, January 6-9, 1992.

Crouch, J.D., "Non-Localized Receptivity of Boundary-Layers," J. Fluid Mech., Vol. 244, 1992, pp. 567-581.

Crouch, J.D., "Initiation of Boundary-Layer Disturbances by Non-linear Mode Interactions," ASME, N. Y. TED - Vo. 114, 1991, pp. 63-69.

Fedorov, A. V., "Excitation and Development of Unstable Disturbances in unstable Boundary-Layers," Ph.D. Dissertation, Moscow Institute of Physics and Technology, 1982.

Fedorov, A. V., and Zhiguler, V. N., "Boundary-Layer Receptivity to Acoustic Disturbances," J. Appl. Mech. Techn. Phys., Vol. 28, 1987, pp. 28-32.

Goldstein, M.E. and Hultgren, L.S., "A Note on the Generation of Tollmien-Schlichting Waves by Sudden Surface-Curvature Change," J. Fluid Mech., Vol. 181, 1987, pp. 519-525.

Goldstein, M.E. and Hultgren, L.S., "Boundary-Layer Receptivity to Long-Wave Freestream Disturbances," Ann. Rev. Fluid Mech., Vol. 21, 1989, pp. 137-166.

Heinrich, R. A., Choudhari, and M., Kerschen, E. J., "A Comparison of Boundary-Layer Receptivity Mechanisms," AIAA-88-3758.

Jordinson, R., "The Flat-Plate Boundary-Layer- Part I: Numerical Integration of the Orr-Sommerfeld Equation," J. Fluid Mech., Vol. 43, 1970, pp. 801-811.

Kerschen, E. J., "Boundary-Layer Receptivity," AIAA-89-1109, 1989.

Kerschen, E. J., "Boundary-Layer Receptivity and Laminar-Flow Airfoil Design," NASA Symposium on Natural Laminar Flow, 1987.

Leehey, P. and Shapiro, P. J., "Leading-Edge Effect in Laminar Boundary-Layer Excitation by Sound," IUTAM Symposium, Germany, 1980, pp. 321-331.

Mack, L. M., "Linear Stability Theory and the Problem of Supersonic Boundary-Layer Transition," AIAA Journal, Vol. 13, 1975, pp. 278-287.

Malik, M. R., "LST and PSE for Boundary-Layer Transition Prediction," Proc. 1st Bombardier International Workshop on Aircraft Icing/Boundary-Layer Stability and Transition, Montreal, Canada, 1993.

Morkovin, M. V., "Critical Evaluation of Transition from Laminar to Turbulent Shear Layer with Emphasis on Hypersonically Traveling Bodies," Air Force Flight Dynamics Lab., AFFDL-TR-68-149, Dayton, Ohio, 1969.

Nishioka, M. and Morkovin, M. V., "Boundary-Layer Receptivity to Unsteady Pressure Gradients: Experiments and Overview," J. Fluid Mech., Vol. 171, 1986, pp. 219-261.

Panton, R. L., Incompressible Flow, Wiley Interscience, New York, 1984.

Rae, W. H. and Pope, A., Low-Speed Wind Tunnel Testing, John Wiley and Sons, New York, 1984.

Reshotko, E., "Disturbance in a Laminar Boundary-Layer Due to Distributed Surface Roughness," Turbulence and Chaotic Phenomena in Fluids (Ed., T. Tatsumi), 1984, pp. 39-46.

Reshotko, E., "Stability and Transition of Boundary-Layers," Progress in Astro. and Aero., Vol. 112, 1988, pp. 278-311.

Sandborn, V. A., Resistance Temperature Transducer, Metrology Press, Colorado, 1972.

Saric, W. S., Hoos, J. A., and Kohamo, Y., "Boundary-Layer Receptivity: Part I. Freestream Sound and 2-D Roughness Strips," College of Engineering and Applied Sciences Report CEAS-CR-90191, Arizona State University, 1990.

Saric, W. S., Hoos, J. A., and Radeztsky, R. H., "Boundary-Layer Receptivity of Sound with Roughness," ASME Paper, Boundary Layer Stability and Transition to Turbulent, 1991.

Schubauer, A. B. and Skramstad, H. K., "Laminar Boundary-Layer Oscillations and Transition on a Flat Plate," Research Paper - RP 1772, Vol. 38, 1947.

Smith, A. M. and Gamberoni, N., "Transition Pressure Gradient and Stability Theory," Douglas Aircraft Co., Rep. ES 26-388, El Segundo, Calif., 1956.

Smith, J., "The Effect of Localized Heating on Boundary-Layers Stability and Receptivity," Master Thesis, George Washington University, 1995.

Squire, H. B., Proc. R. Soc., Ser. A, Vol. 142, 1933, pp. 621-828.

White, F. M., Viscous Fluid Flow, McGraw Hill, Inc., New York, 1979.

Wiegel, M., "Acoustic Receptivity of Laminar Boundary-Layers Over Wavy Walls," Master Thesis, Illinois Institute of Technology, 1992.

Wiegel, M. and Wlezien, R. W., "Acoustic Receptivity of Laminar Boundary-Layers Over Wavy Walls," Shear Flow Conference, Orlando, FL, July 6-9, 1993.

Wlezien, R. W., "Measurements of Boundary-Layer Receptivity at Suction Surfaces," AIAA No. 89-1006.

Wlezien, R. W., Parekh, D. E., and Island, T. C., "Measurement of Acoustic Receptivity at Leading Edges and Porous Strips," Appl. Mech. Rev., Vol. 43, No. 5, 1990.

Wlezien, R. W., "Measurement of Acoustic Receptivity," 25thAIAA Fluid Dynamics Conference, Colorado Springs, CO, June 20-23, 1994.

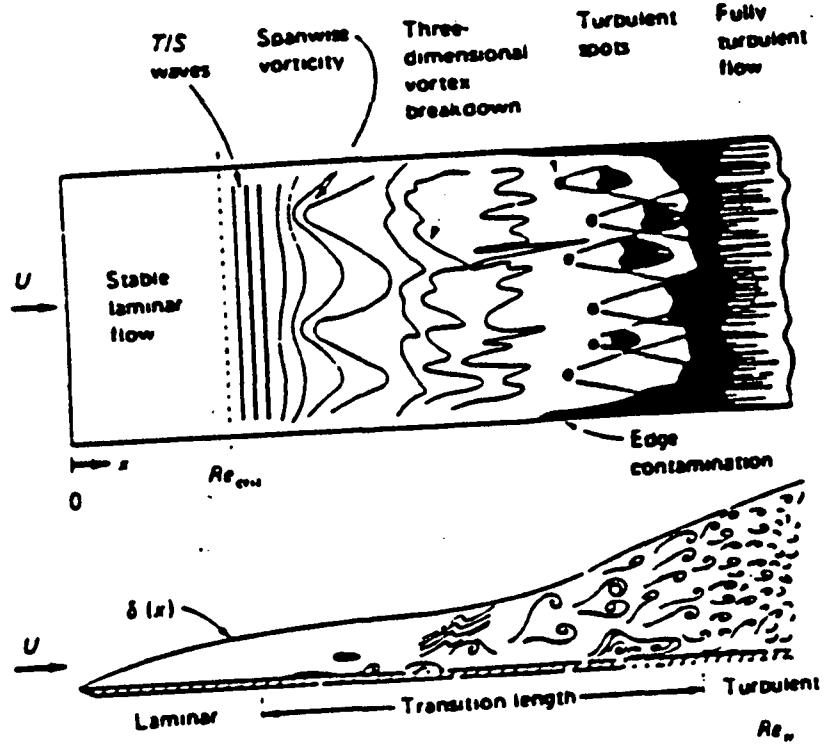

Figure 1. Description of the Boundary-Layer Transition Process

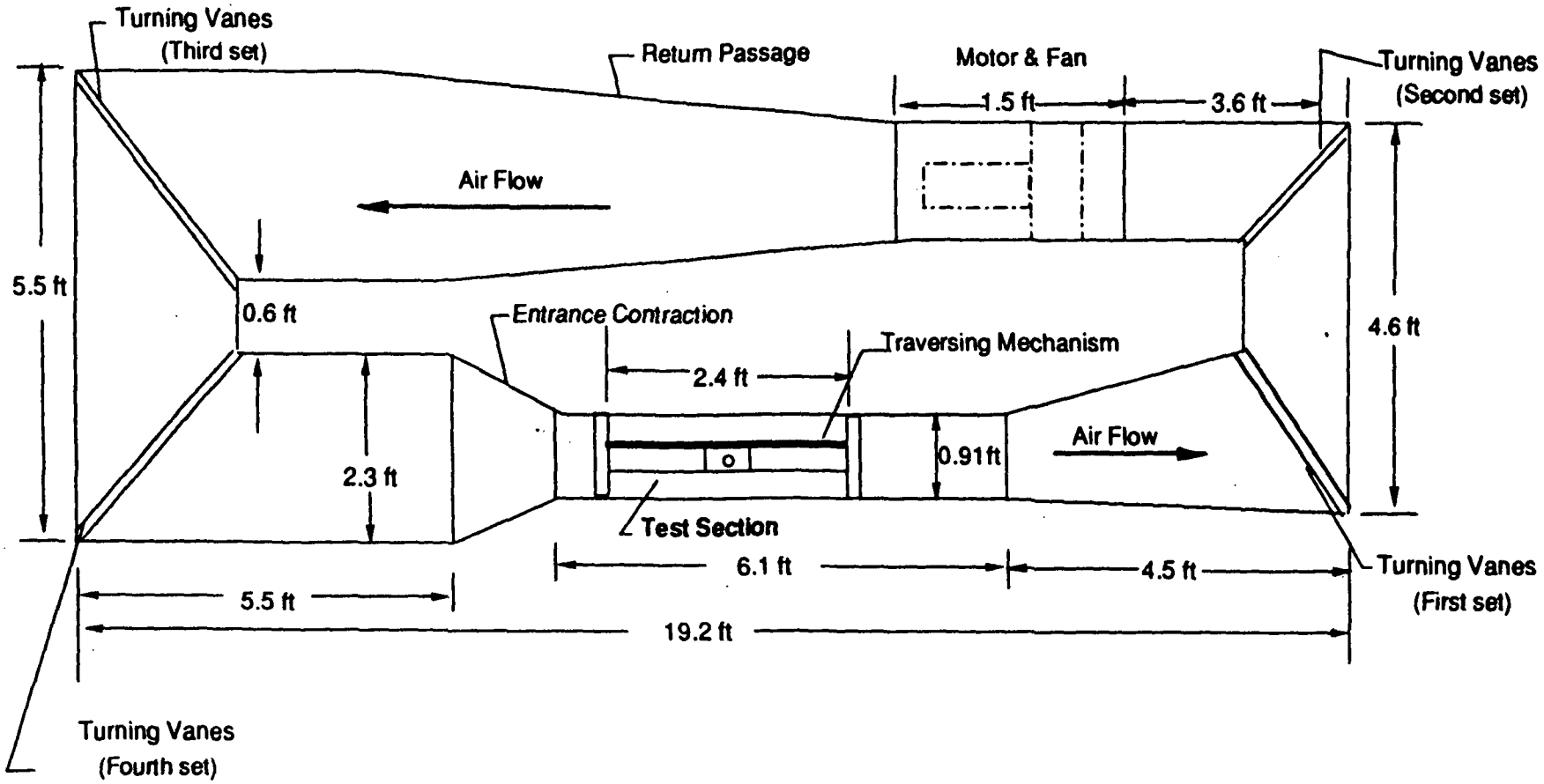

Figure 2. Schematic of Plan View of 2'X3' Laminar-Flow Boundary-Layer Wind Tunnel at NASA Langley Research Center

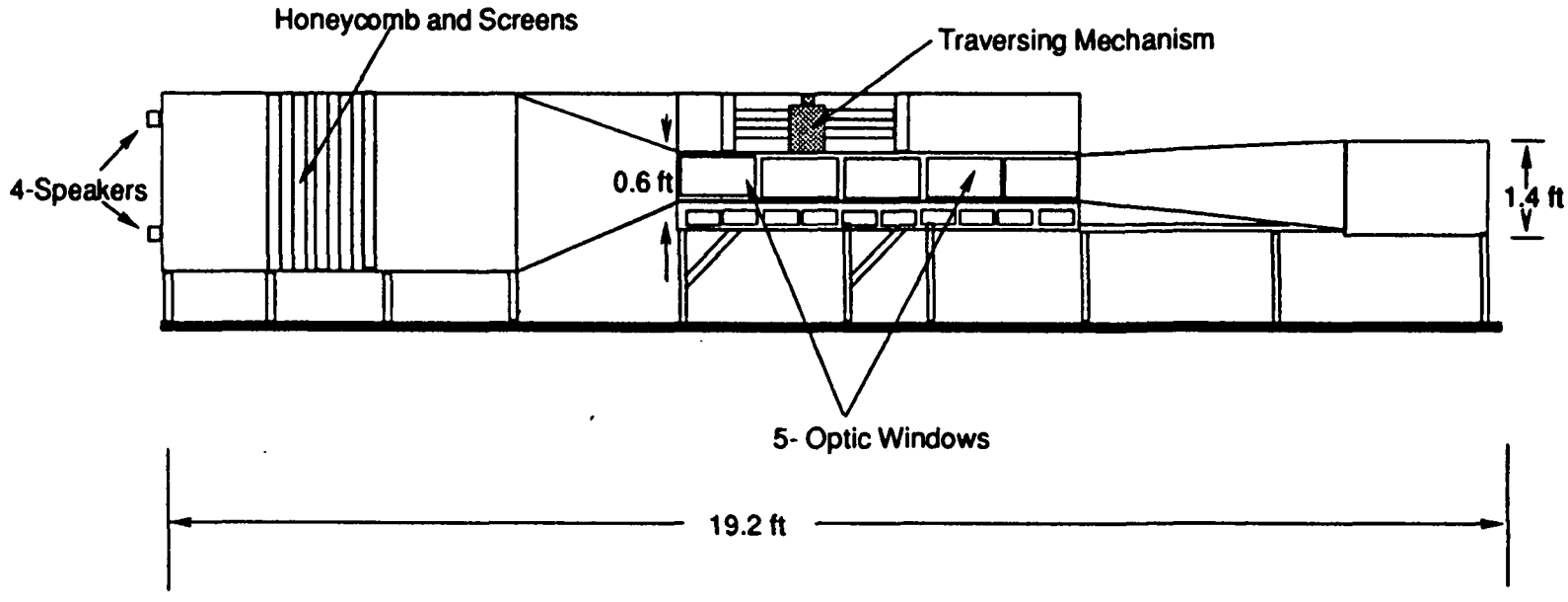

Figure 3. Schematic Side View of 2'x 3' Laminar Flow Boundary Layer Wind Tunnel at NASA Langley Research Center

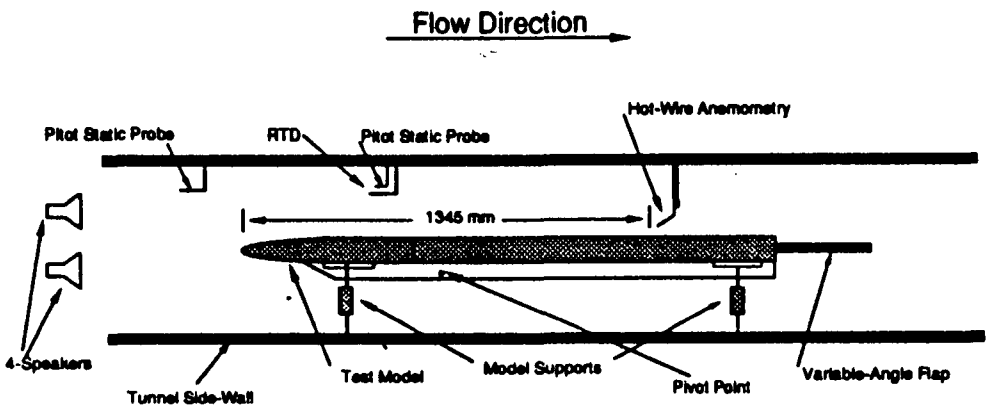

Figure 4. Schematic of Side View of Test Section with Test Model

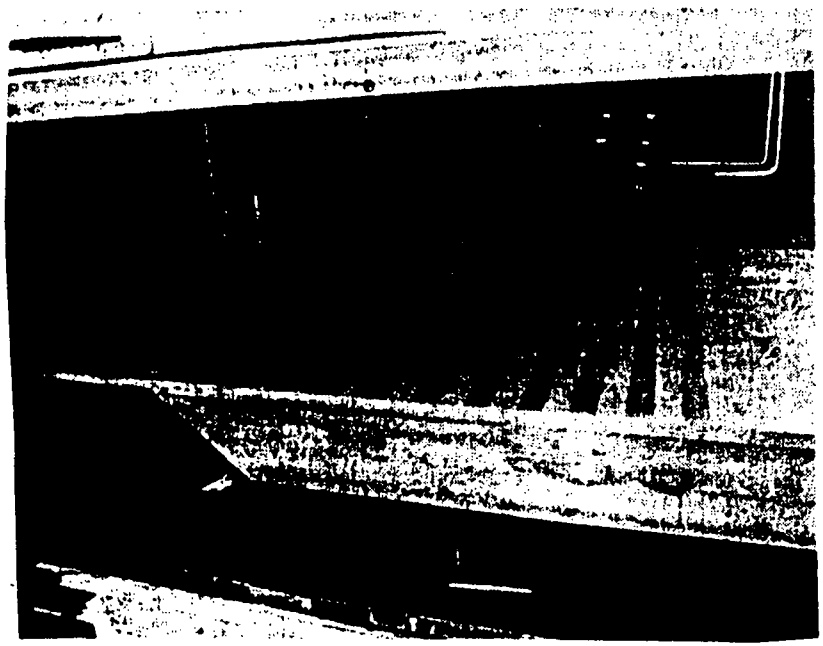

a)

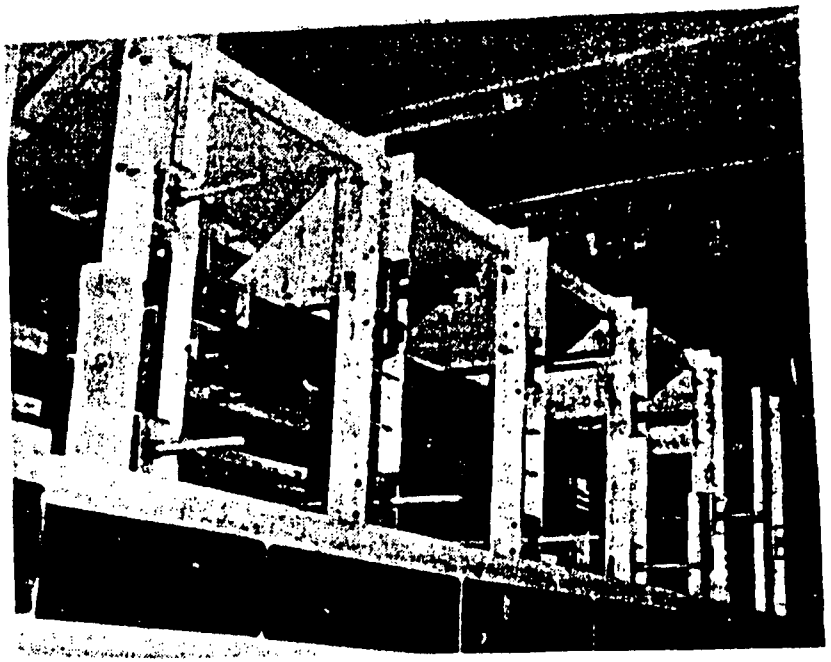

b)

Figure 5. Photographs of Test Facility

a) Test Model with Eleven Strips Attached

b) Top View of the Test Section

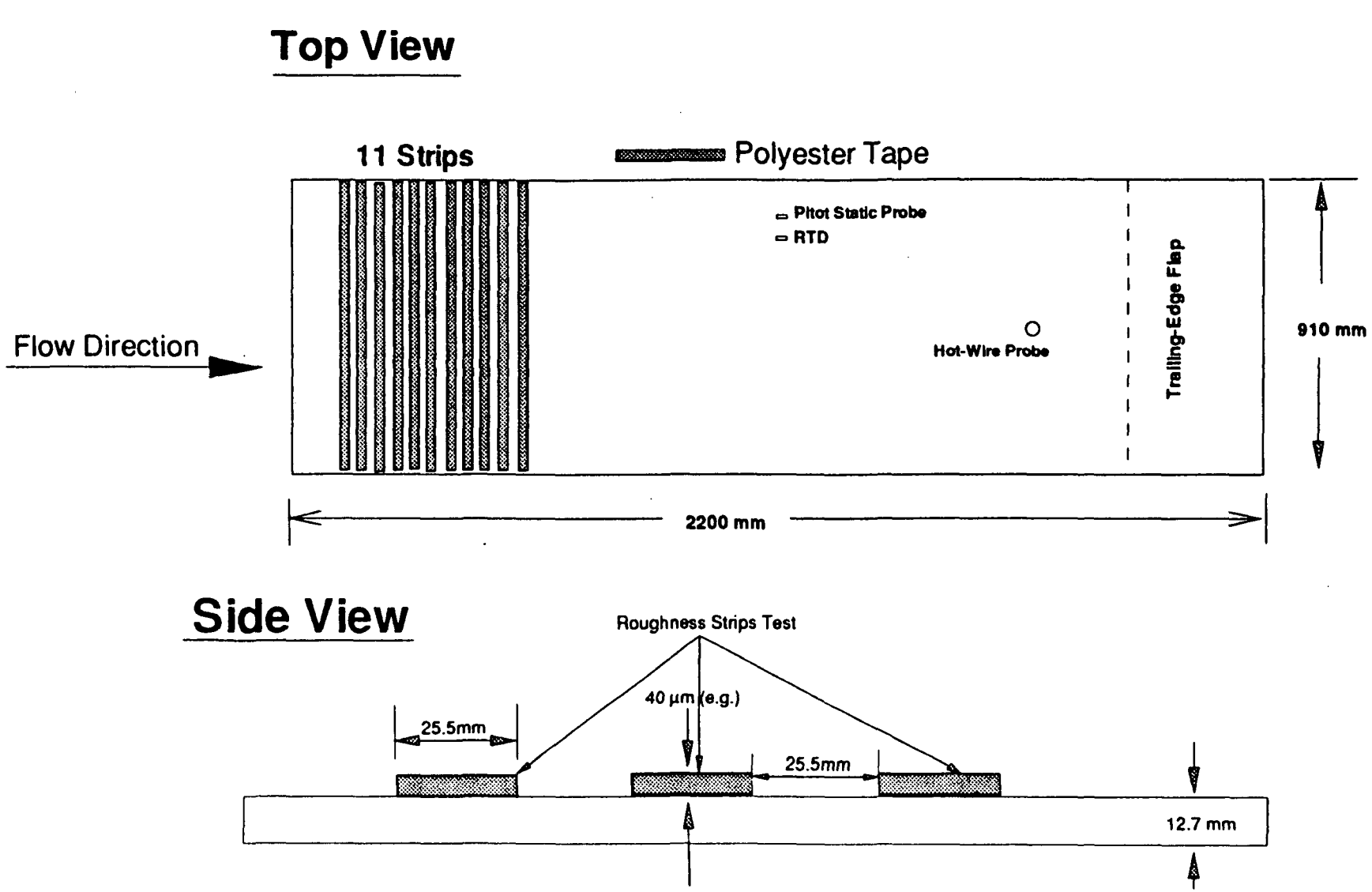

Figure 6. Schematic of Top and Side Views of Test Model

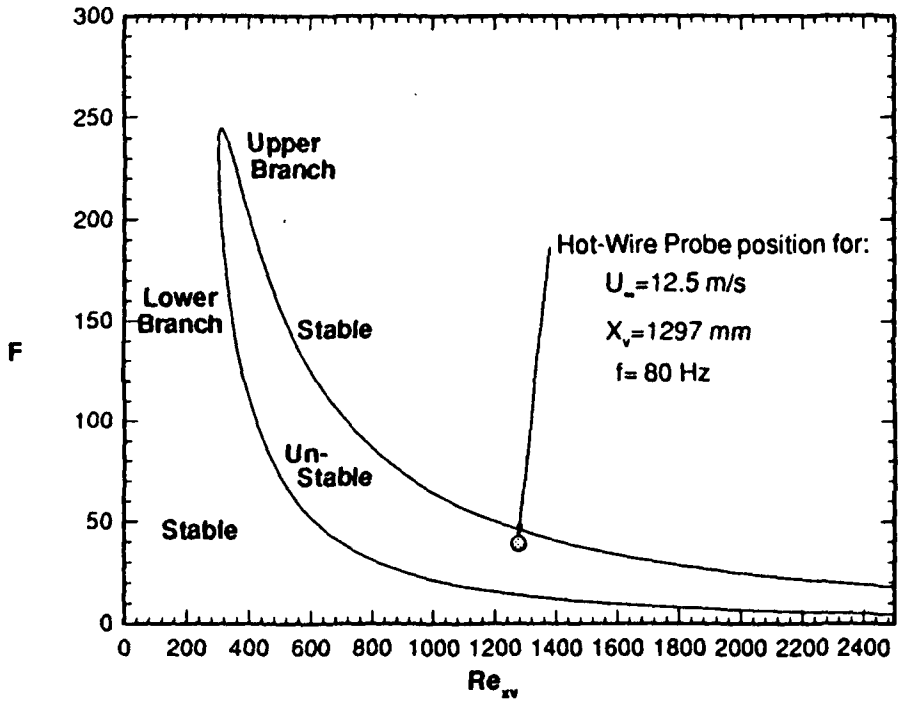

Figure 7. Neutral Stability Curve with Hot-Wire Sensor Position Shown at Experimental Condition

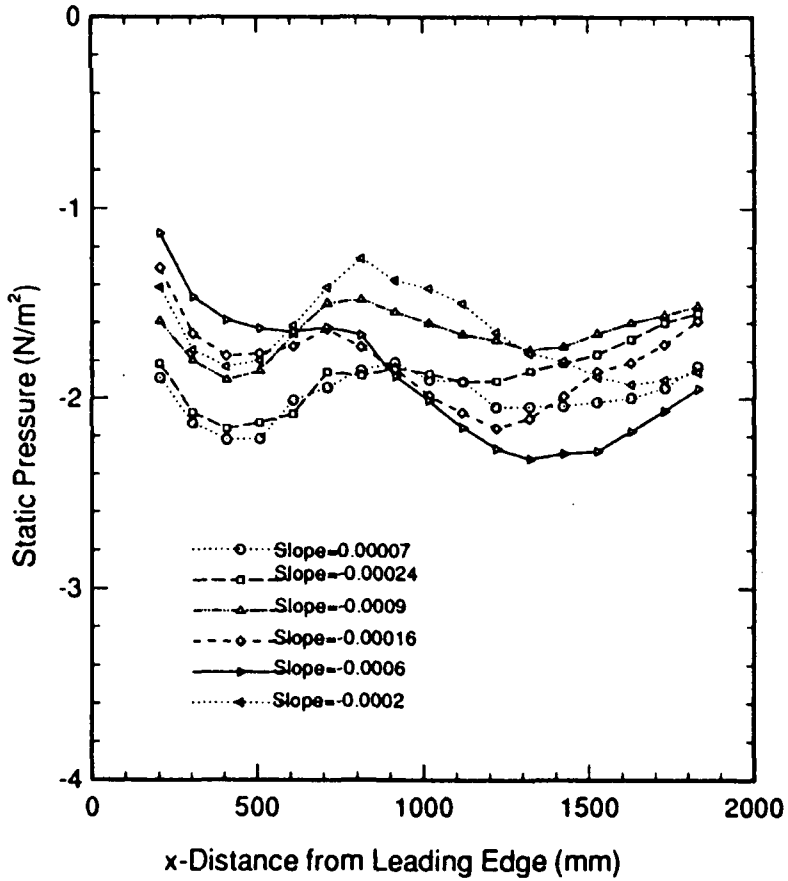

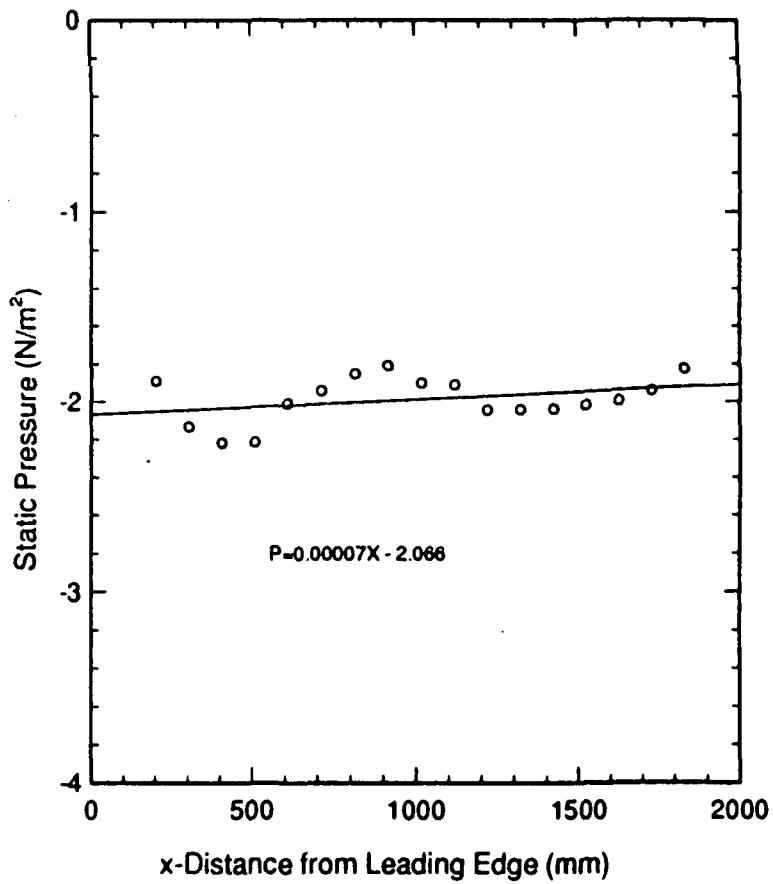

Figure 8. ChordWise Static Pressure Distribution

A. For Six Positions of Test-Section Ceiling

B. For Selected Position of Test-Section Ceiling for Present Experiment

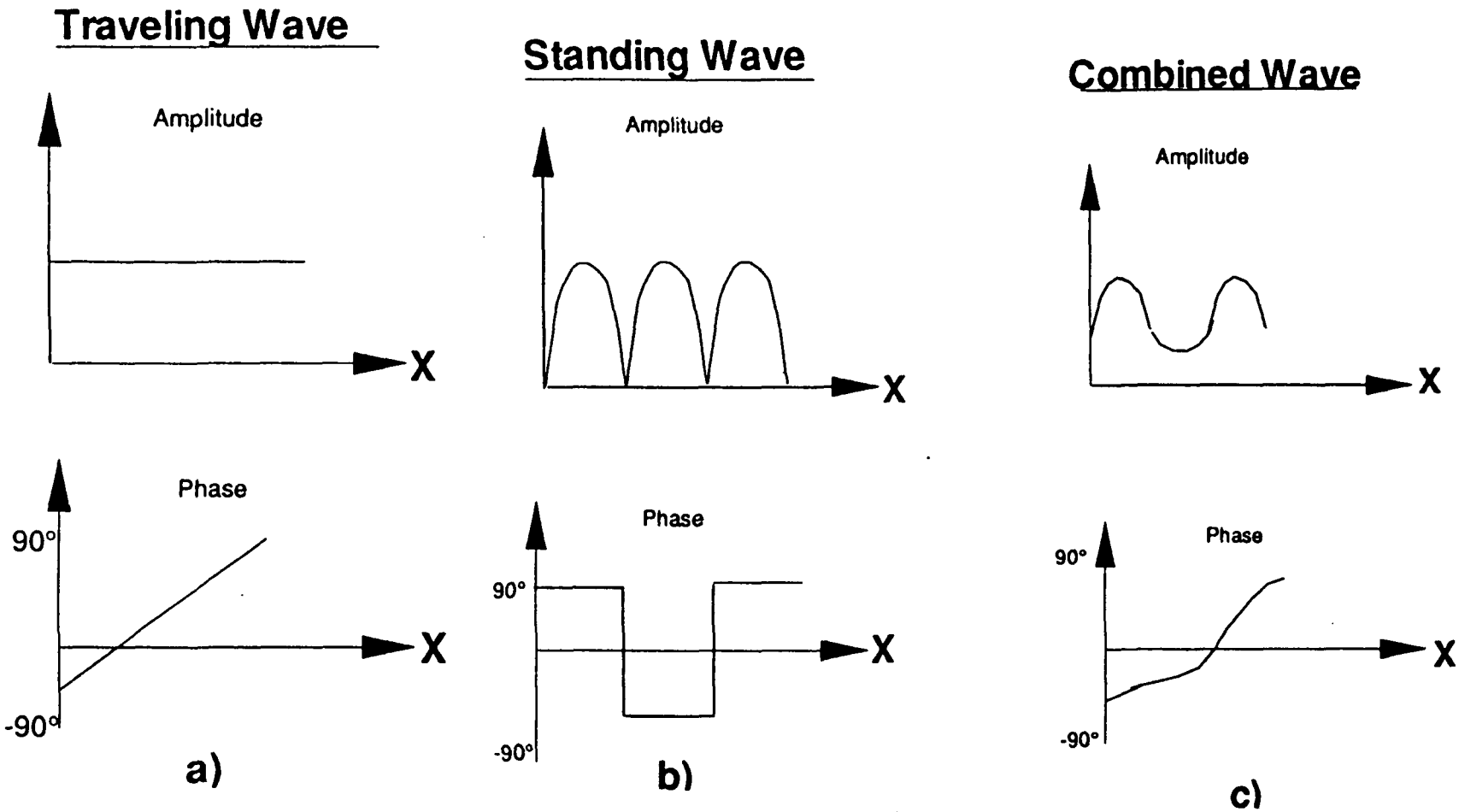

Figure 9. Variation of Amplitude and Phase of a Plane Acoustic Wave

a) Pure Traveling Wave

b) Pure Standing Wave

c) Combination of Traveling and Standing Waves

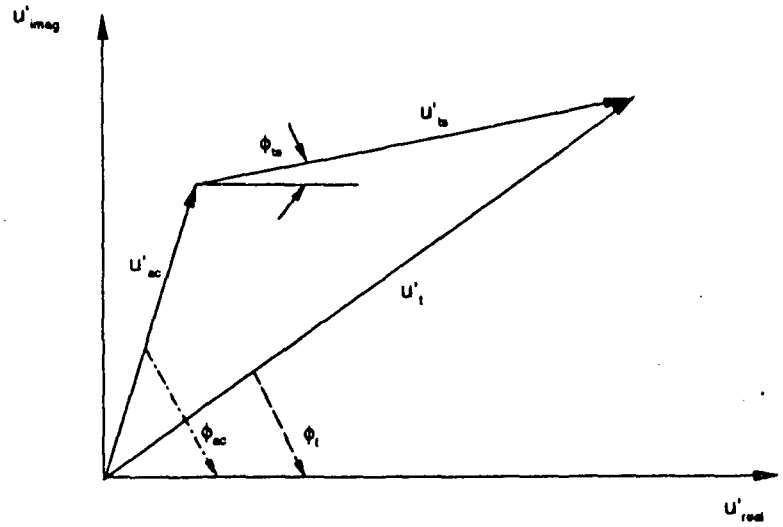

Figure 11. Schematic of Decomposition in the Complex Domain for T-S Wave and Stokes-Layer Wave

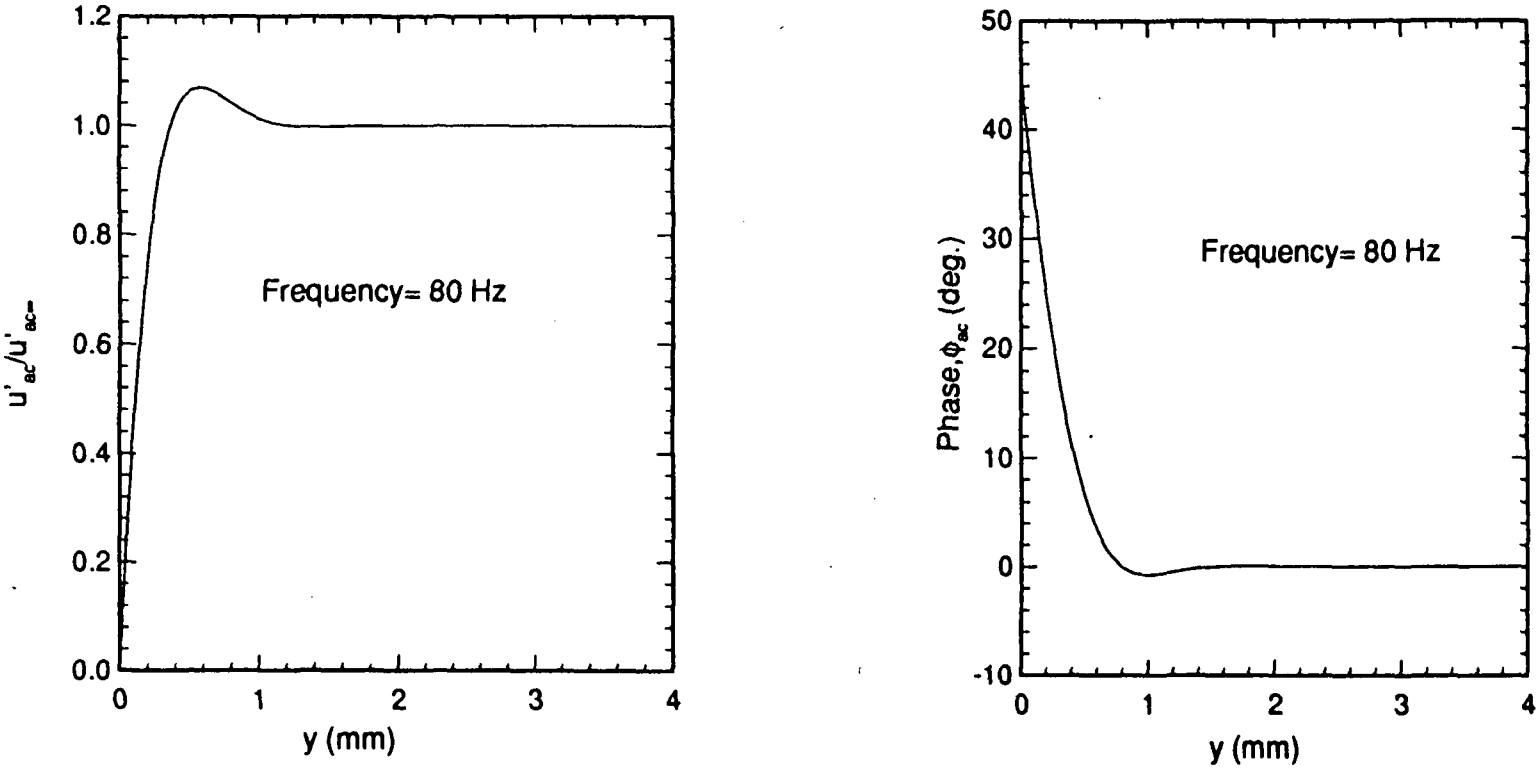

Figure 10. Variation of Stokes-Layer Waves Normal to the Test Model

a) Amplitude

b) Phase

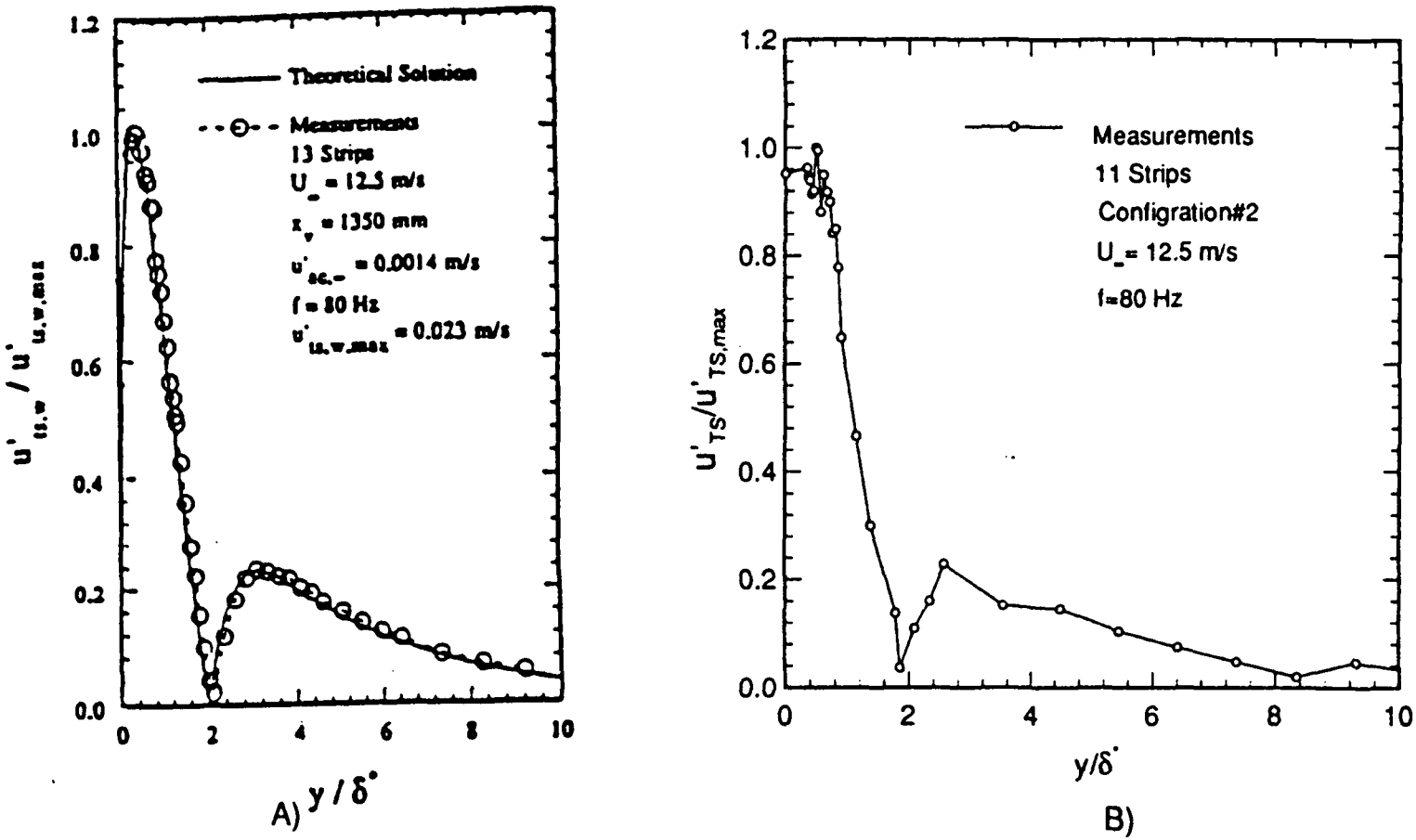

Figure 12. Mode Shape of T-S Wave due to Surface Roughness Receptivity

A)Typical Theoretical Data and Experimental Measurements of Mode Shape

B)Present Experimental Measurements of Mode Shape

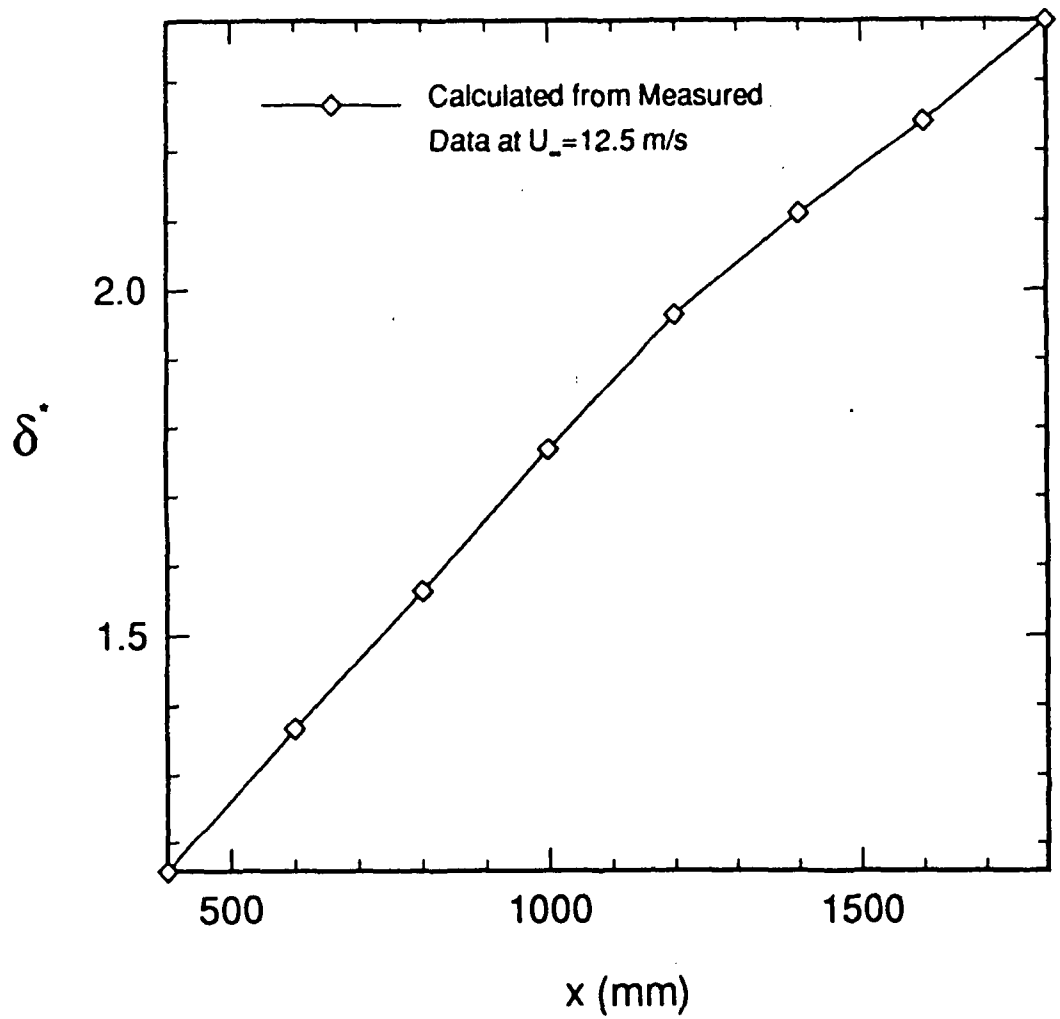

Figure 13. Boundary-Layer Displacement Thickness Vs. Streamwise Distance from the Leading Edge for Freestream Velocity of 12.5 m/s

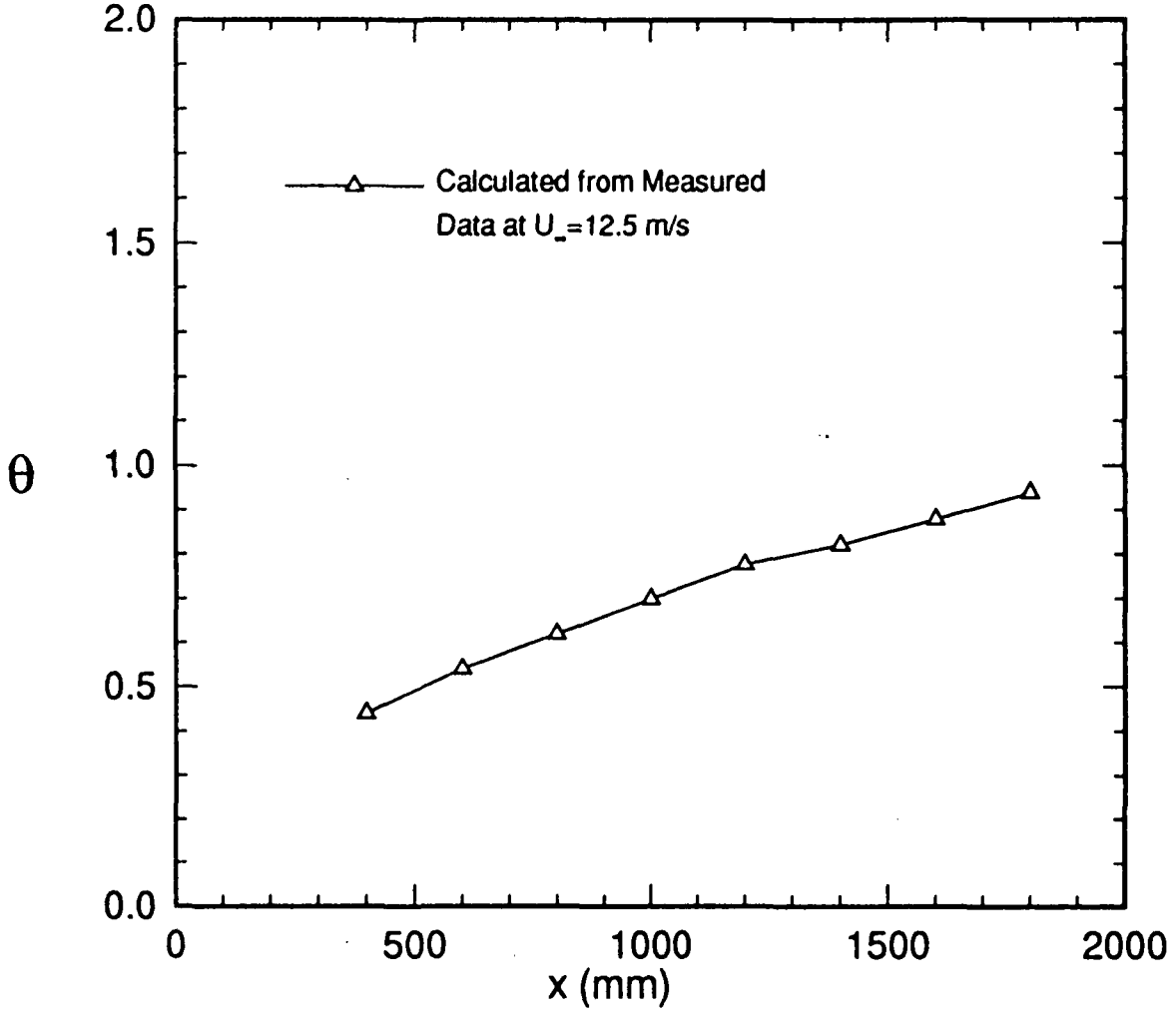

Figure 14. Boundary-Layer Momentum Thickness Vs. Streamwise Distance from the Leading Edge for Freestream Velocity of 12.5 m/s

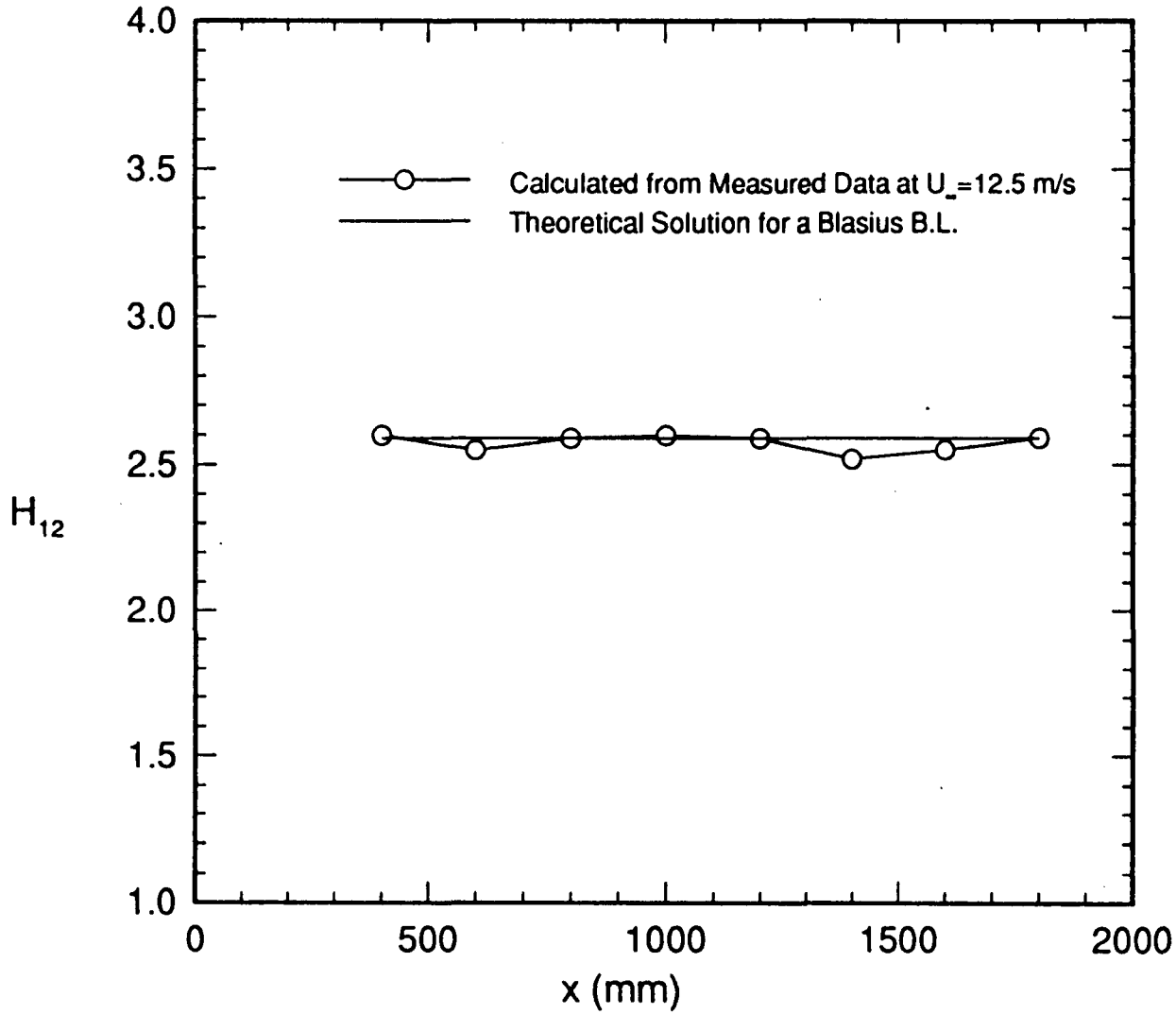

Figure 15. Boundary-Layer Shape Factor Vs. Streamwise Distance from the Leading Edge for Freestream Velocity of 12.5 m/s

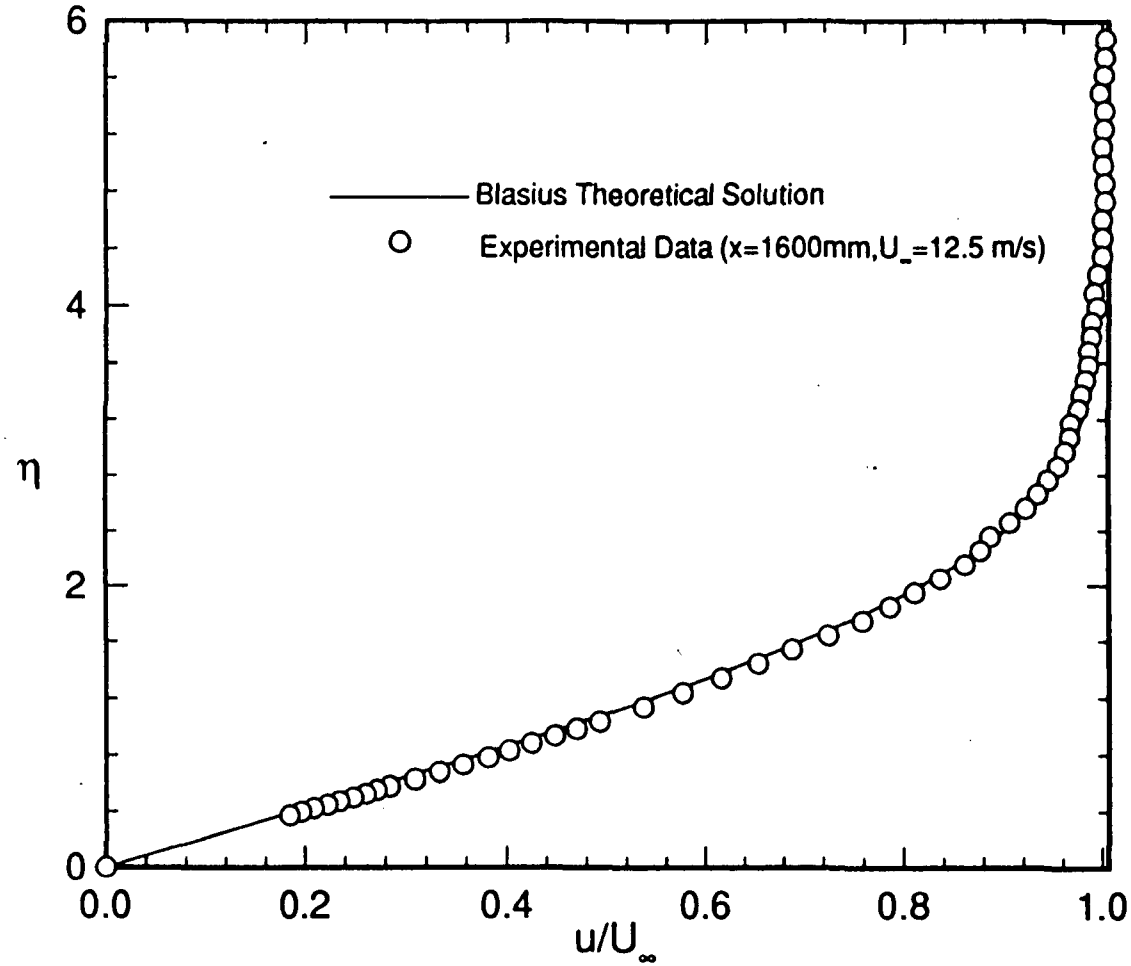

Figure 16. Experimental Data and Theoretical Solution for Nondimensional Velocity at x=1600 mm

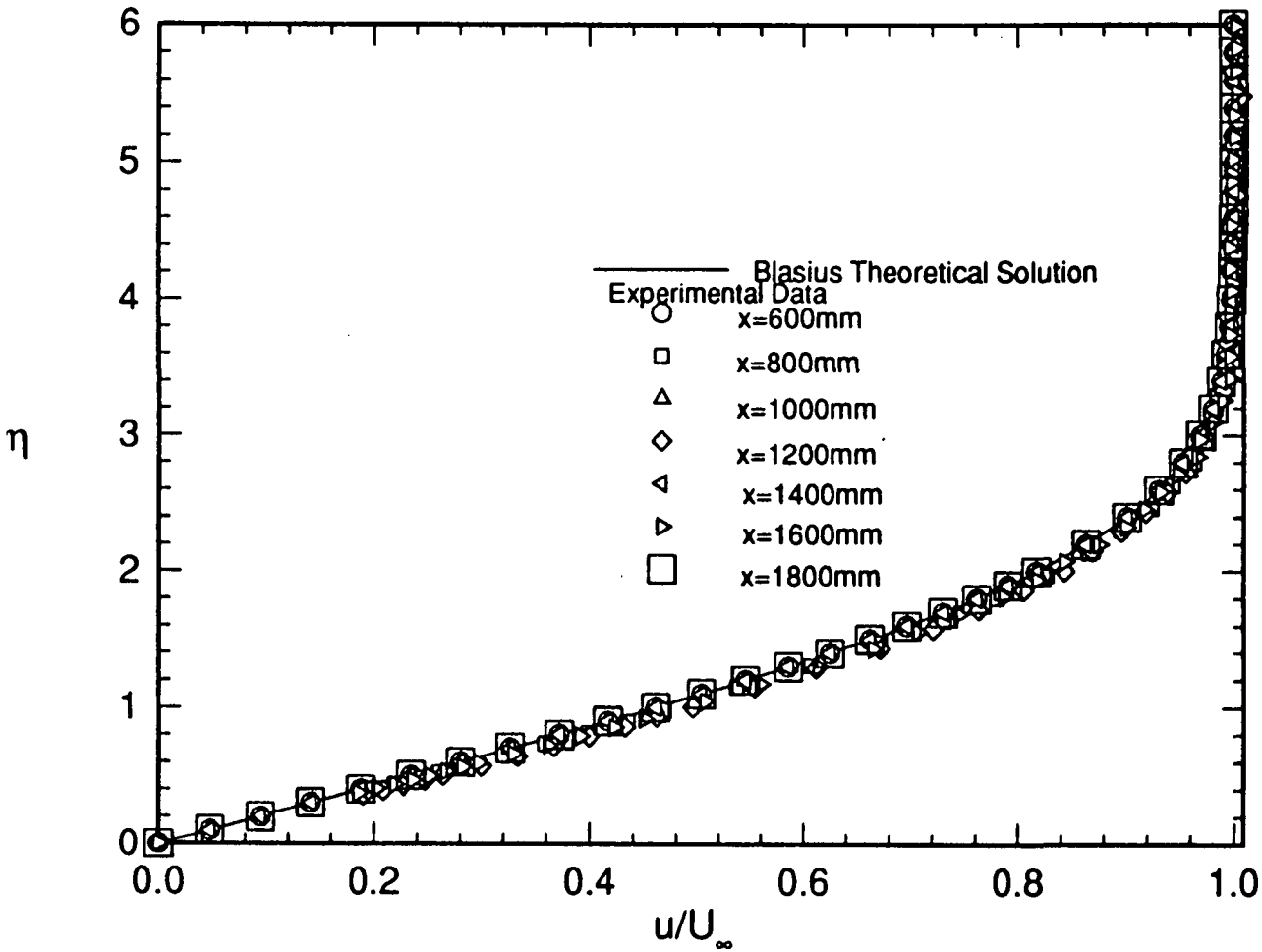

Figure 17. Experimental Data and Theoretical Solution for Nondimensional Velocity at Seven Streamwise Locations

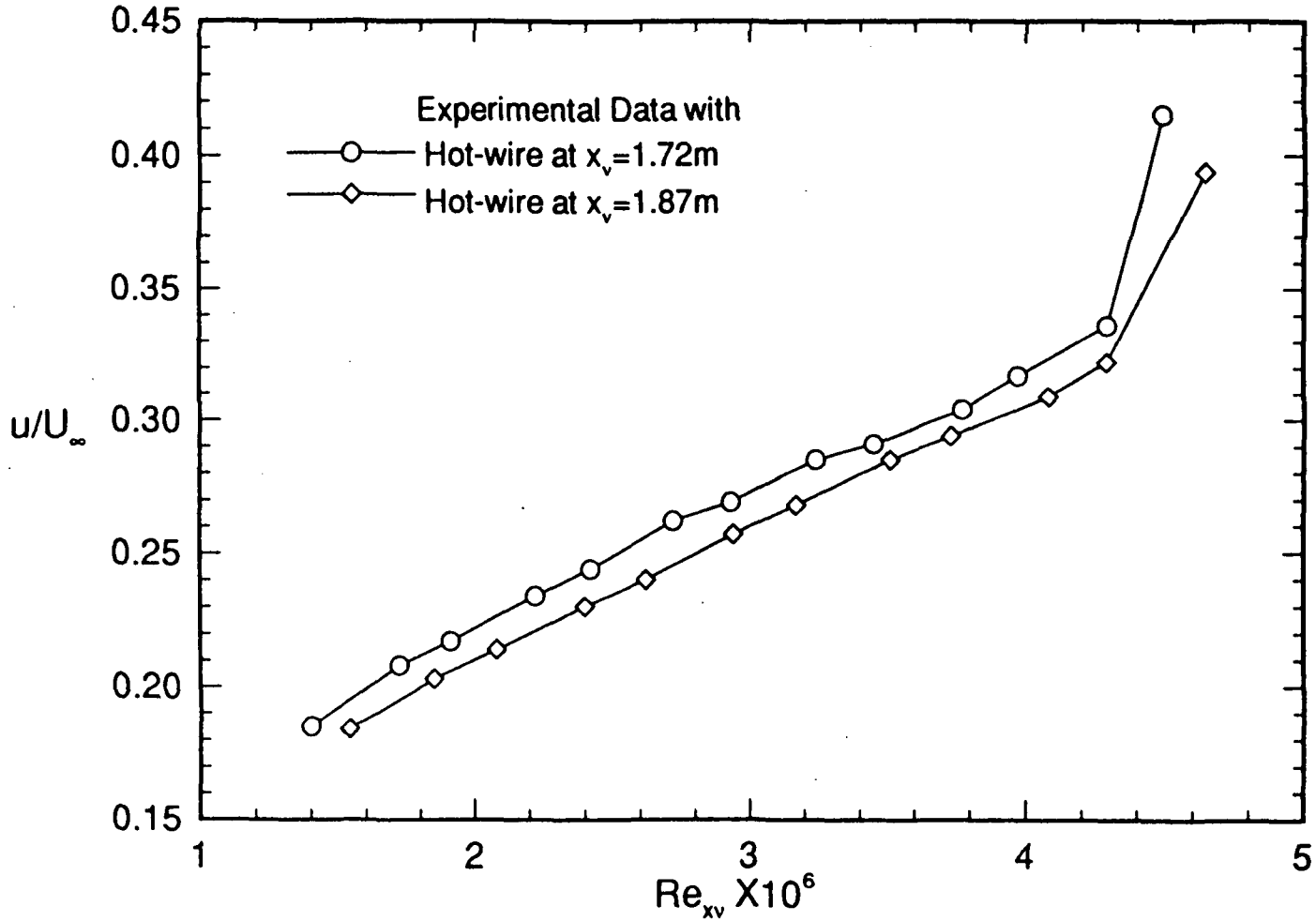

Figure 18. Nondimensional Velocity Vs. Reynolds Number for Transition Reynolds Number Determination (Hot-Wire Probe at x_v=1.72 and 1.87 m)

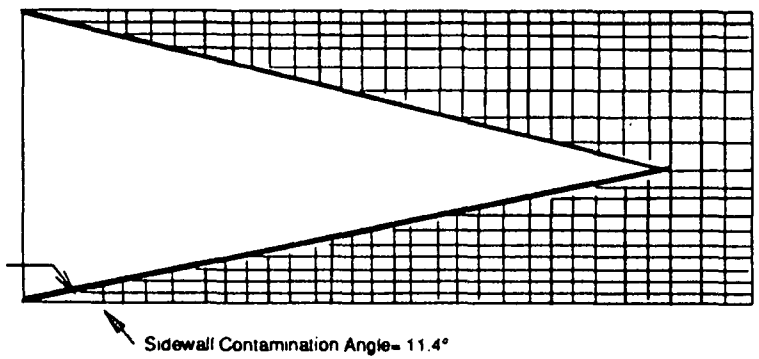

(A)

(B)

Figure 19. A. Schematic of Sidewall Contamination Test (Top View of Test Plate)
B. Photograph of Sidewall Contamination Test (Top View of Test Plate)

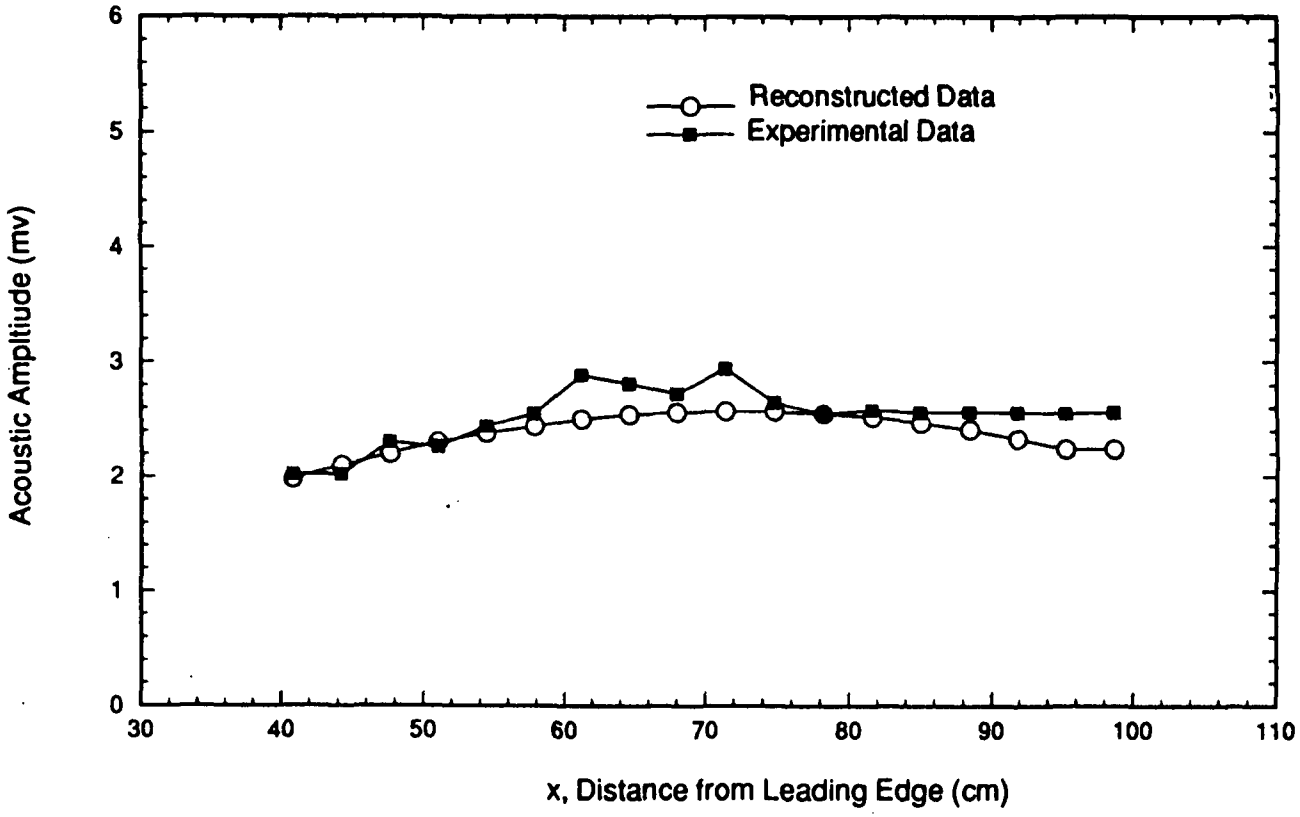

Figure 20. Measured and Reconstructed Amplitude of Acoustic Component of Freestream Disturbance Vs. Streamwise Distance from Leading Edge (f=120 Hz, 1-upstream speaker)

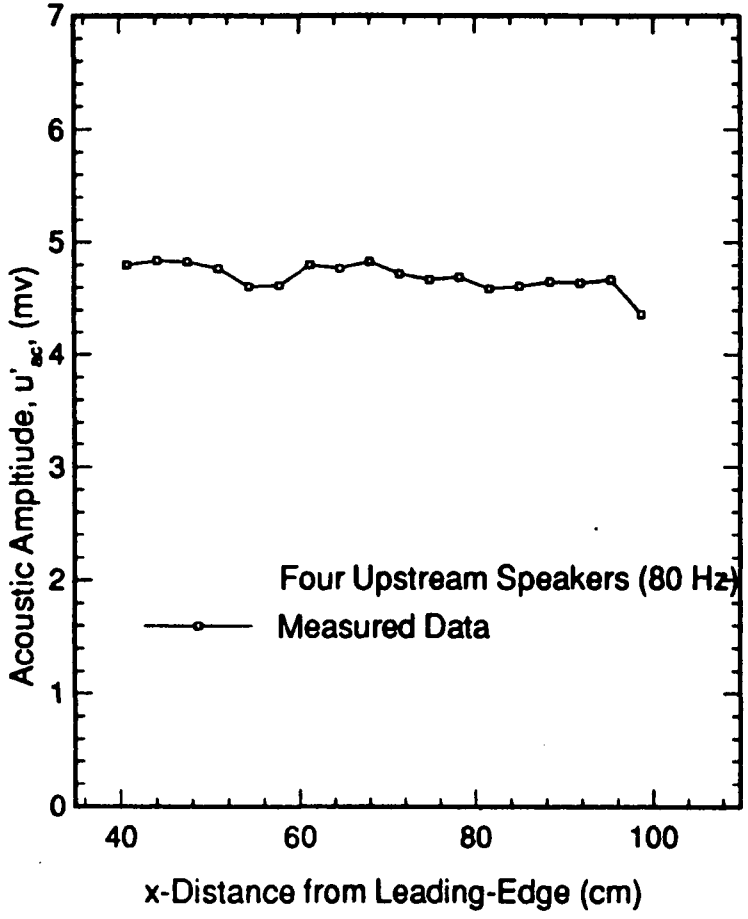

a)

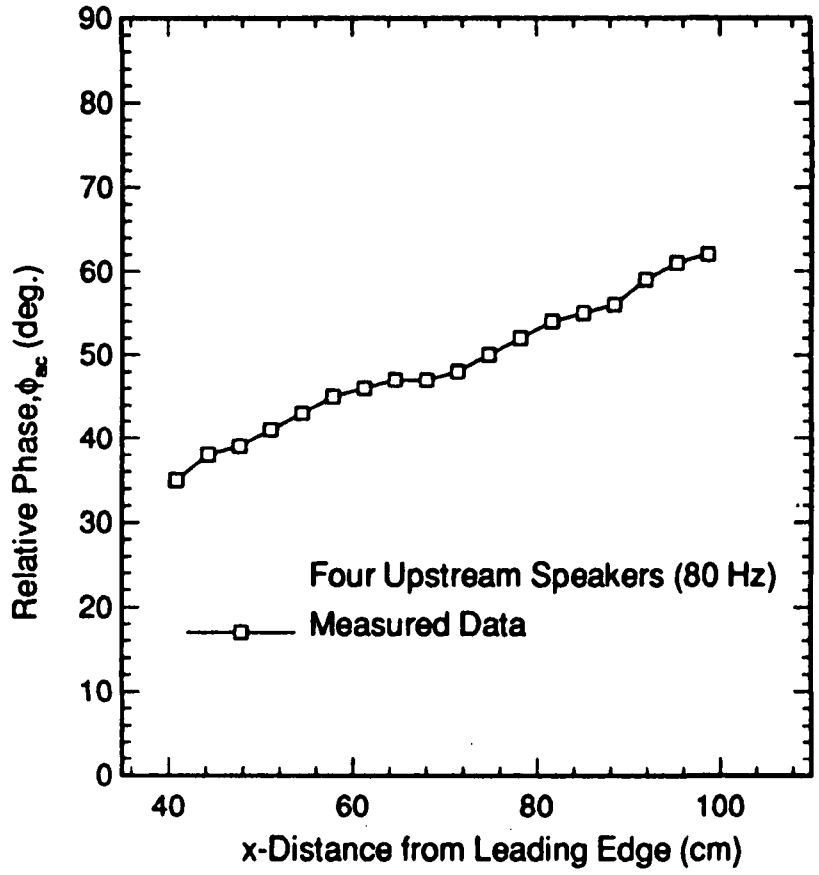

b)

Figure 21. Measured Acoustic Component of Freestream Distrurbances vs. Streamwise Distance from Leading Edge
a) Amplitude
b) Relative Phase

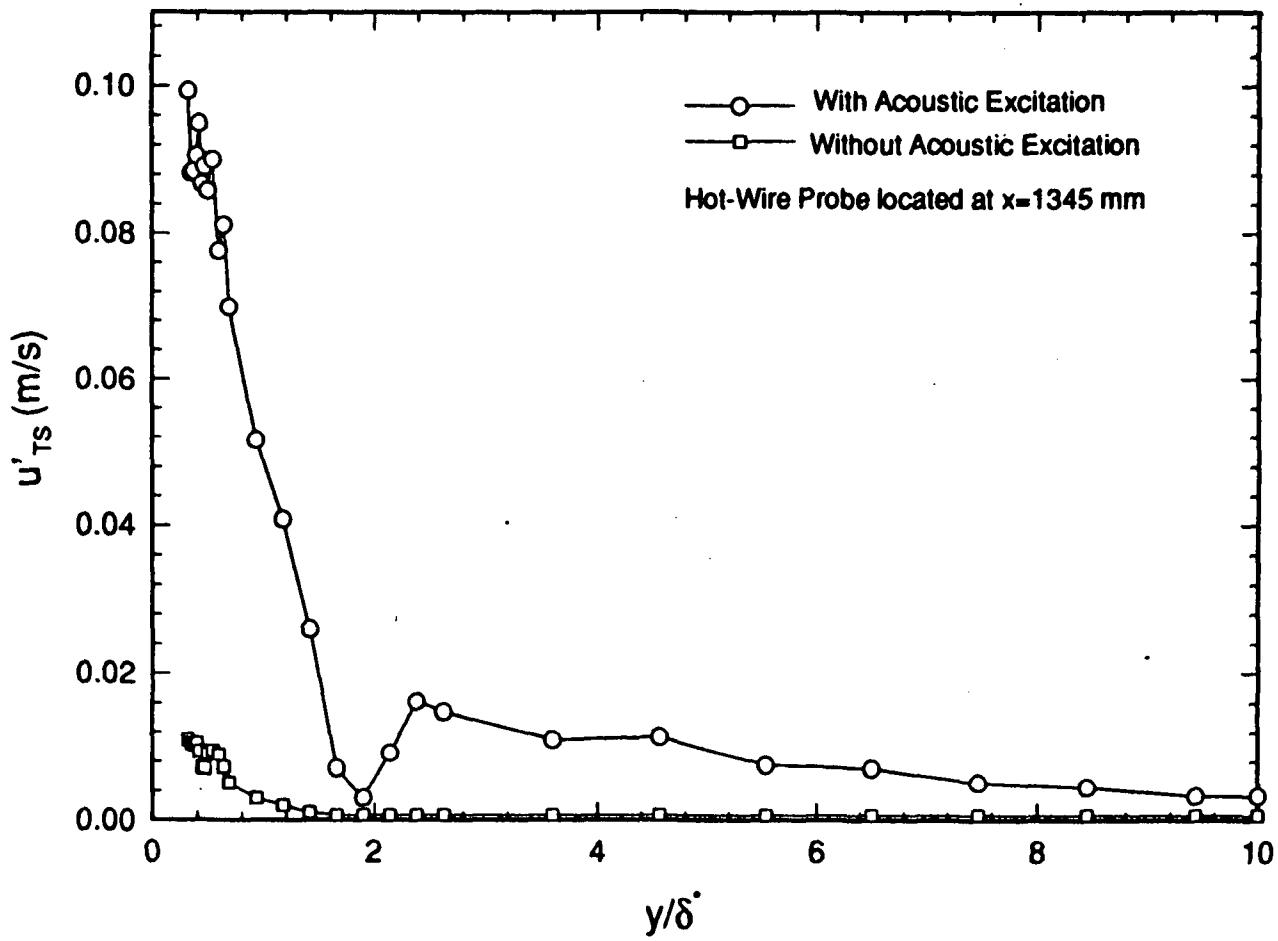

Figure 22. Fluctuating Velocity Component of T-S Wave Vs. Nondimensional Distance above the Test Plate with and without Acoustic Excitation at x=1345 mm from the Leading Edge for Configuration# 3

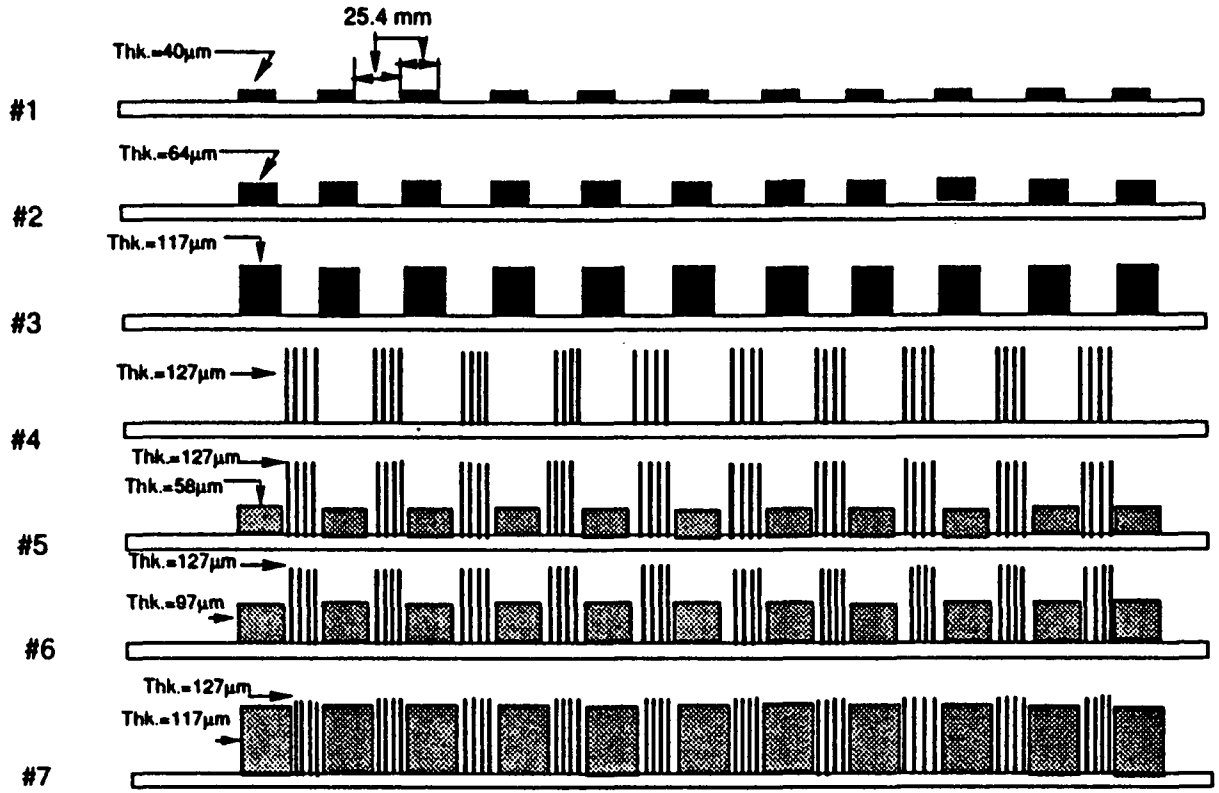

Figure 23. Schematic of Surface Roughness Configurations Tested at U_∞ = 12.5m/s

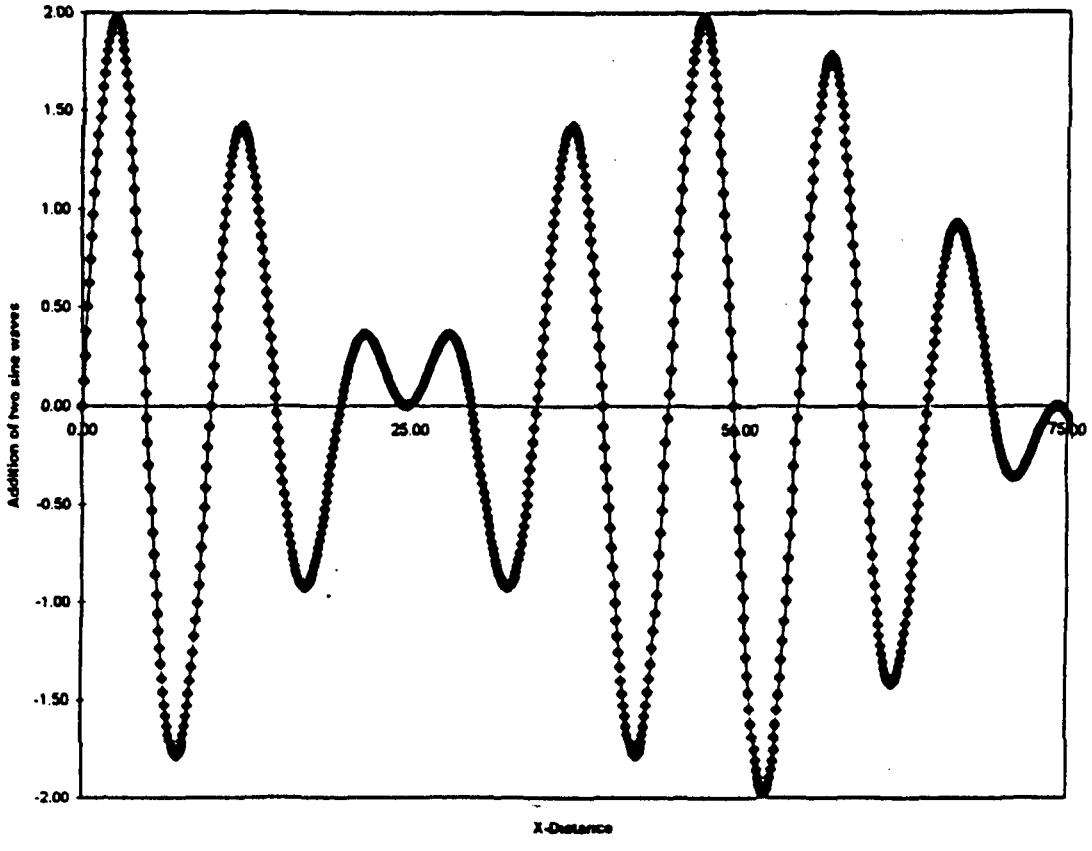

Figure 24. Typical Mathematical Model of Addition of Two Sine Waves

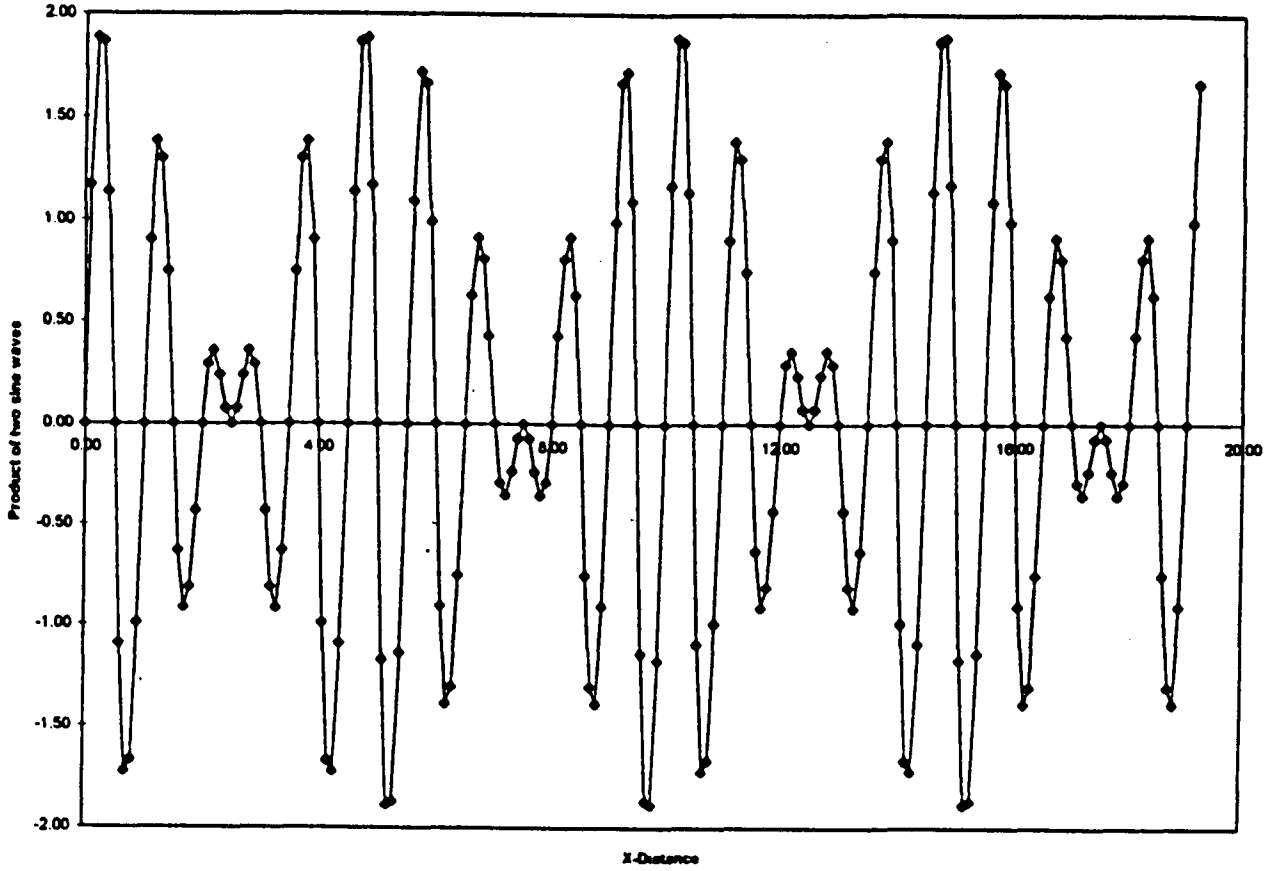

Figure 25. Typical Mathematical Model of Product of Two Sine Waves

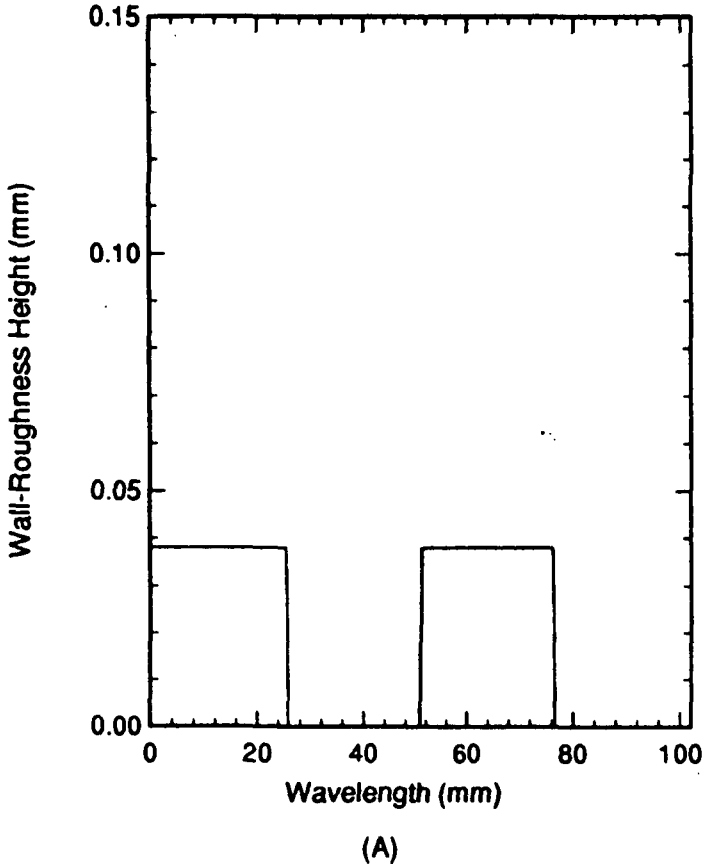

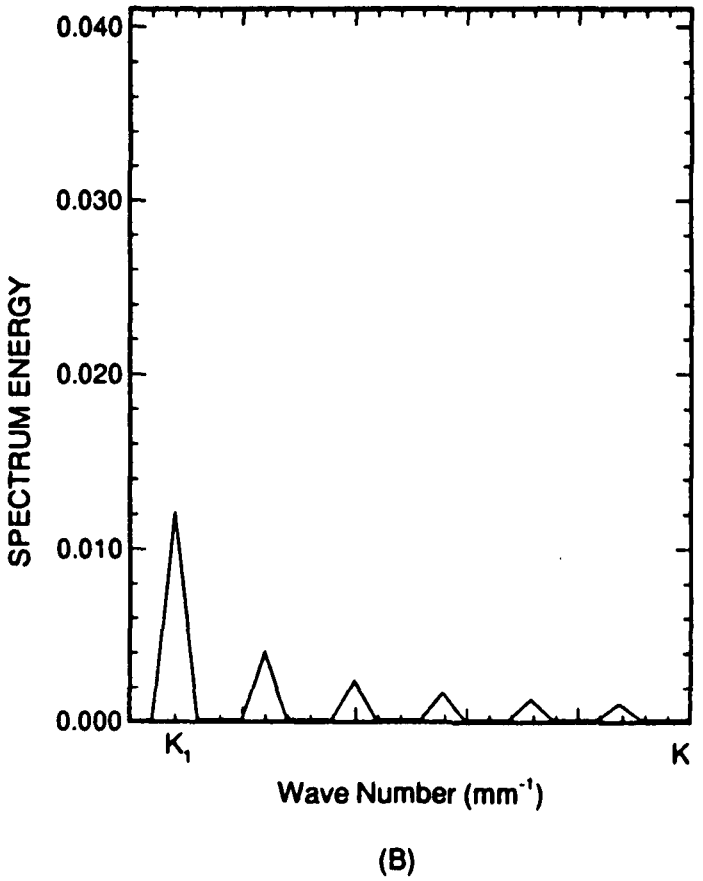

Figure 26. A. Surface Roughness Elements and
B. Power Spectrum Analysis of Surface Roughness Elements
for Configuration #1

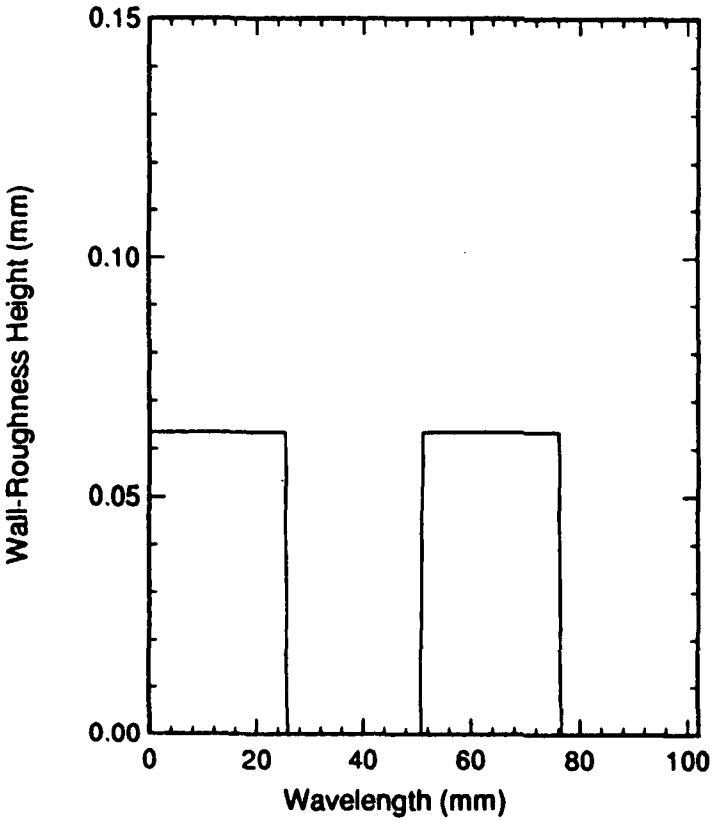

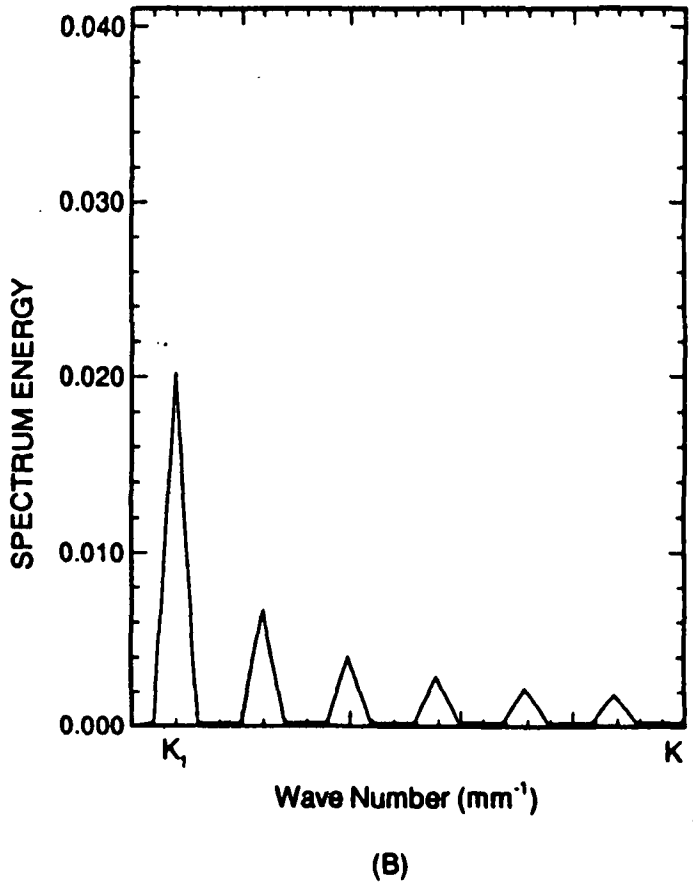

Figure 27. A. Surface Roughness Elements and
B. Power Spectrum Analysis of Surface Roughness Elements
for Configuration #2

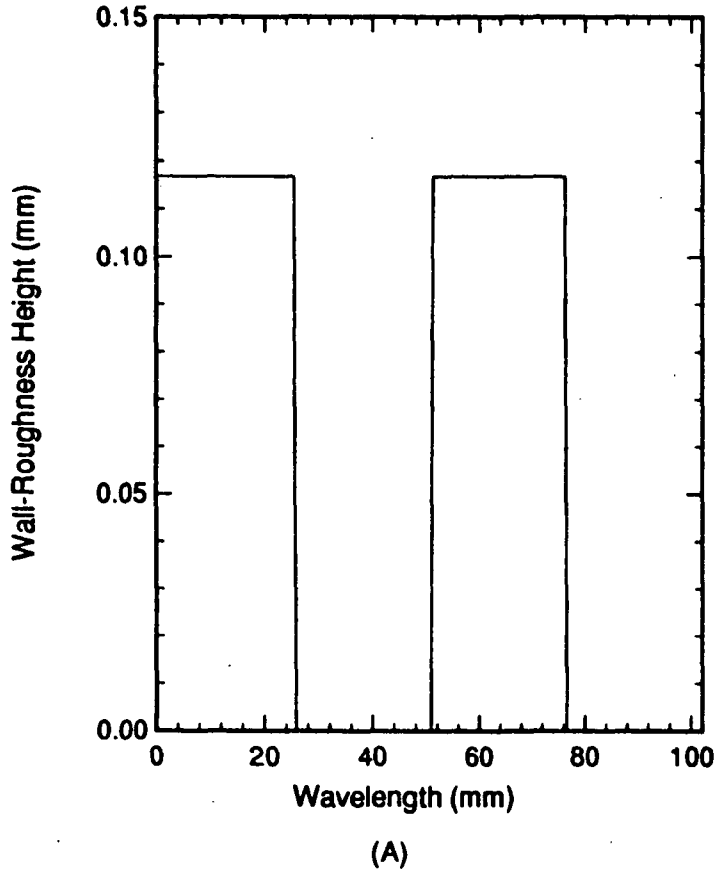

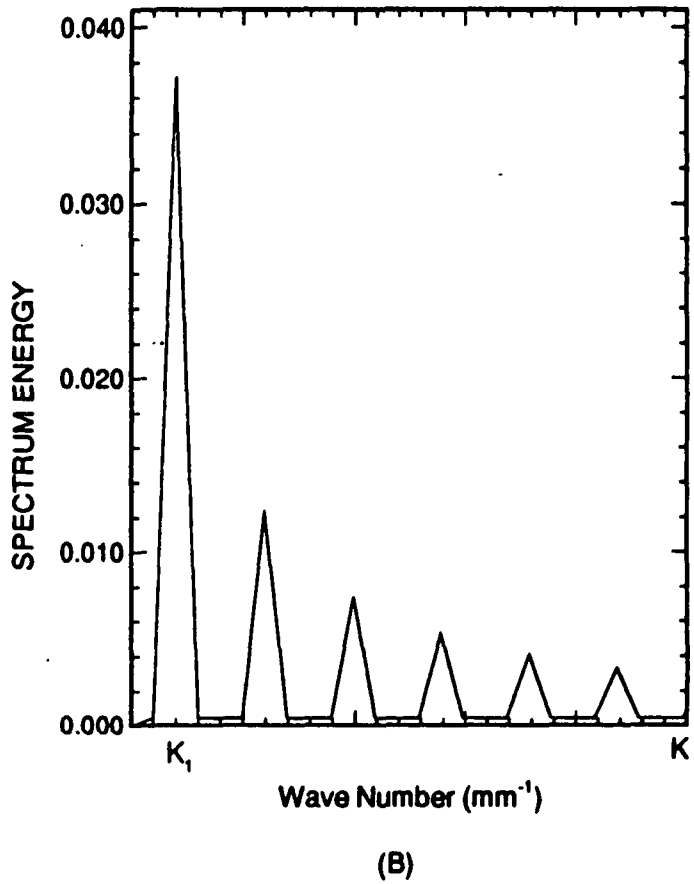

Figure 28. A. Surface Roughness Elements and
B. Power Spectrum Analysis of Surface Roughness Elements
for Configuration # 3

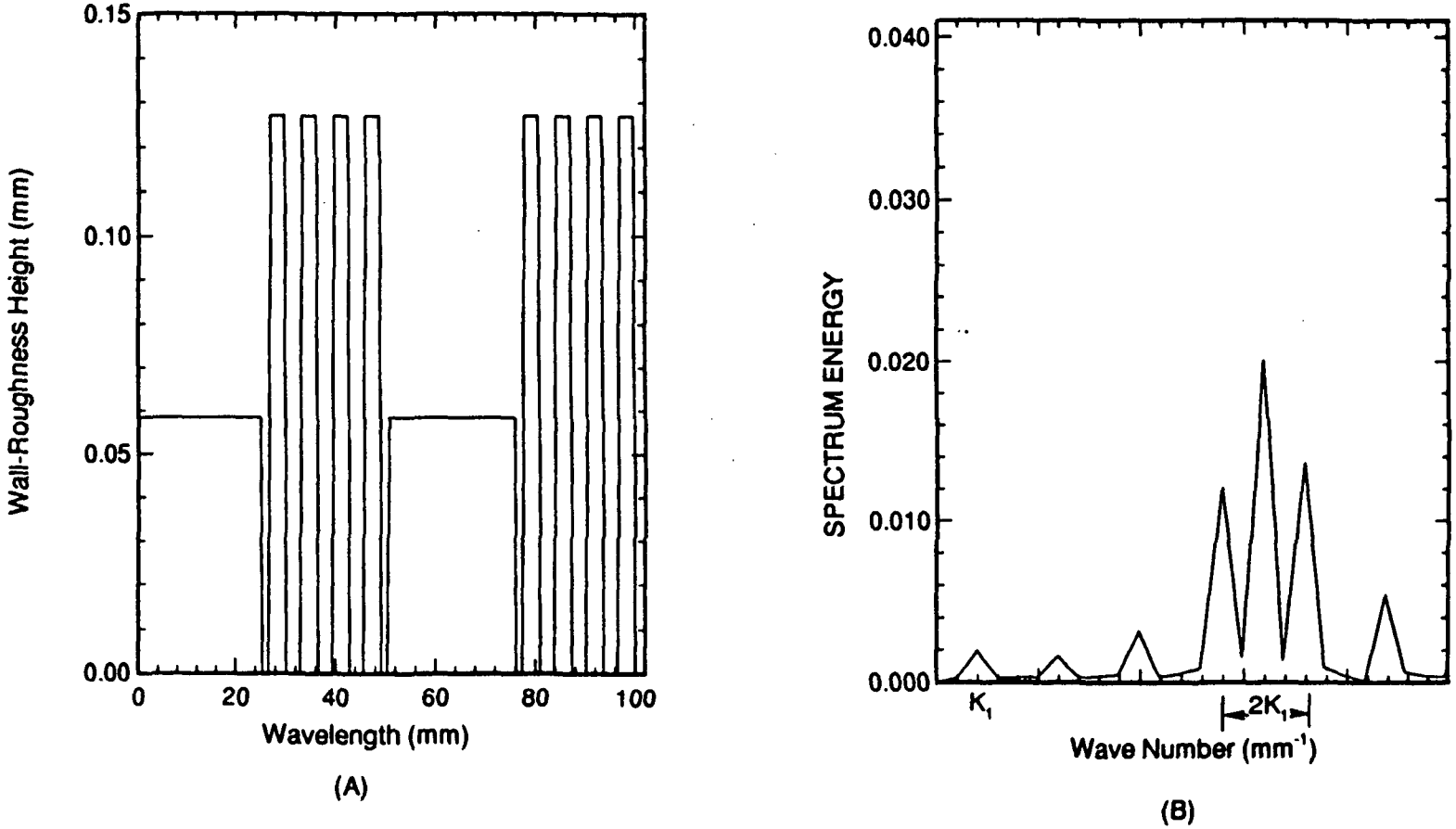

Figure 29. A. Surface Roughness Elements and
B. Power Spectrum Analysis of Surface Roughness Elements for Configuration #5

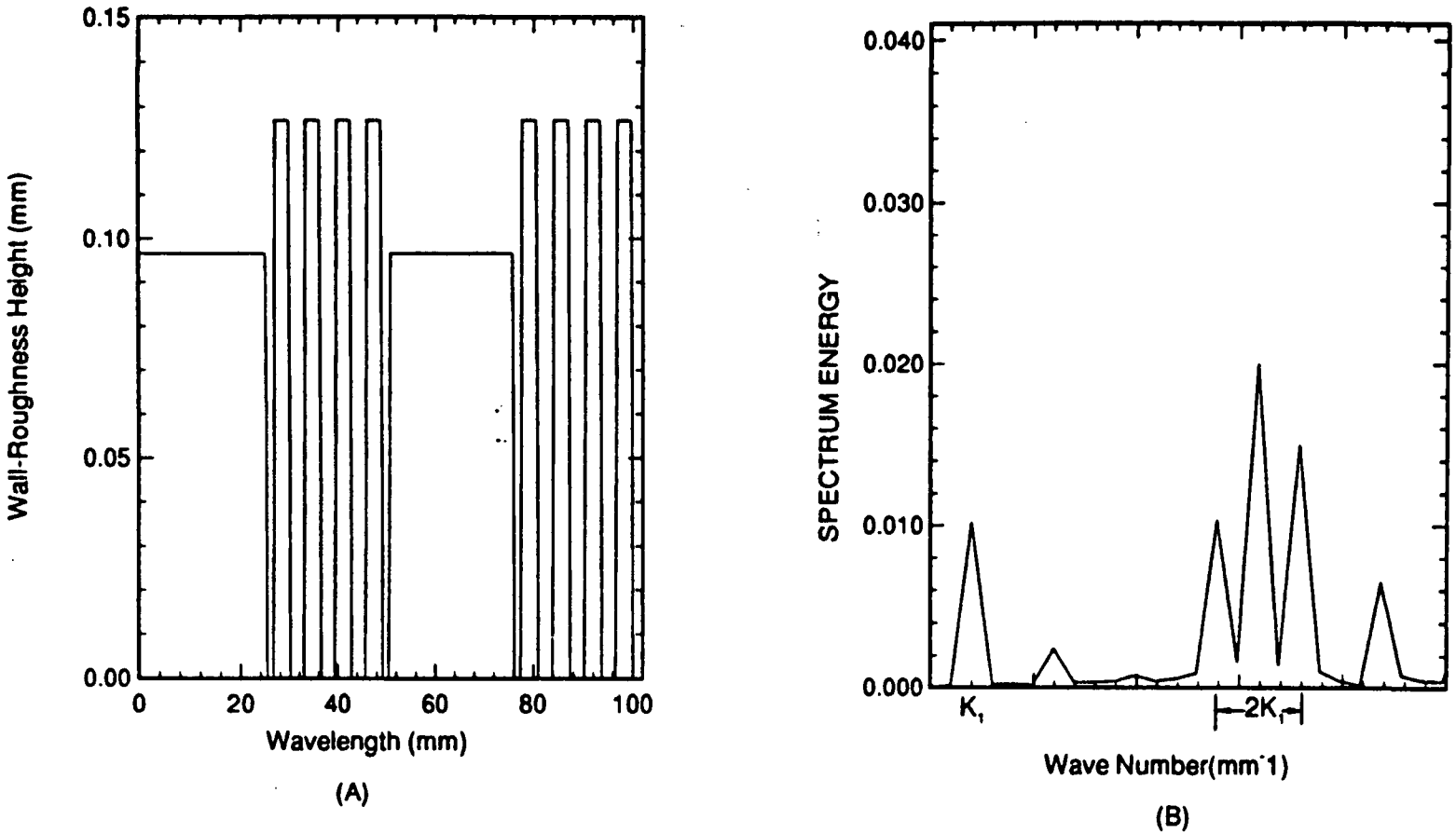

Figure 30. A. Surface Roughness Elements and
B. Power Spectrum Analysis of Surface Roughness Elements
for configuration #6

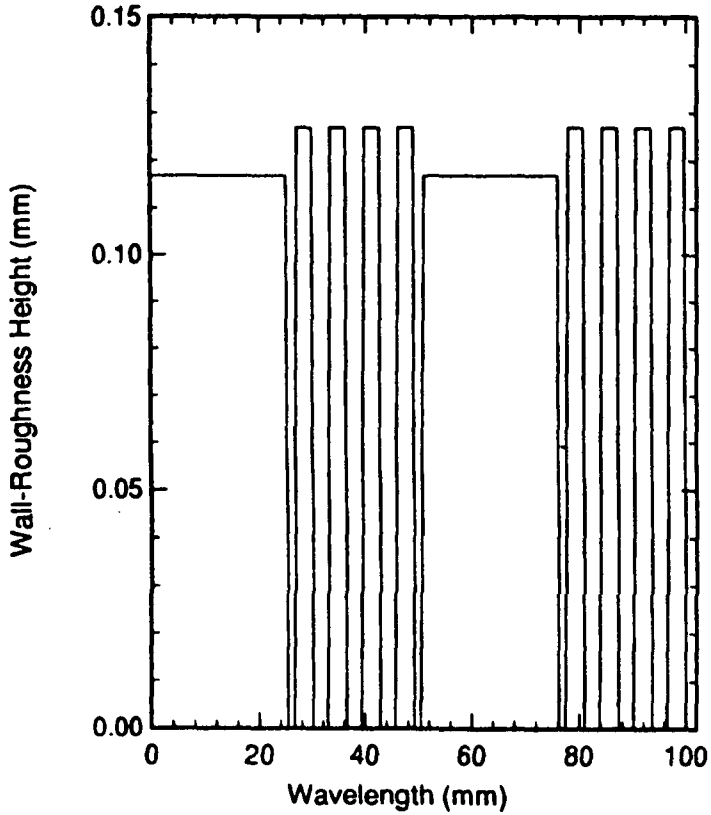

(A)

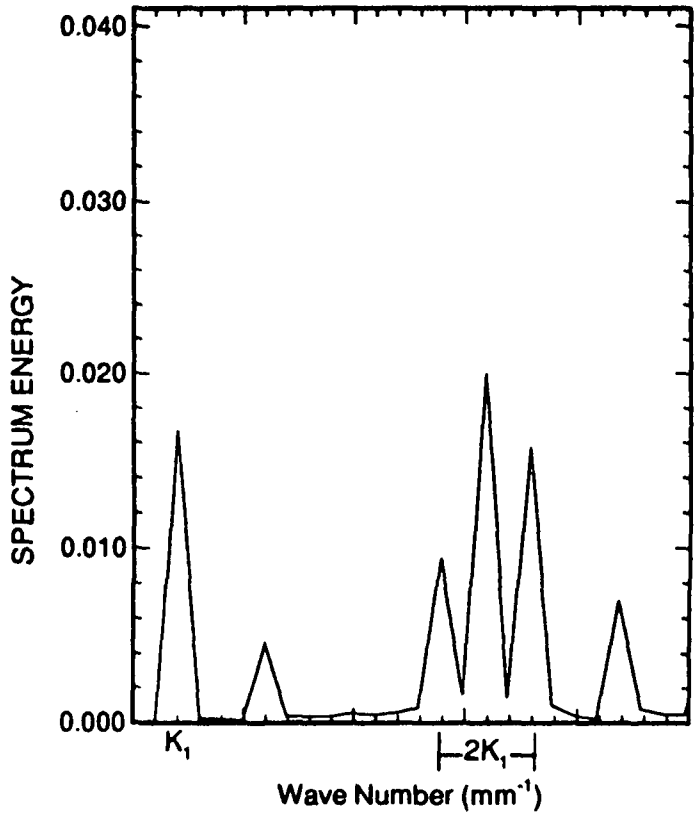

(B)

Figure 31. A. Surface Roughness Elements and

B. Power Spectrum Analysis of Surface Roughness Elements for Configuration # 7

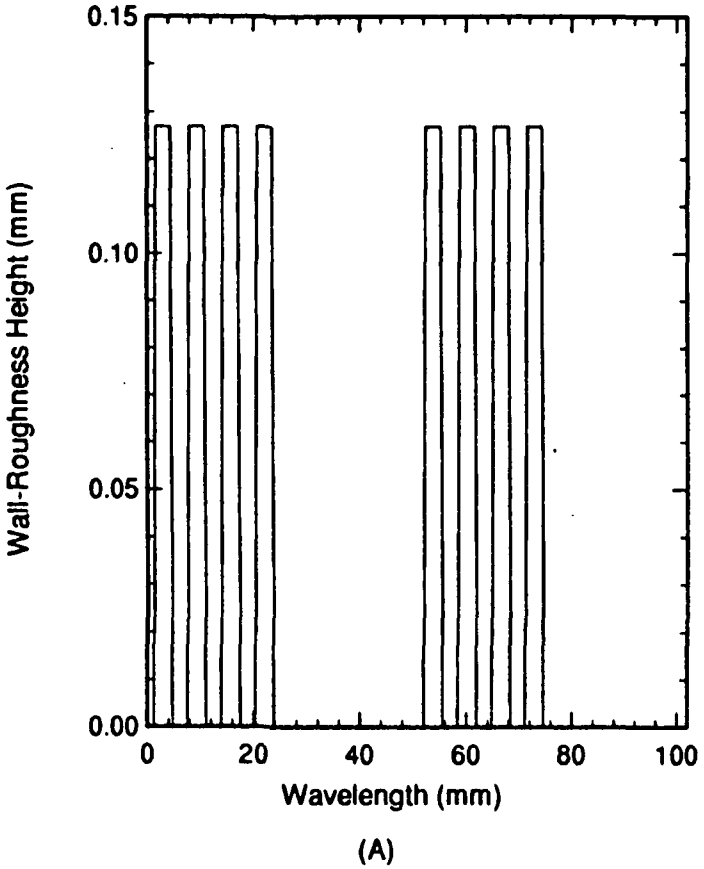

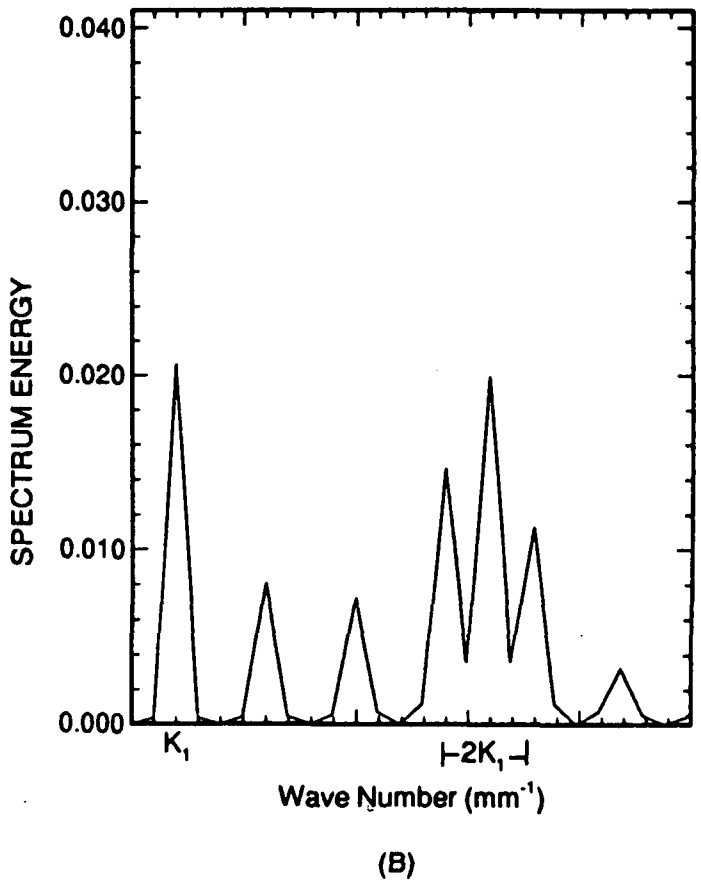

Figure 32. A. Surface Roughness Elements and
B. Power Spectrum Analysis of Surface Roughness Elements
for Configuration # 4

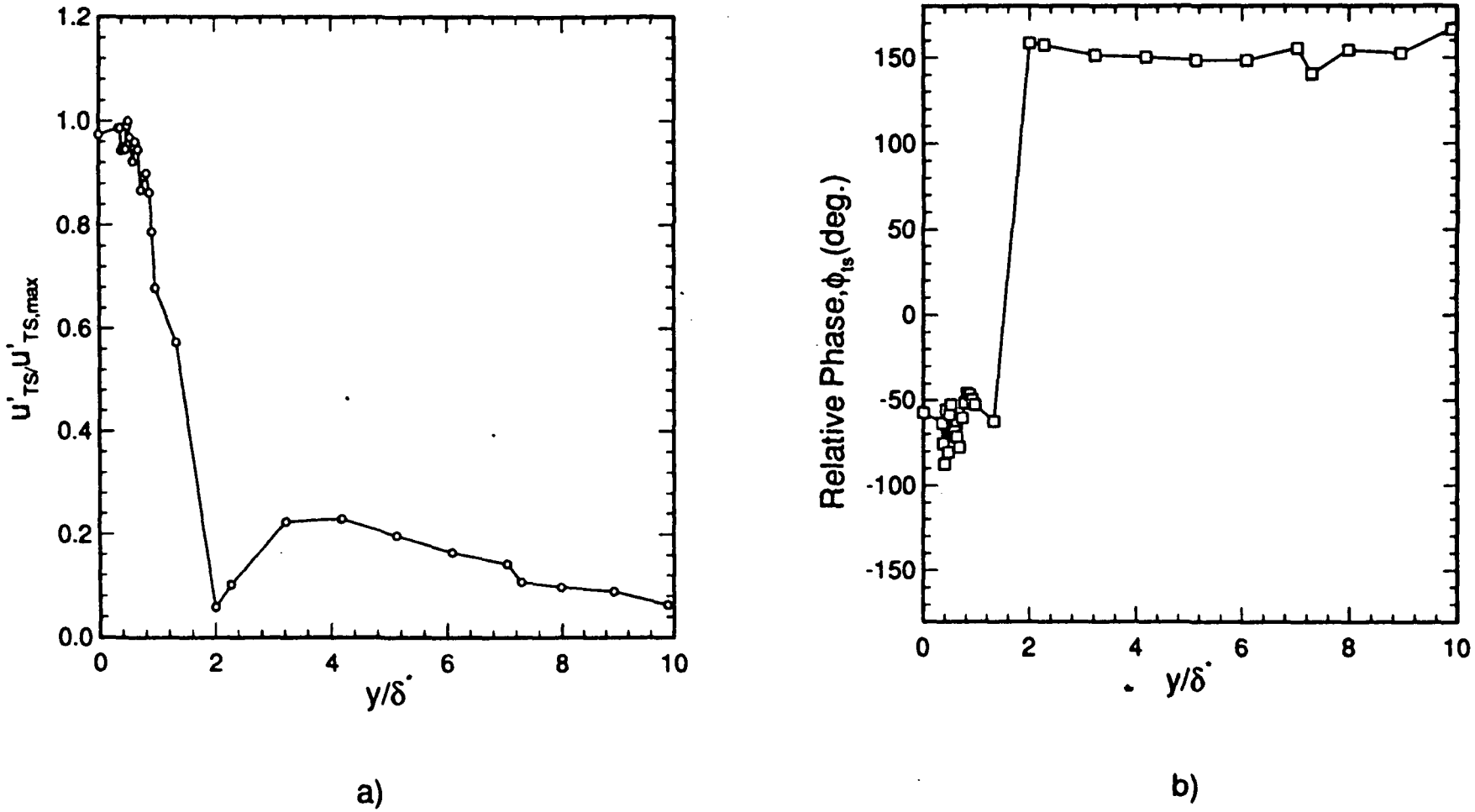

Figure 33. Mode Shape of T-S Wave due to Surface Roughness for Configuration# 1, x=1345 mm, U_∞=12.5 m/s
a) Amplitude and b) Relative Phase

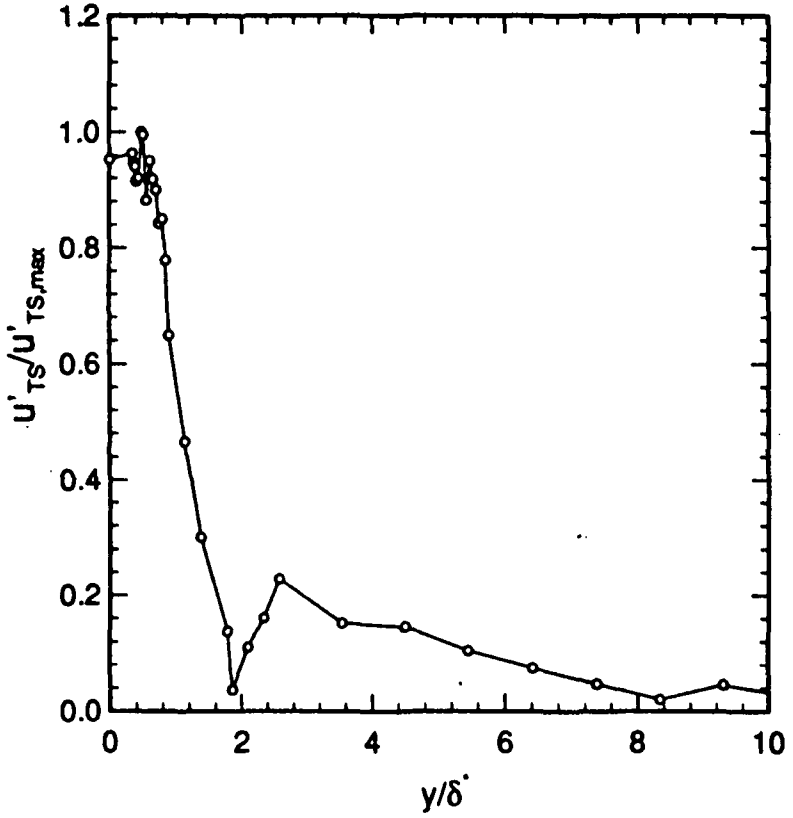

a)

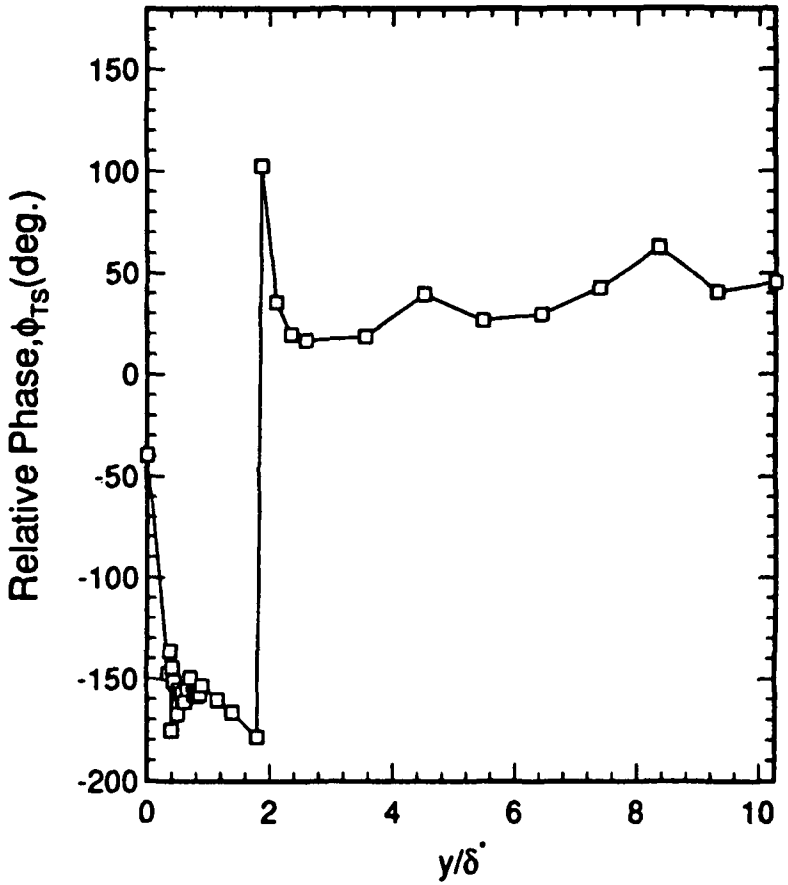

b)

Figure 34. Mode Shape of T-S Wave due to Surface Roughness for Configuration #2, x=1345 mm, U_∞=12.5 m/s
a) Amplitude and b) Relative Phase

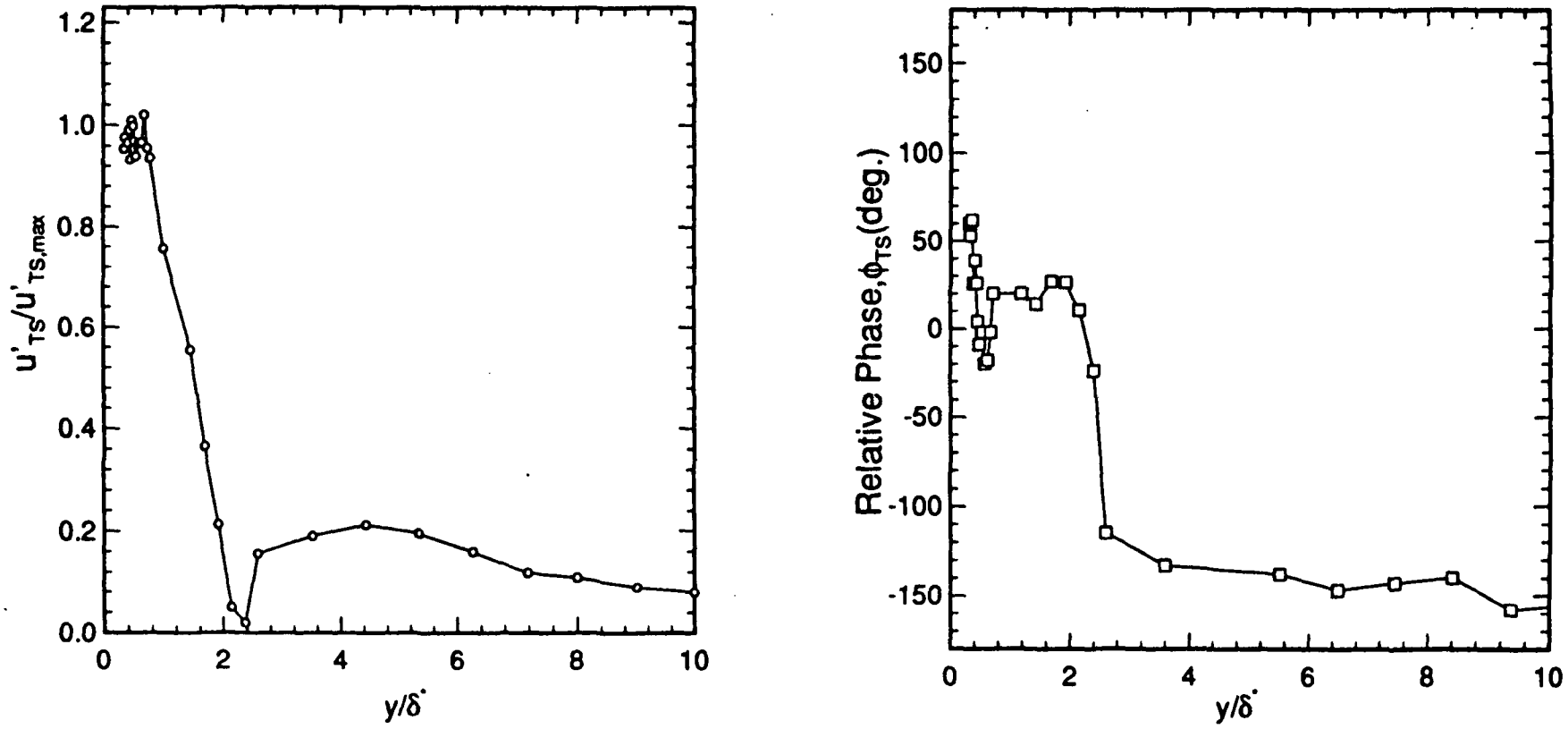

a) b)

Figure 35. Mode Shape of T-S Wave due to Surface Roughness for Configuration #3, x=1345 mm, U_∞=12.5 m/s
a) Amplitude and b) Relative Phase

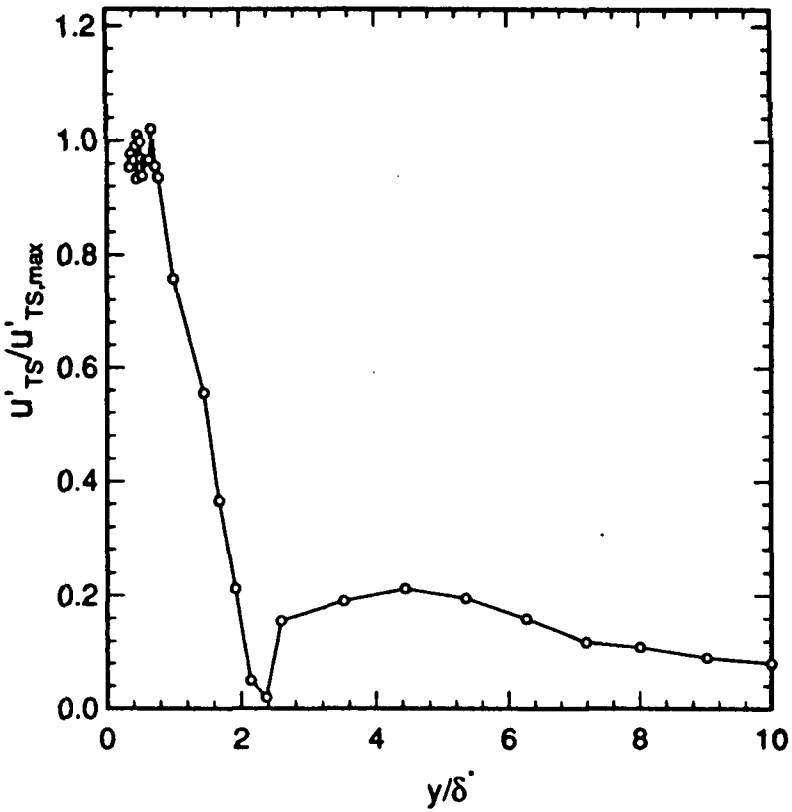

a)

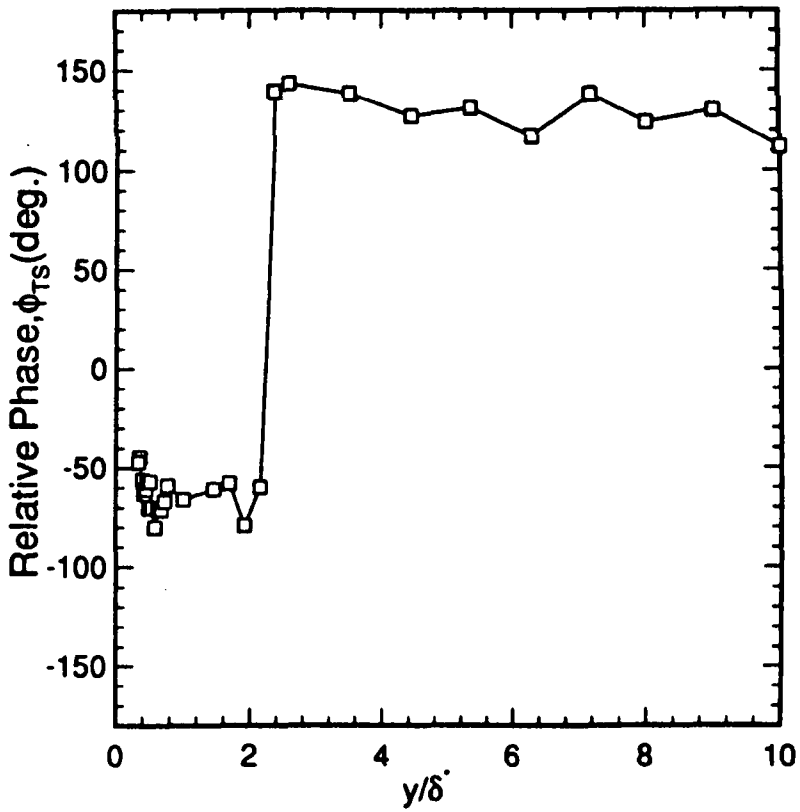

b)

Figure 36. Mode Shape of T-S Wave due to Surface Roughness for Configuration # 4, x=1345 mm, U_∞=12.5 m/s
a) Amplitude and b) Relaative Phase

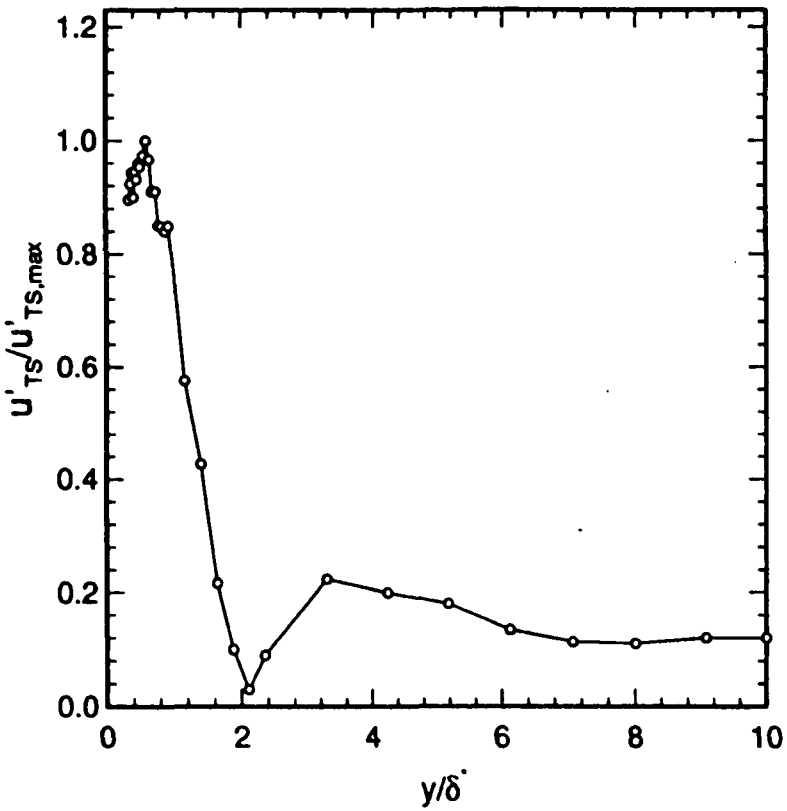

a)

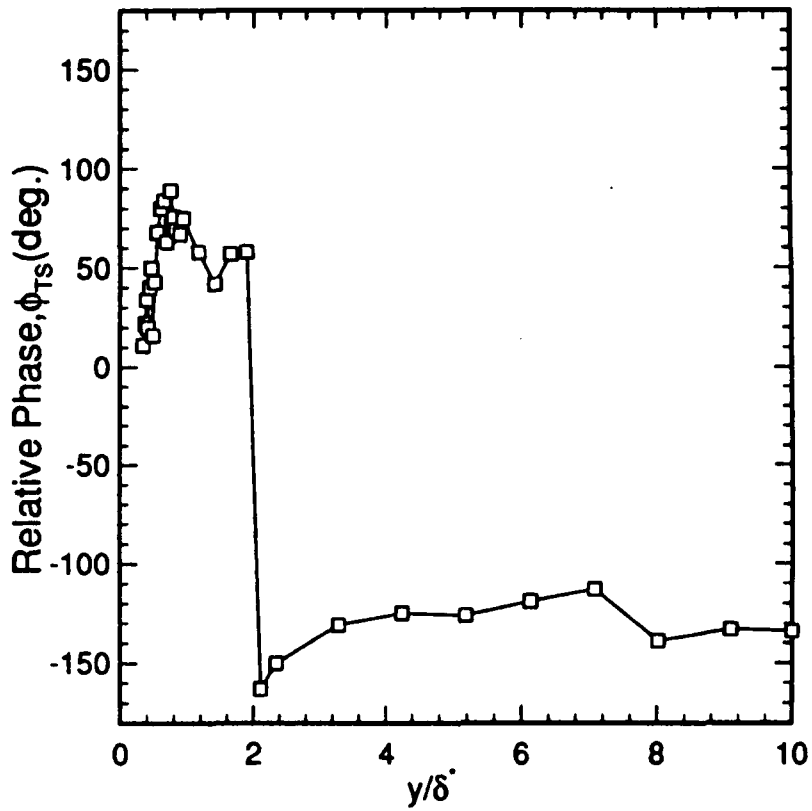

b)

Figure 37. Mode Shape of T-S Wave due to Surface Roughness for Configuration #5, x=1345 mm, U_∞=12.5 m/s
a) Amplitude and b) Relative Phase

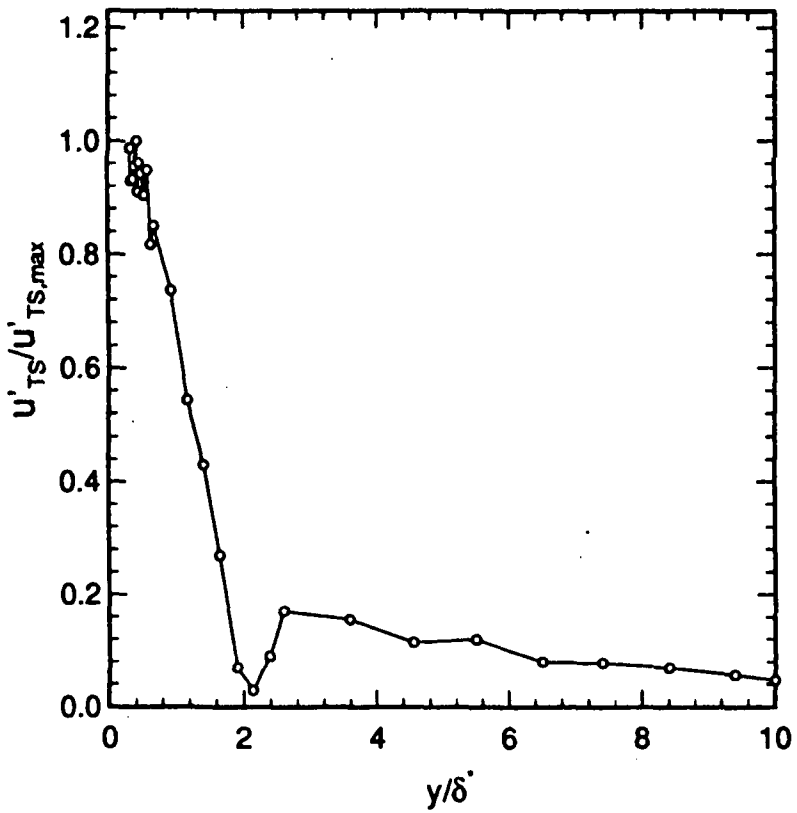

a)

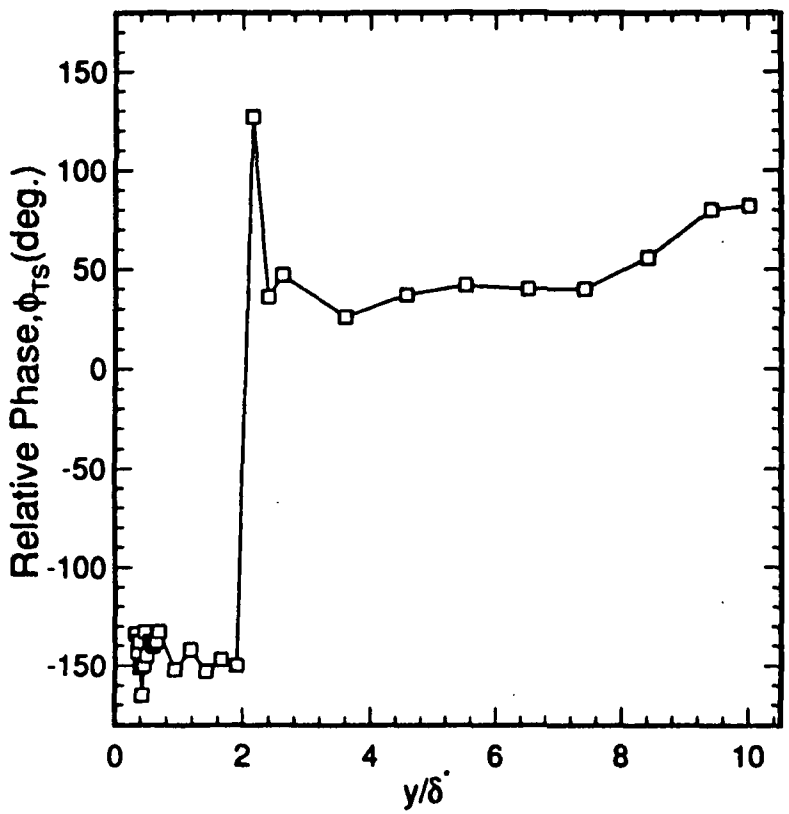

b)

Figure 38. Mode Shape of T-S Wave due to Surface Roughness for Configuration #6, x=1345 mm, U_∞=12.5 m/s
a) Amplitude and b) Relative Phase

88

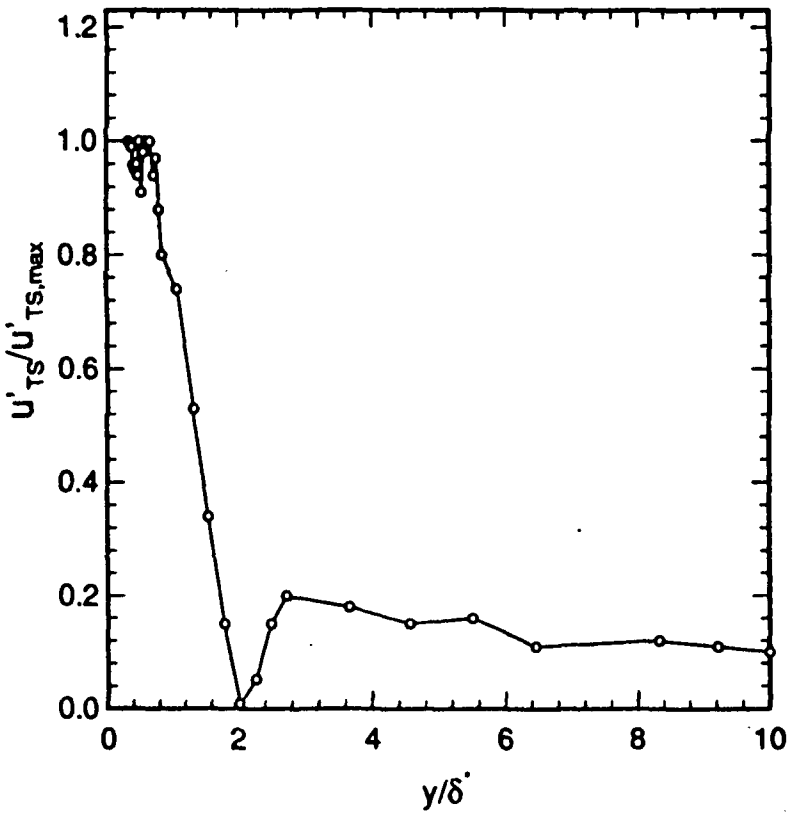

a)

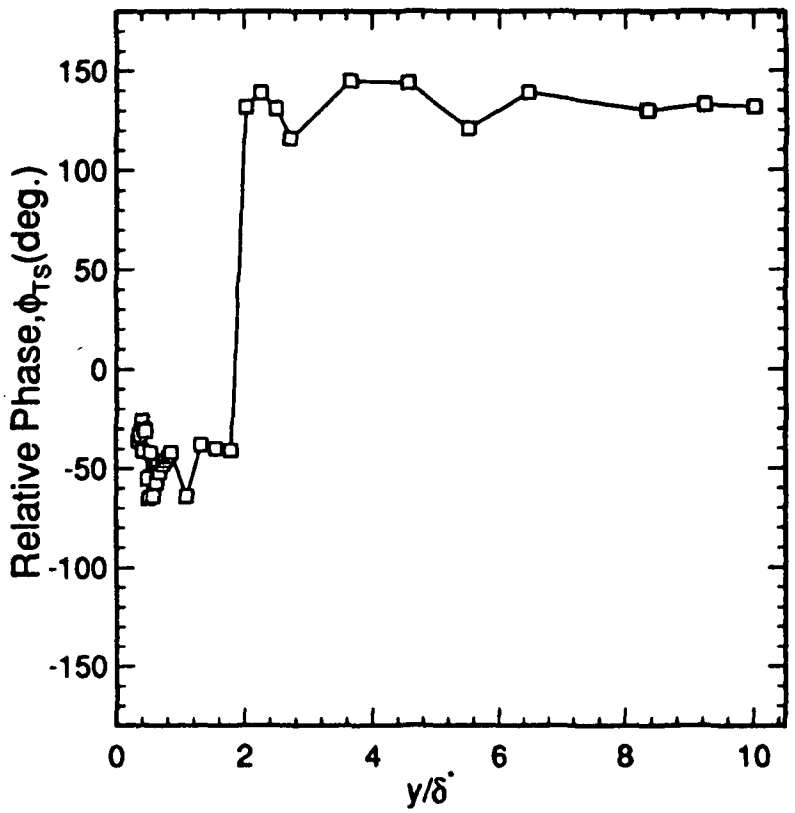

b)

Figure 39. Mode Shape of T-S Wave due to Surface Roughness for Configuration # 7, x=1345 mm & U_∞=12.5 m/s
a) Amplitude and b) Relative Phase

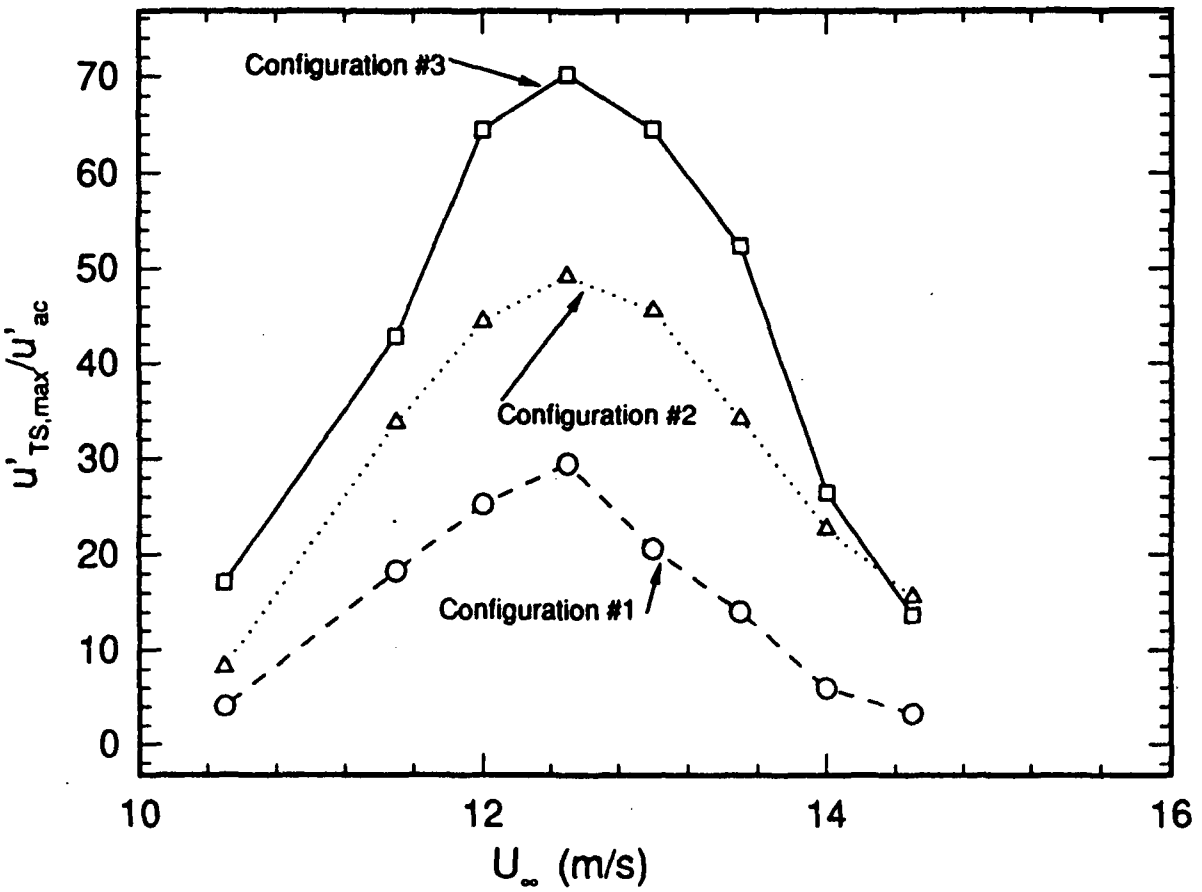

Figure 40. Ratio of Maximum T-S wave Amplitude to Acoustic Wave Amplitude Vs. Detuning Parameter for Configurations #1, #2, and #3

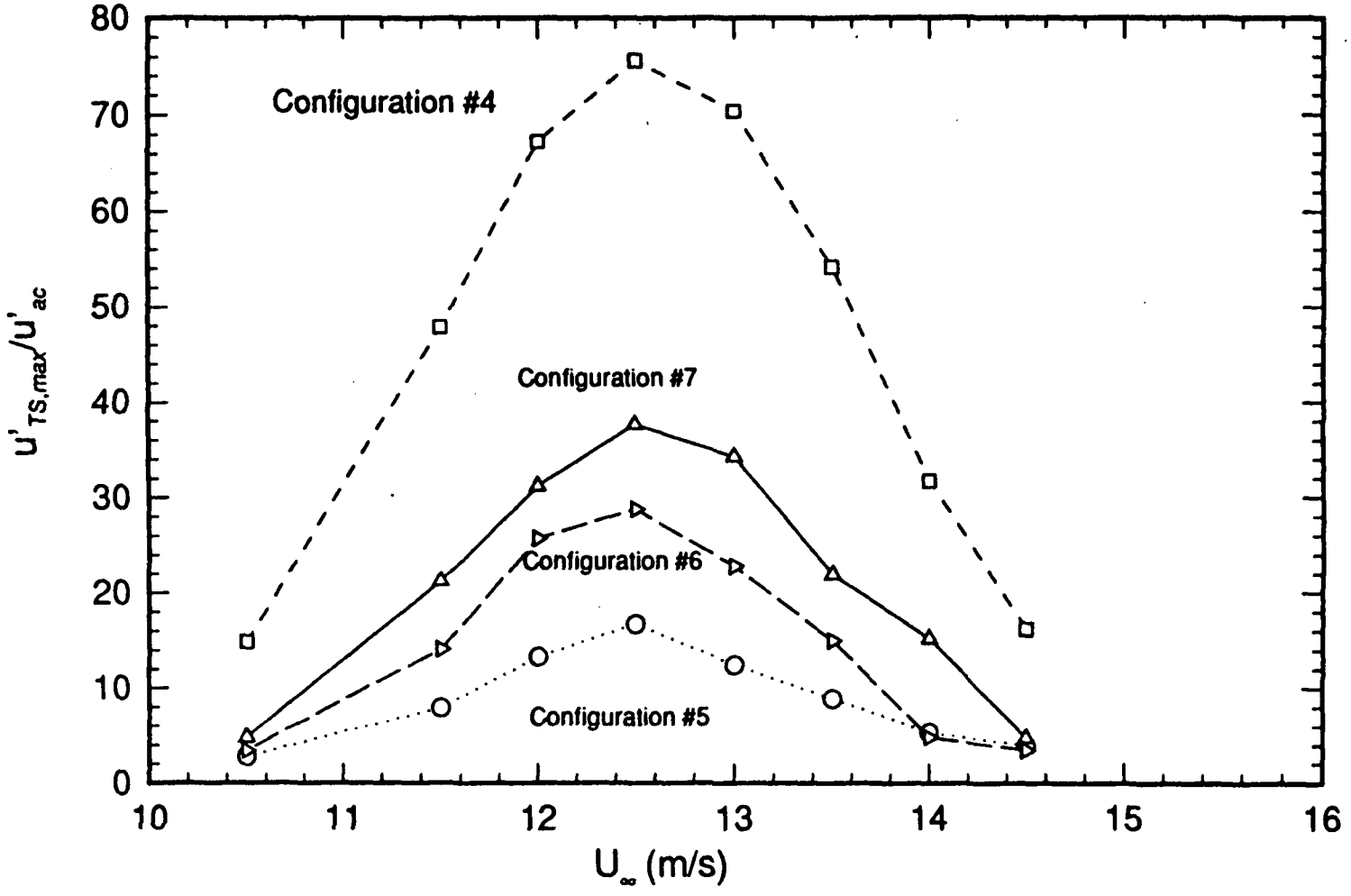

Figure 41. Ratio of Maximum T-S Wave Ampltitude to Acoustic Wave Amplitude Vs. Detuning Parameter for Configurations #4, #5, #6, and #7

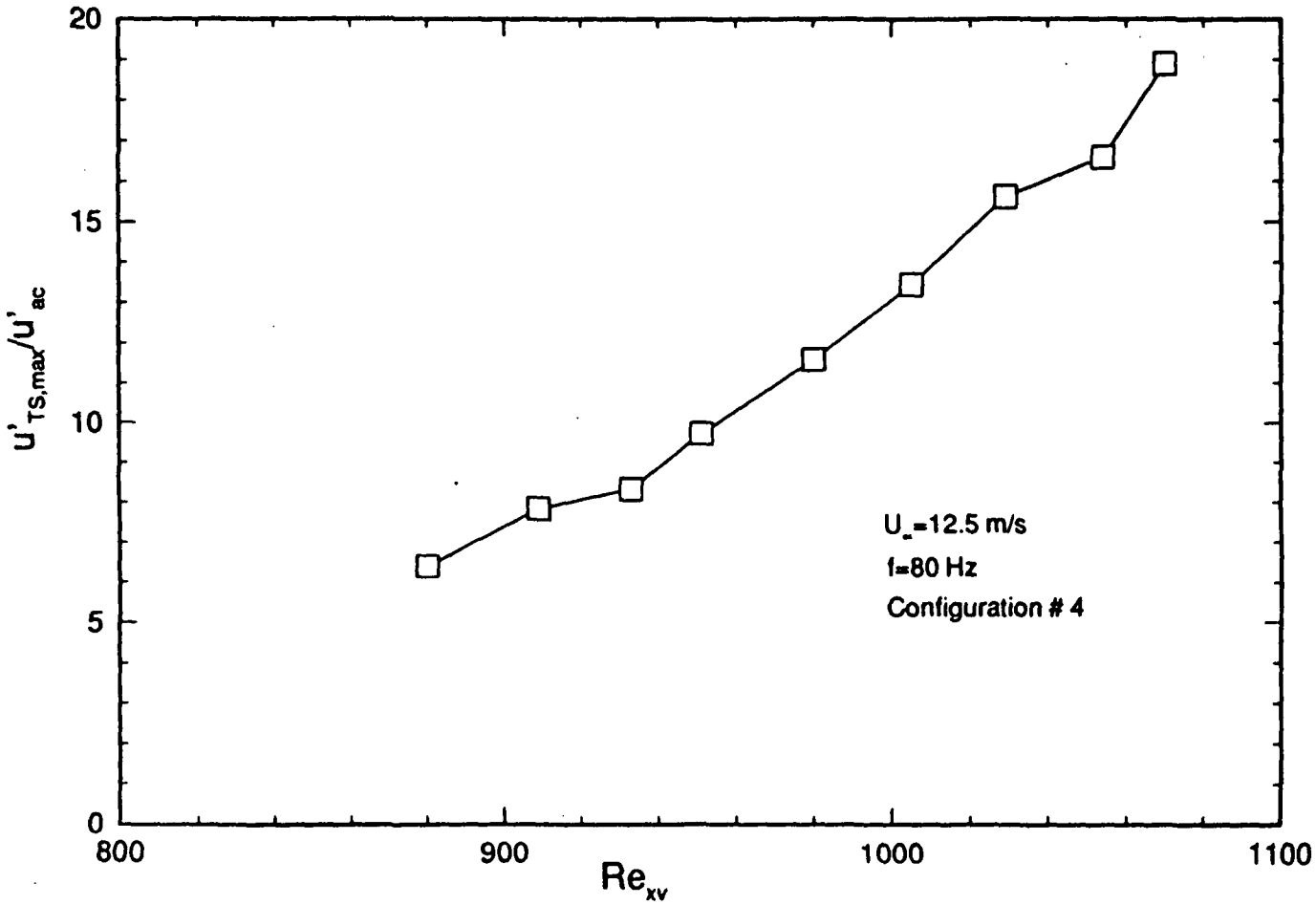

Figure 42. Normalized Streamwise T-S Wave Amplitude Vs. Boundary-Layer Reynolds Number

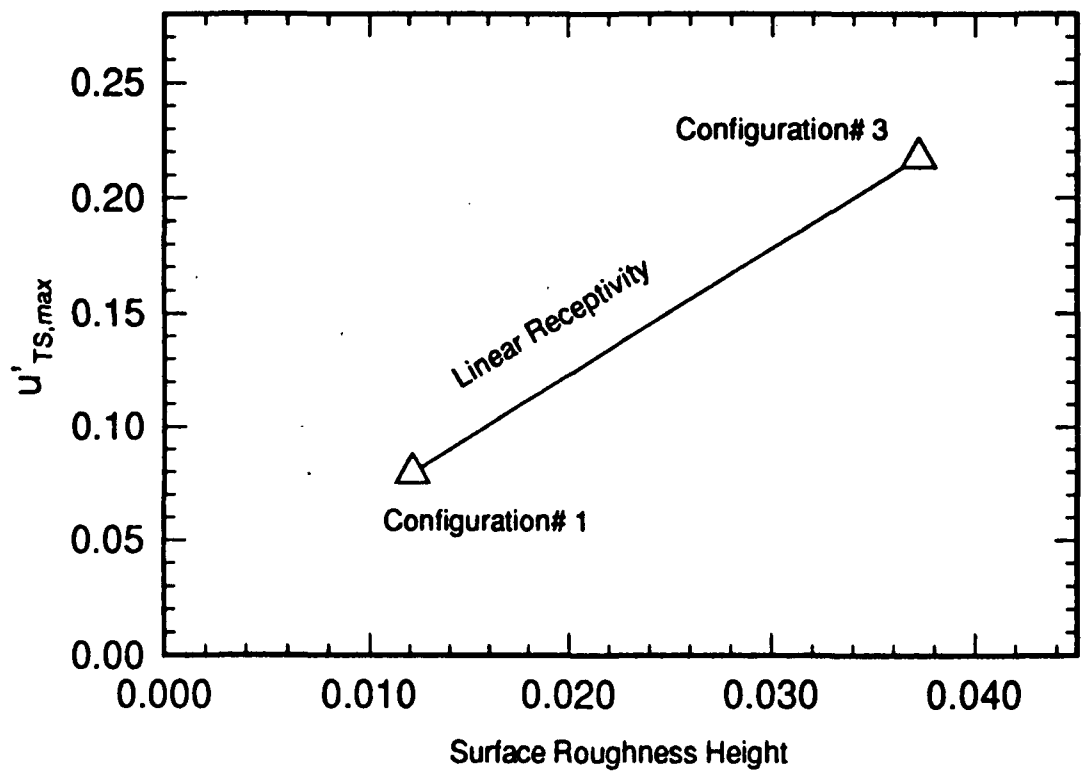

Figure 43. Maximum T-S Wave Amplitude Vs. Surface Roughness Height for Configurations #1 and #3

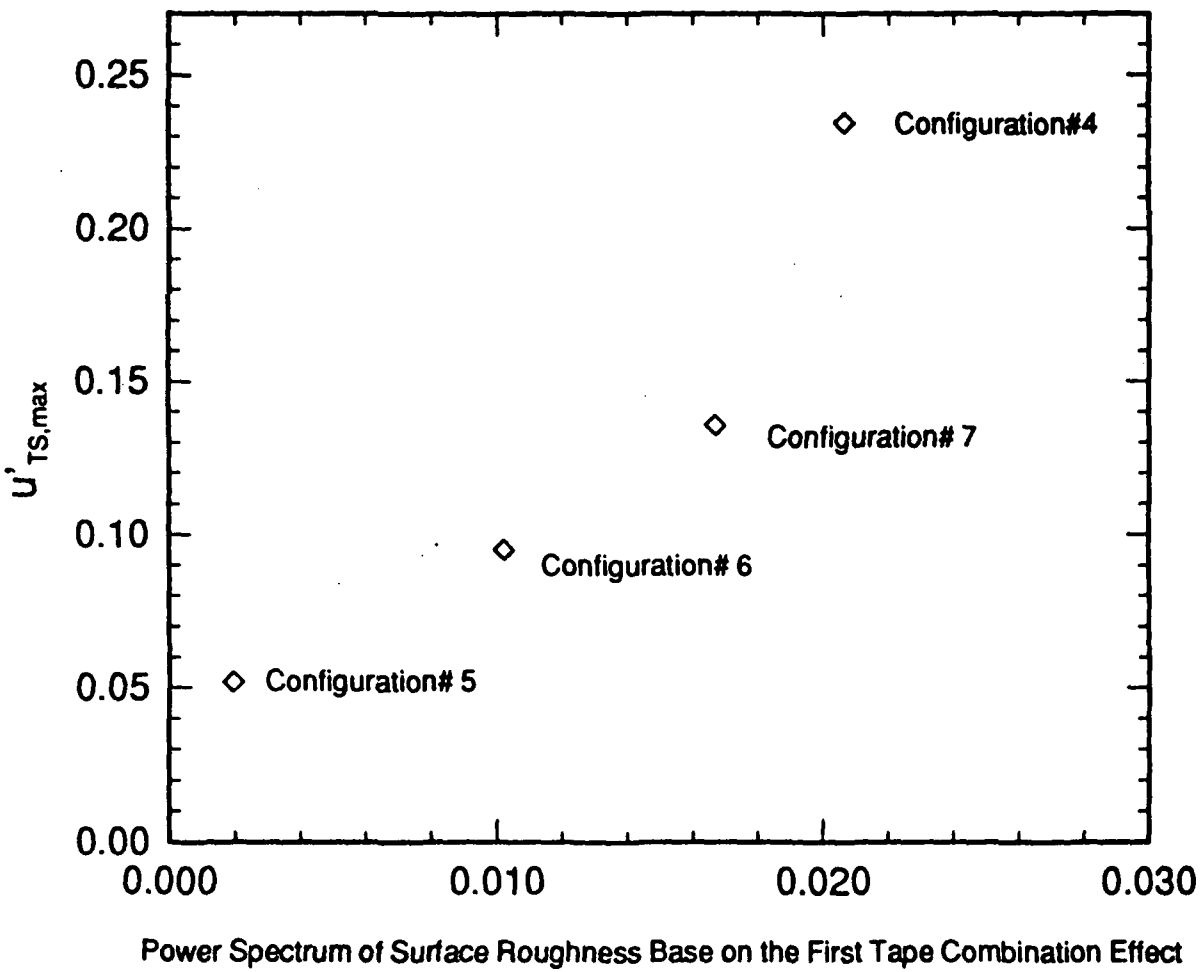

Figure 44. Maximum T-S Wave Amplitude Vs. Surface Roughness Height for Configurations #4, #5, #6, and #7

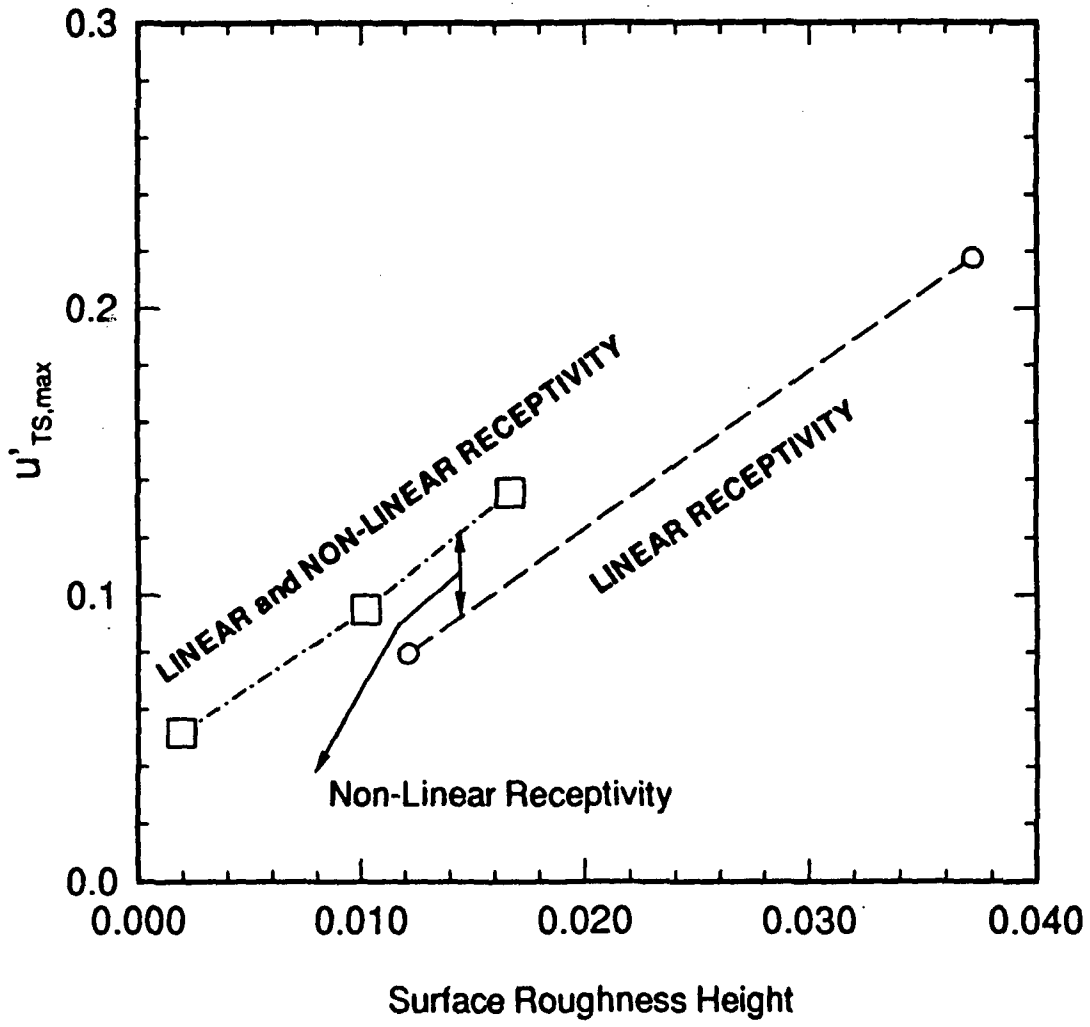

Figure 45. Linear and Non-Linear Receptivity due to Surface Roughness